JUNE 2019

Ph.D. in Civil Engineering

SAAD ABDULRAZZAK MUKHLIF

REPUBLIC OF TURKEY

GAZİANTEP UNIVERSITY

GRADUATE SCHOOL OF NATURAL AND APPLIED SCIENCES

IMPROVING THE STRUCTURAL BEHAVIOR OF HOLLOW CORE SLABS USING SELF-COMPACTING GEOPOLYMER CONCRETE WITH STEEL FIBER

PH. D. THESIS

IN

CIVIL ENGINEERING

BY

SAAD ABDULRAZZAK MUKHLIF

JUNE 2019

IMPROVING THE STRUCTURAL BEHAVIOR OF HOLLOW CORE SLABS USING SELF-COMPACTING GEOPOLYMER CONCRETE WITH STEEL FIBER

PH. D. Thesis

in

Civil Engineering

Gaziantep University

Supervisor

Assoc. Prof. Dr. Nildem TAYŞİ

Co. Supervisor

Asst. Prof. Dr. Mehmet Tolga GÖĞÜŞ

By

SAAD ABDULRAZZAK MUKHLIF

JUNE 2019

I hereby declare that all information in this document has been obtained and presented in accordance with academic rules and ethical conduct. I also declare that, as required by these rules and conduct, I have fully cited and referenced all material and results that are not original to this work.

Saad abdulrazzak MUKHLIF

ABSTRACT

IMPROVING THE STRUCTURAL BEHAVIOR OF HOLLOW CORE SLABS USING SELF-COMPACTING GEOPOLYMER CONCRETE WITH STEEL FIBER

MUKHLIF, Saad abdulrazzak
Ph.D. in Civil Engineering
Supervisor Assoc. Prof. Dr. Nildem TAYŞİ
Co. Supervisor Asst. Prof. Dr. Mehmet Tolga GÖĞÜŞ
June 2019
104 pages

In recent times, concrete technology has been regarded as one of the most viable suggestions for recycling of industrial wastes such as Fly Ash (FA) and Ground Granulated Blast Furnaces Slag (GGBFS). One such development is the use of Self Compacting Geopolymer Concrete (SCGC) whereby the scientific researchers have used some types of solid wastes to improve the performance of concrete. This research involves the study of SCGC and hollow reinforced unit slabs. The thesis consisted of two stages. The first part reports the impact of GGBFS content on the fresh and hardening properties of primarily FA based SCGC. The SCGC mix was formulated with a constant binder content of 500 kg/m3 and at an alkaline-to-binder (a/b) ratio of 0.50. The FA were substituted with GGBFS with various replacement percentages by weight. The second stage includes testing and studying the structural performance of a number of steel fiber reinforced hollow core geopolymer concrete slabs. Twenty-one slabs, which have the same dimensions of 1000x350x125 mm, were cast. These slabs were divided into groups according to steel fiber contents, and each group there were three panels; Solid (SO), Rectangular Hollow (RH) and Circular Hollow (CH). These parameters had the effect of providing variable characteristics of this concrete in terms of the failure modes exhibited, crack strength, ultimate strength, deflection and ductility index.

Key word: Self-Compacting Geopolymer Concrete (SCGC), Fresh Properties, Fracture Energy, Hollow Core Slab (HCS), Steel Fiber (SF).

ÖZET

KENDİLİĞİNDEN YERLEŞEN ÇELİK ELYAFLI JEOPOLİMER BETON KULLANILARAK ÜRETİLEN BOŞLUKLU DÖŞEMELERİN DAVRANIŞLARININ İYİLEŞTİRİLMESİ

MUKHLIF, Saad abdulrazzak
Doktora Tezi, İnşaat Mühendisliği Bölümü
Tez Yöneticisi: Doç. Dr. Nildem TAYŞİ
Dr. Öğr.Üyesi Mehmet Tolga GÖĞÜŞ

Haziran 2019
104 sayfa

Son zamanlarda beton teknolojisi, uçucu kül ve öğütülmüş yüksek fırın cürufu gibi endüstriyel atıkların geri dönüşüm ile kullanılmasını en uygun önerilerden biri olarak kabul etmektedir. Bu gelişmelerden biri de kendiliğinden yerleşen jeopolimer betonun (SCGC) kullanılmasıdır ve bu bilimsel araştırmada da betonun performansını artırmak için bazı katı atık türleri kullanılmıştır. Bu araştırma, kendiliğinden yerleşen jeopolimer beton ve boşluklu döşeme çalışmalarını içermektedir. Tez iki aşamadan oluşmaktadır. İlk bölüm, cüruf içeriğinin, uçucu kül tabanlı jeopolimer betonun yaş ve sertleşmiş özellikleri üzerindeki etkilerini bildirmektedir. Jeopolimer beton karışımı, 500 kg / m3'lük bir sabit bağlayıcı içeriği ve 0,50'lık bir alkali-bağlayıcı (a/b) oranında formüle edilmiştir. Uçucu kül oranı ağırlığa göre çeşitli yüzdelerde cüruf ile değiştirilmiştir. İkinci aşama ise, bir dizi çelik elyafla güçlendirilmiş boşluklu çekirdek beton döşemenin yapısal performansının test edilmesini içermektedir. Aynı boyutta 1000x350x125 mm'lik yirmi bir döşeme dökülmüştür. Bu döşemeler çelik elyaf içeriğine göre gruplara ayrılmaktadır, her grupta üç farklı döşeme tipi bulunmaktadır; dolu (SO), dikdörtgen boşluklu (RH) ve dairesel boşluklu (CH). Bu parametreler, göçme modu, çatlak dayanımı, maksimum mukavemet, deplasman ve süneklik indeksi açısından betonun değişken özelliklerinin belirlenmesinde etkilere sahiptir.

Anahtar Kelimeler: Kendiliğinden yerleşen jeopolimer beton (SCGC), yaş özellikler, kırılma enerjisi, boşluklu çekirdek döşeme (HCS), çelik elyaf (SF).

To my great mother, my father's soul

My sisters

My wife, my children

My friends

ACKNOWLEDGEMENTS

First and foremost, I am grateful to **Allah** who has given me the patience and the strength to overcome all obstacles and have reached by His grace at this stage.

Then, I would like to express my deepest gratitude and all thanksgiving for my supervisor, **Assoc. Prof. Dr. Nildem TAYŞİ**, for her helpful comments, provided all the necessary facilities for this study, also its kindness and support to complete this study. Without her supervision and advice, this thesis would not have been possible. I would like also to thank my Co-Supervisor **Asst. Prof. Dr. Mehmet Tolga GÖĞÜŞ** for his continuous help and also facilitate the experimental works.

The author would also like to thank the **Presidency of the Republic of Iraq** and **Iraqi Ministry of Higher Education** for providing this scholarship to finish my Ph.D. study. Also, special thanks to **Gaziantep University** for the real support and laboratory facilities.

I am very grateful for the **spirit of my father** and for my **mother's prayer**, caring and supporting me over the years. Without them, I will not be anywhere close to the position I am in now, **my sisters,** whose encouragement, love and support served as the foundation for all of my past achievements and future endeavors in life.

As well as, I would like to express my deep appreciation my **wife** and **kids**, to whom I dedicate my work. I am thankful for their love and best wishes, which, despite of their physical absence has helped me in the successful completion of my study.

Finally, I would also like to take this opportunity to thank my **close friends** who have participated in completing this thesis

TABLE OF CONTENTS

LIST OF TABLE

Page

LIST OF FIGURE

Page

LIST OF SYMBOLS

g	Gravitational Acceleration.
Y	Coefficient of Friction
W	Centrifugal Acceleration
***F*c**	Compressive Strength
***F*st**	Splitting Tensile Strength
E	Modulus of Elasticity
Gf	Fracture Energy
***F*flex**	Flexural Strength

LIST OF ABBREVIATIONS

GPC	Geopolymer Concrete
OPC	Ordinary Portland Cement
FA	Fly Ash
GGBFS	Ground Granulated Blast Furnace Slag
SCC	Self-Compacting Concrete
SCGC	Self Compacting Geopolymer Concrete
SF	Steel Fiber
Ma	Macro Steel Fiber
Mi	Micro Steel Fiber
SP	Super Plasticizers
NaOH	Sodium Hydroxide
Na_2SiO_3	Sodium Silicate
CSH	Calcium Silicates Hydrates Gel
ASTM	American Society for Testing and Materials
BS	British Standard
TS	Turkish Standard
LVDT	Linear Variable Displacement Transducers
HCS	Hollow Core Slab
SO	Solid Slab
RH	Rectangular Hollow Slab
CH	Circular Hollow Slab

CHAPTER 1

INTRODUCTION

1.1 Background Study

Turkey, like most other industrialized countries, generates a colossal amount of waste materials. The waste utilization process has been one of the major environmental concerns in this country and across the globe. It is estimated that the annual productions of Fly Ash (FA) and Ground Granulated Blast Furnaces Slag (GGBFS) in Turkey are about 15 million tons and 600,000 tons respectively [1]. For this, the careful selection and utilization of these wastes offer the easiest approach of introducing sustainable product designs in the construction industry.

In recent times, concrete technology has been regarded as one of the most viable suggestions for recycling of industrial wastes such as FA and GGBFS. One such development is the use of Self Compacting Geopolymer Concrete (SCGC) whereby the scientific researchers have used some types of solid wastes to improve the performance of concrete [2]–[4]. Additionally, the concrete technology has occasioned other benefits such as recycling of waste materials, production of lightweight products and reduced use of non-renewable resources [5], [6]. With increasing environmental and social concerns, the adoption of new building technologies is amplified.

Construction activities in many countries have witnessed rapid development. It is worthwhile to note that the construction activities guzzle a lot of resources and at the same time play a major role in the emission of greenhouse gases [7]. In this context, global warming is one of the greatest environmental issues caused by the emission of greenhouse gases like CO_2 to the atmosphere. Waste utilization and reduction of cement consumption Provide the finest opportunity of protecting the environment. Across the globe, cement is used all over the world due to its ease of working, high strength, and great economies. The raw materials used in Ordinary Portland Cement (OPC) manufacturing are widely abundant, but they also have negative effects on the environment. Despite its wide usage, concrete manufacturing is under observation due

to the high emission of carbon dioxide and other greenhouse gases. Approximately 5 % of carbon emissions are from the cement industry with the main constituent in OPC manufacturing being hazardous in nature. The high carbon emissions found in cement manufacturing processes is as the result of the production of carbon dioxide as the waste product caused by the reaction and combustion of fossil fuels [8].

In order to decrease the environmental effects from the manufacture of cement, the struggle for alternative materials must continue. These innovative materials should not only be environmental friendly, but should also prove to be effective construction products. In the recent past, huge attempts have been made to reduce the negative effects on the environment as a result of cement manufacture. One such development is the use of alternative material such as Geopolymer Concrete (GPC) instead of the conventional OPC.[9], [10]

1.2 Geopolymer Overview

The geopolymer technology suggested by Davidovits [11] is one of the most important developments in the concrete world. GPC is an innovative binder material whereby its production involves complete replacement of OPC (zero percentage of cement). GPC prides itself with decent mechanical properties, standard fire and acid resistance and therefore a potential alternative material with comparable properties to OPC. Experimental studies depict less than 80 % carbon dioxide emissions during GPC productions making it a more environmentally friendly construction material when compared to OPC [12], [13]. Additionally, GPC plays a necessary part in the environment in two perspectives. One, it results in reduced consumption of traditional cement which releases vast quantities of carbon dioxide. Two, it utilizes huge quantities of industrial wastes during its manufacturing process.

Conventional low calcium GPC requires heat curing which is already available in the precast industry. The key factors in the selection of source materials for the manufacture of geopolymers include cost, availability, and type of application. Currently, a wide range of mineral deposits and industrial by-products are under investigation with the objective of determining the most suitable materials for the manufacture of geopolymers. Note that FA, silica fume, GGBFS, metakaolin, and red mad can also be used in geopolymers as the source materials [14]. According to Xu and Deventer [15], the most logical source of alumosilicate is FA due to its availability, price and the superior chance for production of GPC [16]. For this purpose, Alkaline

silicate solution is added to activate the raw alumosilicate products such as GGBFS and FA.

In this thesis, FA and GGBFS based GPC were investigated as Pozzolanic materials. The low calcium GPC typically hardens through the process known to as geopolymerisation. In this process, the binder mainly consisting of silica and aluminum is fragmented through the process of dissolution in which both the aluminum and silica ions are released. After dissolution, the condensation process follows whereby the silica and aluminum ions are linked with free oxygen ions to produce the hardened material. Finally, when slag is added into the geopolymer matrix, Calcium Silicate Hydrates (CSH) are produced in union with the geopolymeric gel. The CSH serves the important function of improving the setting time and the compressive strength of GGBFS and FA based GPC [17], [18].

1.3 Research Significance

The following main objectives form the basis of this thesis:

1. To explore the latency and viability of self-compacting concrete made with constituents that are locally available. A thorough study of the mechanical and physical properties of the SCGC will be discussed.

The problem with the self-compacting concrete is that it has little cracking resistance, low tensile strength, and limited ductility. However, these curbs can be eliminated by the addition of fibers into the concrete mix [19], [20]. The fibers improve the ductile character of the concrete structure by possibly increasing the post-cracking energy absorption. Addition of Steel Fibers (SF) also contributes to its low cost as compared to the ordinary self-compacting concrete [21]–[23].

In normal cases, the self-compacting concrete exhibit a homogenous flow with the addition of SFs. The homogenous flow goes a long way in ensuring an improved concrete flowability. Geometry, size, and content of SFs can greatly affect the properties of self-compacting concrete. As such, great care is normally exercised when adding the appropriate SFs content [24].

2. To produce lightweight slabs as a result of reduced cross-sectional areas of slabs.

Hollow Core Slab (HCS) panels, also known as void slabs, are super materials in engineering due to low seismic zones, relatively small weight and cheap price. Considerably noticeable is the opening that is created through the panel, which reduces

its total weight. Also, these openings can be used for passing mechanical, thermal and electrical equipment through it- mainly in large constructions like high-rise buildings, bridges, offshore structures and malls. The resource efficient HCS are precast concrete slab systems with hollow cavities which consistently extend throughout the length of the slab with the aim of decreasing both the cost and weight of slabs. Additionally, HCS utilizes the embedded voids to disguise mechanical and electrical runs. The HCS has a wide variety of applications ranging from bridge deck units, wall panels and also as spandrel members. Due to their lightweight nature, HCS span up to 18 meters without supports or columns. The slab system can thus be utilized in both the roof and floor systems requiring long clear spans such as bridges, conference rooms and auto parks [25]. For this, it is paramount that experimental investigations are conducted for these slab systems. The type of SF and the shape of the hollow core will be the main parameters of these analyses.

1.4 Outline of the Thesis

The Thesis comprises of six chapters as outlined below:

- Chapter One: Provides a brief introduction and the objectives of this research thesis
- Chapter Two: Gives a detailed review of available literature pertaining to GPC, SCGC, and HCS. It also reviews the previous research studies related to the present research work.
- Chapter Three: Displays the experimental works with a description of material properties and lab tests, including testing of fresh and hardened properties of SCGC. Also casting and testing procedures of HCS.
- Chapter Four: Illustrates the results obtained from the testing program. Moreover, the effects of experimental parameters on the fresh and hardened properties of SCGC are discussed.
- Chapter Five: Discusses the characteristics of stress-strain curves of HCS with or without SF. The constitutive relationships for stress-strain are studied in detail for HCS.
- Chapter Six: Presents a summary of conclusions based on the present study, as well as the most important recommendations for future studie

CHAPTER 2

LITERATURE REVIEW

2.1 Introduction

This chapter endeavors to provide a deep insight into the philosophy of GPC and to achieve this aim, the contents of Chapter two are primarily organized into three sections:

- The first section provides a general introduction to GPC, including history, material, application, and advantages.
- The second focuses on SCGC and the difference between GPC.
- The third section talks about the HCS as a structural member, performance, and review of the experimental investigations implemented on HCS system

2.2 Pozzolanic Materials

A pozzolan is simply defined as a finely divided aluminous or siliceous material that reacts with calcium hydroxide in presence of moisture to form composites that possess cementitious properties through chemical reactions [26].

FA and GGBFS are the common most used pozzolanic materials in the conventional cement concrete. The substitution of cement of these pozzolanic materials largely decreases the early-age strength of concrete, but at the same time improves a number of late-age properties of concrete. This study focused on FA and GGBFS pozzolanic materials due to their widespread use.

2.2.1 Fly Ash

FA is an inorganic waste product generated in thermal power stations during the firing of powdered coal at temperatures of approximately 1200°C. At ambient temperatures FA is capable of reacting with $Ca(OH)_2$ to form compounds with cementitious properties [27]. Physically, FA is in the form of gray powdered particles and mostly comprising of sphere-shaped glassy particles. The characteristic of the FA depends on

numerous factors, such as the type of power plant, the composition of feed coal, the chemical composition of the coal, burning system and the conditions of deposition of FA. Generally, FA is obtained from both electric and steam-fired coal plants. In most cases, the coal is pulverized or crumpled and then blown with hot air as it moves into the combustion chamber where it ignites, leading to the production of molten mineral residue. The embedded boiler tubes extract the heat from the boilers cooling the flue gas and at the same time causing the molten mineral residue to harden and form ash status. Coarse ash particles as referred to as bottom ash, fall to the bottom of the combustion chamber, whereas the lighter fine ash particles also termed as FA remain suspended in the flue gas. Prior to exhausting the flue gas, FA is removed by particulate emission control devices, such as electrostatic precipitators or filter fabric bag houses [28]. Figure 2.1shows the FA producing process.

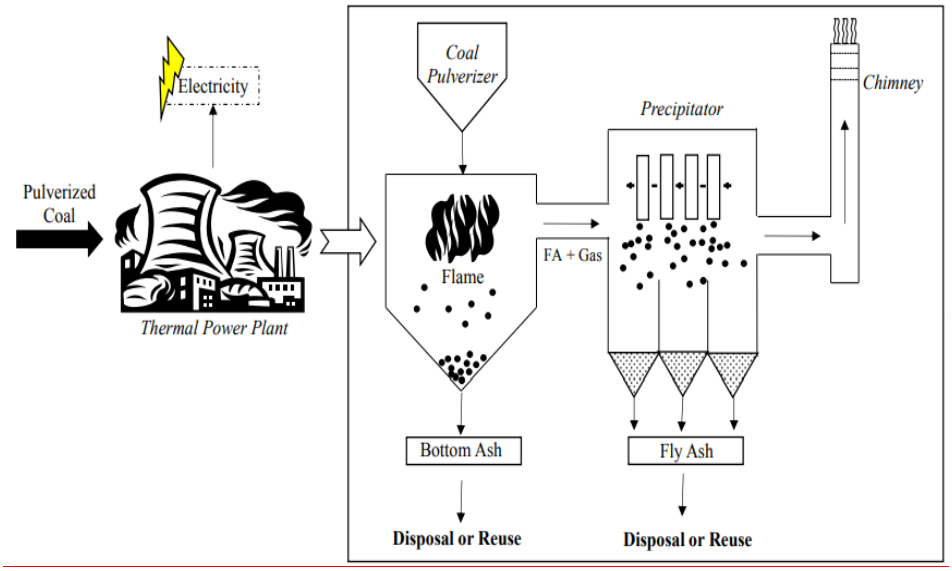

Figure 2.1 The process of producing fa in a power plant [29]

GGBFS commonly referred to as "slag" is fine glassy material produced when the molten blast furnace slag is promptly cool chilled by immersion of water. In most cases, GGBFS is obtained as a by-product of an iron manufacturing process that has calcium alumino-silicate microstructure. The GGBFS comprises of alumino-silicates and silicates of calcium among other metal bases which are produced in molten conditions concurrently with iron in the blast furnace [30]. In other words, GGBFS is a waste product of blast furnaces used in the manufacture of iron. The blast furnaces are operated at extremely high temperatures of approximately 1500^0C and are served with a cautiously controlled mixture of iron ore, coke, and limestone. During the

manufacturing process, the iron core is reduced to iron with the remaining forming a slag that floats above the iron. The slag is then systematically taped off from the furnaces in molten form and immediately quenched by large quantities of water to produce GGBFS. This cooling process optimizes the cementitious properties of GGBFS and results in the production of granules similar to those of coarse sand. The last process involves drying and grounding of the granulated slag to fine powder producing the GGBFS which is also referred to as the “Slag cement”.

In the built environment, GGBFS is a renowned alternative to concrete. For this, its development is very timely especially since the urge for waste utilization across the globe is on a rise. Being a waste material the effective use of GGBFS serves as a step forward to a greener environment. That said, it is paramount to note that the use of GGBFS does not degrade or reduce the strength of concrete. The process of GGBFS production is as shown in Figure 2.2 [31].

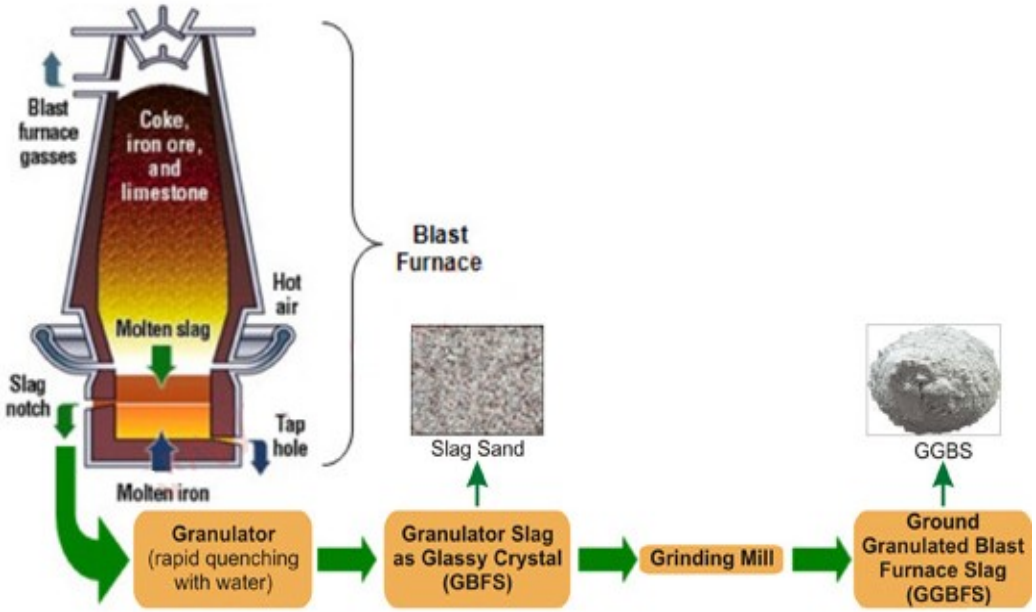

Figure 2.2 GGBFS production process [31]

2.3 Geopolymer Concrete (GPC)

Geopolymerization refers to a synthesis reaction that integrates minerals chemically [32]. In this context, a "geopolymer" may be defined as a solid stable material comprising of aluminosilicates compounds formed through the alkali silicate or/and alkali hydroxide activation process [33].

The three common types of polysialates as distinguished by Davidovits are as depicted in Figure 2.3 and Figure 2.4.

Poly (sialate)

(-Si-O-Al-O-)

Poly (sialate-siloxo)

(-Si-O-Al-O-Si-O-)

Poly (sialate-disiloxo)

(-Si-O-Al-O-Si-O-Si-O-)

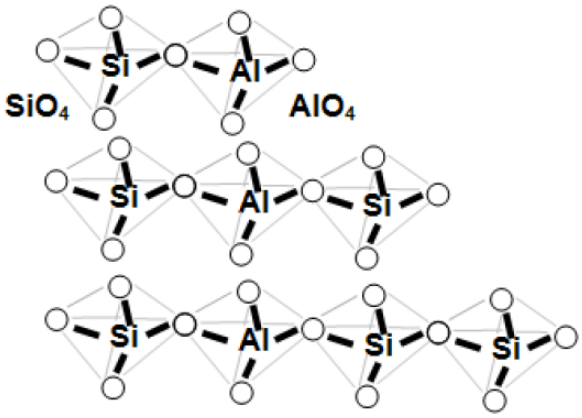

Figure 2.3 Common types of polysialates

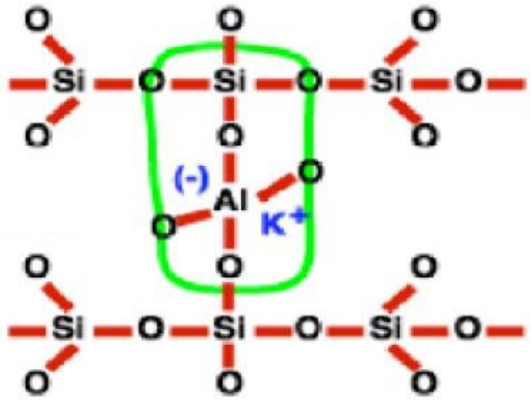

Figure 2.4 Typical chemical structure of polysialates [33]

In geopolymerization also known to as geosynthesis, alumino-silicate oxides chemically react with polysilicates to yield three-dimensional polymeric bonds under extreme alkaline conditions. In other words, the reaction is better defined as a chemical process that integrates minerals (polymeric bonds) to form the final geopolymer material as the main building block [8].

In this case, the polysilicates mostly used are the potassium silicate or sodium silicate in either amorphous non-crystalline or glassy crystalline structure [11], [14]. Geopolymer process mostly depends on the following factors:

- The concentration of the alkaline solution
- The composition of binder material (Chemical and mineralogical)
- Curing temperature, and
- Water content

The silica to aluminum ratio plays a very important role in determining the strength of the GPC. This ratio just as in the case of geopolymer process depends on the concentration of the alkaline solution, starting a material chemical composition, curing time and the curing temperature. Studies by Fernández- Jiménez et al. [34] suggest that a fraction of the aluminum and silica ions are not reactive in the binder. This was investigated by the use of different FA types and the percentage of reactive silica in all sample materials were found to be the same but varied in aluminum. A detailed geopolymerization process is discussed in the next section with the aim of ensuring a better understanding of the binder process of GPC.

2.3.1 Reaction Mechanism of Geopolymer

The main constituents of geopolymers are the alkaline liquids and the source materials. It is important that source materials be rich in Aluminium (Al) and Silicon (Si). Clay and Kaolinite are some of the natural resources examples that are rich in Al and Si. Alternatively, by-product materials, for example, FA, GGBFS, silica fume, red mud, and rice husks can be used as the source materials. In most cases, the decision for the source material to use is determinate with factors such as cost, application, availability, and particular demand of the end users [35].

Figure 2.5 demonstrates a simplified geopolymerization reaction mechanism and also outlines the key processes occurring in the transformation of a solid alumino-silicate source into a synthetic alkali alumino-silicate.

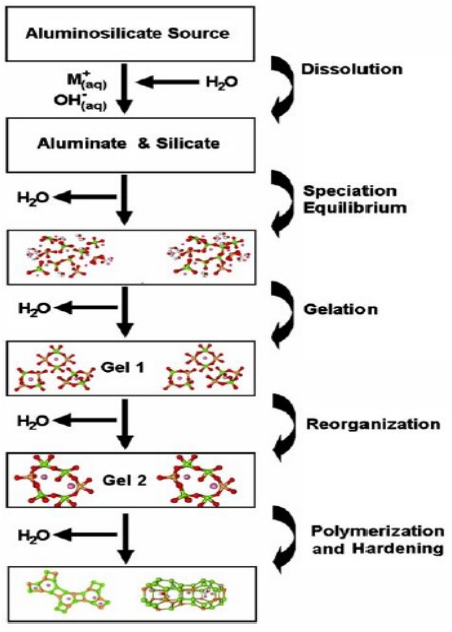

Figure 2.5 Conceptual model for geopolymerization [36].

During geopolymerization, sluggish growth of the crystalline structure is evident after the nucleus of the polymerized gel achieves its critical size. The matrix crystalline process is relative to the rate at which the precipitation occurs with slow alkali and ash reactions allowing the development of a well-structured crystalline environment. In the context of this, zeolitic precursors are regarded as the most hardened geopolymer types of cement.

The end product of geopolymerization is an amorphous, semi-crystalline material that is cementitious in nature. Note that the chemical structure of the geopolymer material produces is comparable to natural zeolitic materials but with amorphous microstructures.

The process of polymerization involves a considerably fast chemical reaction under favorable alkaline conditions on Si-Al minerals resulting in a 3-dimensional polymeric ring and chain structure that consists of Si-O-Al-O bonds [37]. Importantly, the produced gel product contains alkaline cations that equally compensate for the charge deficit linked with the aluminum for silicon substitution [38]. An intermediate, aluminum-rich phase is first formed which then gives way to a more stable, silicon rich three-dimensional gel product in the form of $Q_4(nAl)$, which is dependent upon curing conditions and the activator type [39].

The chemical reaction during polymerization proceeds without the involvement of water and instead any water is expelled out during the curing and drying process. This is in direct contrast to the hydration reactions that activates when Portland cement is mixed with water producing compounds such as calcium hydroxide and calcium silicate hydrate. The contrast between the two plays a significant role in both the chemical and mechanical properties of the resultant GPC. Additionally, it renders it more resistant to water ingress, alkali-aggregate reactivity, heat and chemical attack [35]. The schematic development of a geopolymer material from the initial activation stage to the final microstructure formation is as depicted by Equation (2-1) and Equation (2-2) [37], [40].

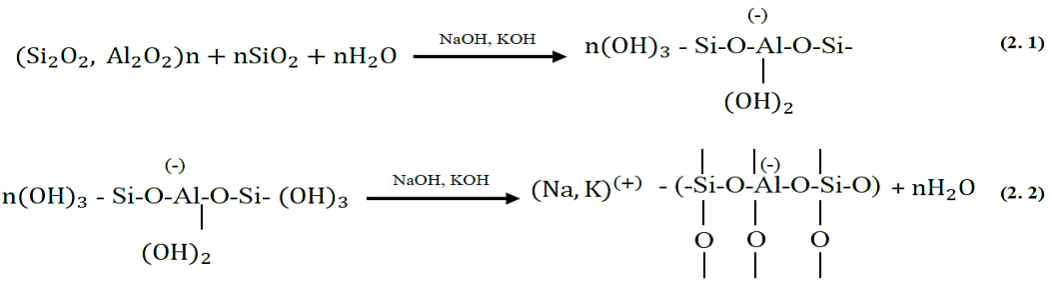

(2. 1)

(2. 2)

2.3.2 Source Materials

As stated earlier, geopolymers are produced through the alkali-activating process to form cementitious materials. The three most used raw binders for the geopolymarization process include GGBFS, coal FA and calcined clays (metakaolin). For a more efficient process, the binder materials should have very high levels of Aluminium and Silicon in their amorphous form. The various binder materials that have been studied and used to produce GPC mixes are as listed below

- GGBFS
- Calcium Kaolin (Metakaolin)
- Silica Fume
- Class F – FA
- Class C – FA
- Any natural minerals containing high levels of Al and Si.
- Alibite and,
- Red Mud

2.3.2.1 Fly Ash-Based Geopolymer Concrete

FA particles are finer than cement and spherical in shape. The size of the FA particles ranges from 1 to 150 micrometers. Chemically, it mainly contains silicon oxide (SiO_2), aluminum oxide (Al_2O_3), calcium oxide (CaO), and iron oxide (Fe_2O_3). It also contains some elements in smaller amounts such as sulfur, magnesium, titanium, sodium, and potassium. In normal concrete, FA is used in the construction industry as a replacement of cement up to 60 % [41]. Calcium hydroxide that results from the hydration of cement reacts with the silicon oxide in the FA particles to form a gel of calcium silicate hydrate (C-S-H). The use of FA in normal concrete improves its workability and at the same time reduces the water content due to the spherical shape of its particles.

Moreover, it improves concrete density and durability due to the small particle size that acts as filler [40], [42]. It also enhances the confinement of the GPC by increasing the particle packing and reducing its porosity.

The properties of FA vary widely based on the chemical composition and the impurities of the source coal prior to combustion, and the properties of the combustion process [43]. Two main types of FA present include Class F, and Class C. The most commonly used type of FA in the production of GPC is Class F. It is more analyzed in literature than Class C due to its large availability, sufficient silica and alumina content, and low water demand [44], [45]. However, Class C-FA contains more Ca than Class F [43]. Generally, FA has less amount of Ca than GGBFS. Precursor materials with a high amount of CaO were reported to give higher strength GPC. It was also reported that it reduces the setting time of concrete. Moreover, it was found that this type of binder material improves the mechanical properties of geopolymers, especially when cured at ambient temperatures. This was justified by the formation of calcium silicate hydrate (C-S-H) compound in materials containing a high amount of CaO along with the alumino-silicate hydrate in the geopolymer reaction [45].

2.3.2.2 Ground Granulated Blast Furnace Slag Based Geopolymer Concrete

GGBFS has a chemical structure that contains sufficient calcium for use in charge-balancing the aluminum. It was found that GGBFS particles based reaction depends on the size of the particles. Particles greater than 2 micrometers react slowly, while particles less than 2 microns in size react faster and approximately need 24 hrs to be reacted completely in both normal and GPCs [43]. The main components of GGBFS are:

- CaO (30-50 %).
- MgO (1-18 %)
- Al_2O_3 (8-24 %) and
- SiO_2 (28-38 %),

The higher content of CaO in GGBFS typically reveals a significant increase in compressive strength of concrete. Note that for any given source of GGBFS, the properties especially the chemical composition remains reasonably constant compared to FA.

The addition of GGBFS to FA based GPC was found to have a positive impact on the strength of concrete even when added in smaller amounts such as 4 %. However, the overall impact depends on the type and concentration of the activating solution, and the percentages of GGBFS and FA relative to each other [44].

2.3.3 Alkali Activator

Silica is an element that chemically dissolves in strong alkaline based conditions to form other compounds. The strong alkaline solution should be active during the dissolution process of aluminum and silica since it plays a very important role during the condensation process [45].

The commonly used activators in the geopolymarization process include:

- Sodium Hydroxide
- Sodium Silicate
- Potassium Hydroxide
- Potassium silicate

In this research study, Sodium hydroxide was used as the main activator with additional sodium silicate used to increase the overall silica content in the matrix.

Researchers have found that the best alkaline solution to be used in GPC production is a combination of silicate and hydroxide of either sodium or potassium. However, the use of one alkaline solution like sodium hydroxide (NaOH) is also feasible. It was found that the type of alkaline solution used in the GPC affects the geopolymarization process. NaOH was reported to have a higher rate of geopolymarization reaction than potassium hydroxide (KOH). In light of this, Xu and Van Deventer (2000) proved that sodium hydroxide caused a higher rate of dissolution as compared to that of potassium hydroxide [15]. Conclusively, it is evident that NaOH dissolves the minerals in the source material at a higher rate than KOH [46].

Ravikumar et al. reported that the properties of both the fresh and hardened concrete are significantly affected by the amount of alkaline solution used in the geopolymarization process. An experiment was conducted where different amounts of alkaline solution, 35 %, 40 %, and 45 % (by volume of the mix) were tested. From the results, it was evident that the amount of alkaline solution has a direct relationship with the quality of the GPC in terms of the material properties.

2.3.3.1 Sodium Hydroxide Solution

Sodium hydroxide in an alkaline material mostly produced through electrolysis of sodium chloride brine in a diaphragm electrolytic cell or membrane. Sodium hydroxide is commonly referred to as caustic soda and draws a large number of users especially in the paper industry and manufacturers that use alkaline based materials as one of their raw materials.

Sodium hydroxide is made available in four different forms namely; flakes, beads, solid castings and compounders. Interesting to note is that all these different forms have the same chemical composition.

2.3.3.2 Sodium Silicate Solution

The solutions of alkali silicates can be formed by hydrothermally dissolving reactive silica sources or by dissolving alkali silicate capsules in very hot water to produce their respective alkali hydroxide solution [47]. The equation below demonstrates the hydrothermal dissolving process:

$2MOH + x\ SiO_2 \rightarrow M_2O.\ x\ SiO_2 + H_2O$

2-3

As shown from the equation above, the chemical configuration of the dissolve silicates can be known by use of the following formula: SiO_2 x M_2O where "M" represents either the potassium (K) or the sodium (Na). Note that the silicate solutions are mostly identified by the ratio SiO_2:M_2O. This ratio plays a very critical role during the geopolymarization process. Both potassium silicate and sodium silicate solutions exhibit similar reactive qualities with the only difference being that potassium silicate is more viscous [47]. Studies depicted that the geopolymarization reaction occurred at a much higher rate with the presence of a soluble silicate unlike when only the alkaline solution was used in the process [43].

2.3.4 Factors Affecting Geopolymer Concrete Performance

2.3.4.1 Sodium Hydroxide Concentrations

Research studies on GPC indicate higher compressive strengths when alkaline solutions with high sodium hydroxide concentrations are used [48]–[50]. The reason behind this increase in strength is that stronger bonds are formed as more alumino-

silicates can be dissolved. This may be regarded as one of the determining factors regarding the increase in the compressive strength [51].

The impact of molarity of sodium hydroxide solution to the compressive strength of GPC is as displayed in Figure 2.6

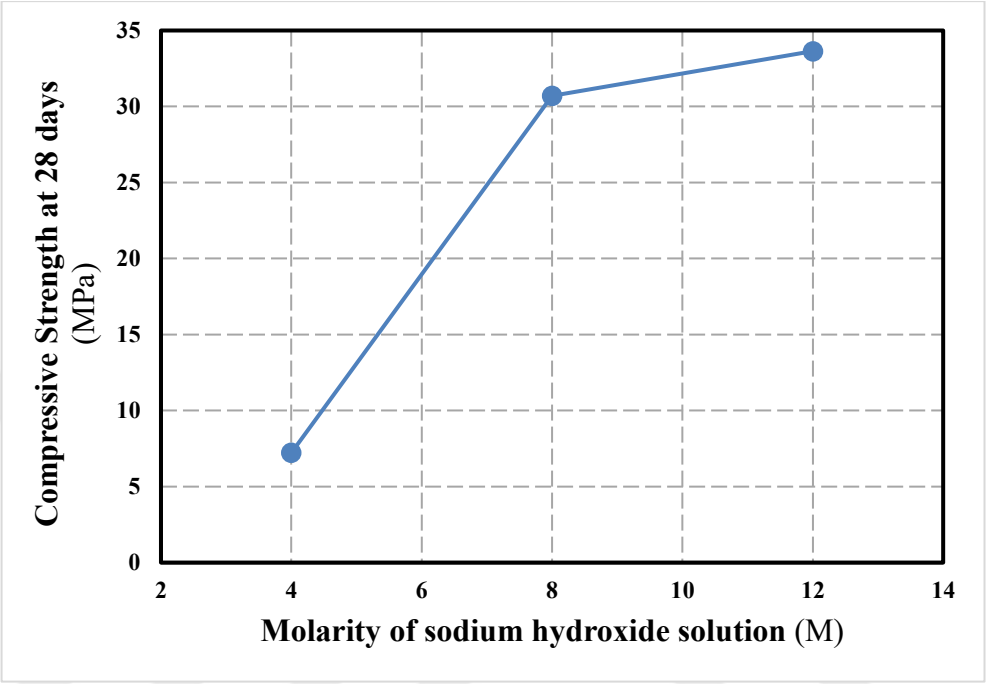

Figure 2.6 Effect of the sodium hydroxide concentration on the compressive strength of the GPC [50]

2.3.4.2 Sodium Silicate-to-Sodium Hydroxide Liquid Ratio

Research indicates that higher compressive strength is yielded with an increase of the silicate solution in the reaction matrix [49], [51]. According to laboratory experiments conducted by Hardjito (2005), an optimum ratio of 2.5 is recommended for obtaining the best results as depicted in Figure 2.7 [52]. Luckily, the addition of the silicate solution is more cost efficient as sodium silicate is relatively cheaper than the sodium hydroxide solution.

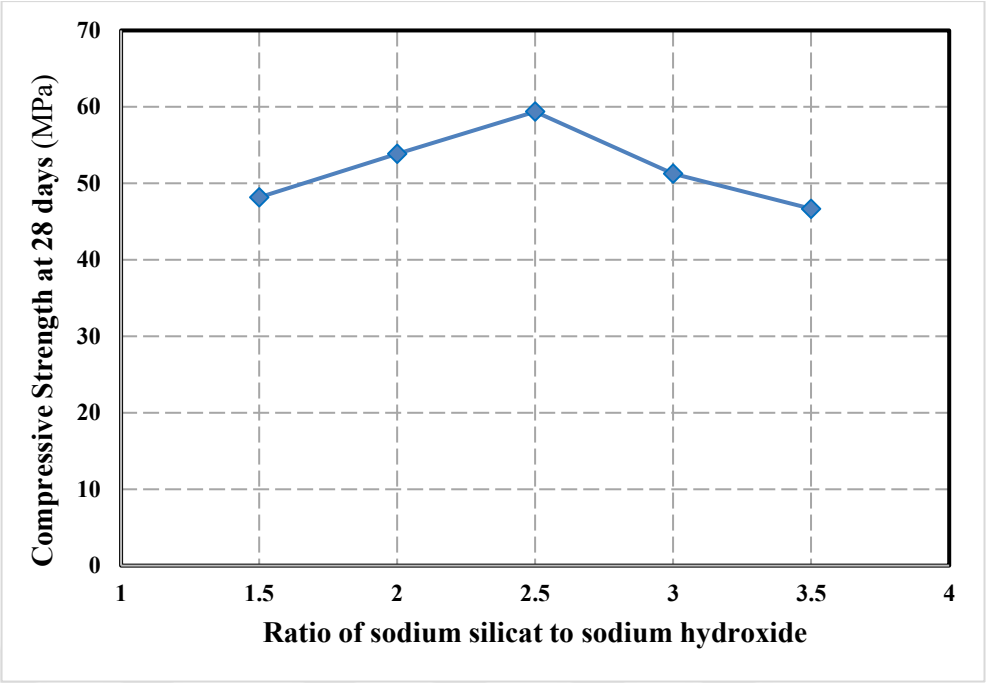

Figure 2.7 Effect of the SS/SH ratio on the compressive strength [52]

2.3.4.3 Curing Type

Literature review indicates that geopolymer binders can be produced through curing in various conditions. In contrast to OPC, geopolymer binders do not need water for curing. Nonetheless, a comparative study of different curing conditions [53] showed that temperature and humidity play a key role in the development of the microstructure and consequently the properties of alkali-activated FA materials. It is important to note that the curing regime highly influences the chemical properties and composition of the final product.

2.3.4.3.1 Ambient Curing

Strength development of geopolymers is highly influenced by the curing temperatures. The curing process calls for fairly higher temperatures than ambient to speed up the setting process. This is especially so for the alumino-silicate materials that have no or very little quantities of calcium compounds. Therefore, to make effective use of the ambient temperature, the addition of GGBFS in the matrix is highly encouraged [54]. Palomo et al [55], in their studies, observed that the mechanical properties rose considerably with temperature and that the degree of reaction was controlled by the curing time. It was noted that at lower temperatures, relatively long periods of time were required in order to achieve the same degree of reaction attained in few hours at

elevated temperatures. For instance, a FA geopolymer paste displayed a degree of reaction of roughly 38 % in 7 days with a curing temperature of 45ºC but relatively the same degree of reaction was achieved when curing was done for 24 h at 65 °C. It was also reported that there exists a temperature and time threshold value after which the mechanical properties (strength) rises slowly, or even decline.

The chemical composition and mechanical properties of geopolymer materials are highly influenced by the curing condition used. Heat curing is the most desired method but it poses practicability concerns especially for cast-in-situ concrete. Importantly to note is that although the use of high temperatures may accelerate the setting and strength developments during early ages, it may not always guarantee similar effects as ambient curing at later ages.

Chindaprasirt et al. [56] suggested that the surface to volume ratio influences the particles exposure to heat and consequently the loss of moisture. This means that particles with high surface to volume ratio are more subjected to the curing heat compared to larger particles with a small surface to volume ratios. Results indicate that curing of reacting mixtures at elevated temperatures fast-tracks the strength development of the resulting product. However, the 28 days of mechanical properties are realized when curing is done at ambient temperatures [56].

2.3.4.3.2 Curing Temperatures

In the geopolymarization process, the curing temperatures play an important role in influencing the rate curing process. That is, the higher curing temperatures the more efficient is the dissolution process [48]. Palomo et al [55], in their research studies, noted that an increase in the curing temperature from 45 °C to 65 °C greatly improved the rate of mechanical properties development. Additionally, Olivia et al [57] observed that heat cured FA based GPC had higher tensile and compressive strengths in addition to low effective porosity all which are important for concrete especially those in the aggressive environment [58].

2.4 Self-Compacting Geopolymer Concrete (SCGC)

The durability of concrete was a major concern in Japan. Conventionally, construction of durable structures commands for adequate concrete compaction by the skilled personnel. The gradual decline in the number of skilled personnel in Japan's construction industry lead to a reduction in construction works quality. For this, an innovative self-compacting concrete was developed with the aim of producing durable concrete units independent of the quality of the ongoing construction work.

Self-compacting concrete attains remarkable compaction by using its own weight and without necessitating for mechanical vibration. This state of the art material was first proposed by Okamura in 1986 [59].

Studies to develop SCC, including a primary study on the workability of this concrete, have been carried out by Ozawa and Maekawa at the University of Tokyo [59], [60]. These models of SCC were first concluded in 1988 by use of materials readily available on the market. The models performed acceptably in terms of denseness after hardening, shrinkage, drying, and hardening, and heat of hydration. One type of this kind is the High-Performance Concrete that can be defined using the three stages of concrete as shown below:

1. Fresh – Ability to self-compact
2. Early on age – Prevents early defects
3. After hardening – Defense ability against exterior factors

According Aitcin [61], High-Performance Concrete may be referred to as concrete with high durability and with relatively low-water cement ratio. For this, the use of high performance concretes has found widespread applications in delivering high durability concrete.

Self-Compacting High-Performance Concrete (SCC) is well known as concrete with good deformability. SCC can be used to fill closely reinforced areas without the need for mechanical vibrations. Additionally, SCC has very high resistance to particle segregations. To achieve outstanding self-compact ability, especially in highly reinforced areas, SCC should deform appropriately without segregating its components. Slump flow test can be used as the evaluation test for estimating the deformability of SCC under its own weight. Since there were no standard tests for assessing the resistance to segregation and the self-compact ability of SCC at the time, researchers developed simple evaluation methods. One such was the use of a U-shaped

apparatus and the time taken for the concrete to flow to a certain distance used to estimate the self-compact ability of the concrete.

High deformability and resistance to segregation of SCC were regarded as very important properties. Interestingly, these material properties are fundamentally opposite in nature and thus SCC is more sensitive to quality fluctuations of materials as compared to conventional concrete when produced at ready-mix concrete plants. It was a tall order to produce SCC with constant quality at the time because the available facilities had not acquired the required quality control units. To improve the manufacturing and handling process, the researchers developed an SCC incorporated with a distinct kind of viscosity agent that they formulated from a biotechnology process.

Nowadays, it is normal to increase the resistance to segregation by use of present production facilities and commonly available materials. As per JSCE, (1999), this type of SCC provides the required self-compact ability principally by reducing the water-powder ratio to achieve the recommended resistance to segregation. Use of superplasticizers is however recommended in order to impart high deformability[62].

The first application of combination type SCC was in the year 1991 for the tower of cable-stayed OPC building and bridge structures. Over the years, the use of this type of SCC has been applied for more complicated and sensitive structures such as the construction of large section tunnels and full sandwiched structures.

As stated above, it has been close to three decades since the first practical application of SCC. Currently, the structures built using SCC vary extensively with each application requiring different mechanical properties. Point to note is that most of the original methods that were used to estimate deformability, self-compact ability and resistance to segregation are still in use up to now. This evidently validates that the initial evaluation tactics were sufficiently effective. Therefore, it is very important to relate these evaluation methods and then come up with new concepts of SCC development for improved manufacturing and handling.

The problem with the self-compacting concrete is that it has little cracking resistance, limited ductility and, low tensile strength. However, these curbs can be eliminated by the addition of fibers [18]. Fibers can improve the concrete structure's ductile character by possibly increasing the post-cracking energy absorption. Addition of SFs also contributes to the low cost of production as compared to the ordinary self-compacting [20]–[22]. In normal cases, the SCC exhibits a homogenous flow with the addition of

SFs which also comes with improved concrete flowability. The geometry, size, and content of SFs can greatly affect the properties of SCC. As such, great care should be carried out when adding the appropriate SFs content [23].

2.5 Fiber Reinforced Geopolymer Concrete

The concepts of using fibers as reinforcements in geopolymers were introduced with an aim of improving the properties of GPC such as ductility, durability, fracture toughness and flexural strength. Steel, glass and synthetic fibers were used as reinforcement in concrete and the research of fibers reinforced concrete is still work in progress [63].

Today, reinforcing fibers are available in a wide variety of materials and can be classified into four primary categories. The categories are defined according to the different material types for fibers. These different materials possess different properties and the fiber material choice is dictated by the end properties required [64]. The types of fibers include the following:

- Steel (both low carbon or stainless)
- Mineral (glass or asbestos)
- Synthetic organic (carbon, cellulose, or polymeric)
- Natural organic (fiber from plants or animals).

SFs are the most commonly used type of fiber for both structural and non-structural applications [65]. Table 2.1 displays the different types of fibers, categories of each type and their various properties.

Table 2.1 Different fiber types [66]

Type of fiber		Specific Gravity	Tensile Strength (MPa)	Elastic Modulus (GPa)
Steel		7.80	1000 – 3000	200
Glass		2.60	2000 - 4000	80
Synthetic	Acrylic	1.16 -1.18	296 -1000	14 - 19
	Carbon I	1.90	1724	380
	Carbon II	1.90	2620	230
	Aramid I	1.44	2930	62
	Aramid II	1.44	2344	117

2.5.1 Steel Fibers (SF)

The concept of using SFs to enhance the characteristics of building materials is very old [18], [67]. The SF reinforced concrete, the presence of randomly oriented SFs hinders micro-cracks mechanisms thereby limiting the crack propagation. This functions to improve the general strength and ductility of the concrete. SFs are typically used to control crack initiation and propagation, decrease brittleness and increase elastic modulus. The addition of fibers into concrete renders it more isotropic, homogeneous and at the same time transforms if from a brittle material to more ductile one [68].

Initially, the fiber was used as secondary reinforcement materials or for crack control functions in less critical sections of the structural elements [69]. But today, its use is widely applied as the main reinforcement in precast elements, industrial floor slabs, and shotcrete. Note that the extra tensile resistance is provided by the present fibers bridging any crack and this resistance depends mainly on the number of fibers implanted over the crack plane. For this, it is important to have a sufficient amount of fibers in the design mix. Another equally important aspect is the tensile strength of the fibers so as to avoid any case of rupturing. Note that ruptured fibers lead to a rapid loss in the load carrying capacity of the resultant concrete structure [70]. Fibers can be produced in different sizes and shapes see Figure 2.8. These variances influence the bonding characteristics between the concrete matrix and the fiber.

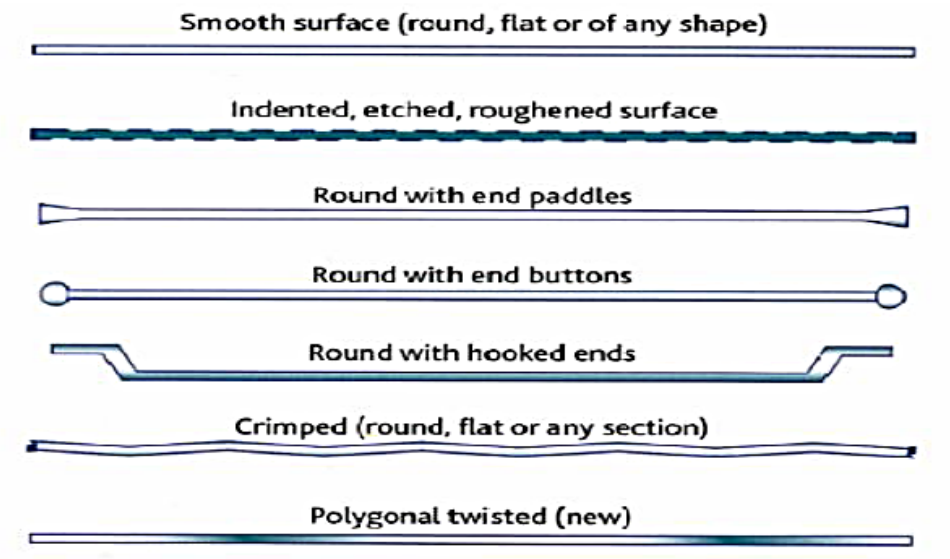

Figure 2.8 Types of steel fibers SF

Bernal et al. [71] conducted a study that involved the addition of SFs into alkali-activated concrete slag. The results depicted a lower compressive strength in GPC as compared to OPC concrete with SFs. The flexural toughness was considerably increased when higher volumes of the SFs were added. In general, the mechanical properties such as the durability performance of concrete was greatly improved. Conclusively, the reinforced GPC and the OPC reinforced concrete showed comparative results as far as their mechanical properties were involved.

Investigations by Ganesan et al. [19] reveal that the overall compressive strength of GPC considerably improves with the addition of the SFs at certain volume proportions. While investigating the mechanical properties of the SF reinforced GPC they discovered that the compressive strength increased from 3.22 % to 8.51 % with 0.25 % to 1.0 % increase in the volume fraction of fibers. They also noted that the modulus of rupture, the splitting tensile strength, Poisson's ratio and the modulus of elasticity of GPC increases greatly with the increase in fiber volume fraction. From their studies, the following were deduced when the fiber volume fractions were increased from 0.25 % to 1 %:

- The Modulus of Rupture increased from 9.4 % to 24 %
- Poisson’s Ratio increase from 14 % to 50 %
- The Modulus of Elasticity increased from 13.7 % to 65 %
- The splitting tensile strength increased from 23.3 % to 61.6 %

A study by Mo et al. [72] investigated the shear behavior and mechanical properties of both the SF-reinforced cement and geopolymer oil palm shell lightweight aggregate concrete. In their studies, fibers of steel were added to cement-based lightweight aggregate concrete and geopolymer lightweight aggregate concrete at various proportions. The test results revealed that the addition of SFs greatly improves the mechanical performance of concrete, particularly in the case of splitting tensile strength. It was also noted that the flexural toughness was enhanced with the addition of the SFs and this was more pronounced in the case of cement-based lightweight aggregate concrete than in the conventional GPC. Additionally, the shear resistance of lightweight aggregate concrete elements improved further with the addition of SFs and the conventional prediction models for the shear capacity of SF reinforced concrete was observed to be conservative for both the geopolymer lightweight aggregate concrete and the SF reinforced cement-based concrete.

2.6 Hollow Core Slab (HCS)

HCS panels, also known as void slabs, are super materials in engineering due to low seismic zones, relatively small weight and cheap price. Considerably noticeable is the opening that is created through the panel, which reduces its total weight. Also, these openings can be used for passing mechanical, thermal and electrical equipment through it- mainly in large constructions like high-rise buildings, bridges, offshore structures and malls.

2.6.1 Historical Background

The concepts of voided slab technology were credited to Purdue University in the early 1990s [73]. The university analyzed 279 mm deep voided slabs spanning 2.7 m and 6.1 m. During the studies, the following were conducted:

- 50 mm toppings of lumber wearing surface and LWAC were added above the ribs of the flange.
- The slabs were then loaded with iron weights after one month of placement.

In the 6.1 m slab, results showed that the reinforcing steel started yielding at a live load of 25 kPa. At mid-span, the tension failure occurred at an ultimate load of 34 kPa and with a deflection of about 75 mm. On the other hand, the reinforcing steel in the 2.7 mm slab began to yield at a live load of 32 kPa and the slab eventually failed at an ultimate load of 42 kPa.

Application of the voided slab in the construction of a housing project in Chicago, IL by the United States Housing Authority was discussed through a case study published in the year 1941. The project comprises of 125 building structures that range from two to four stories. In order to optimize costs, the structural engineers considered five different floor slab systems including, one-way ribbed slab made from removable pans, a solid slab and three different options of ribbed slab made using hollow clay blocks of varying dimensions. The major cost and design factor was the requirement by the local authorities that all the ceilings of the buildings must be plastered to laid down specifications and standards. As much as the architect proposed for the use of solid slabs, the structural engineers desired for a better base for the plaster. From the investigations, clay tile systems permitted plaster to be smeared directly to the tiles but the ribbed slab made using removable pans required the use of metal lath before plastering. The tile and joist slab system was considered as the winning option the

preceding systems were associated with additional costs such as the labor costs for removal of the forms and the actual cost of lath. Precast concrete HCSs are innovative voided slab technique commonly applied in floor systems of high rise steel frame and precast buildings [74]. The slab depths typically range between 150 mm to 600 mm, but the slabs with deeper depths are more preferred since they are cost-effective for larger spans. The elimination of formwork during the construction process results in fast construction and further reduces construction costs.

A case study describing the use of Tube HCSs THCS systems in an industrial complex in Irvine, CA as published in the year 1983 is also worth reviewing. The functional requirements of the large complex demanded clear slab spans of above 12m in addition to live loads of more than 6 kPa. It was established that the THCS system provided the finest combination in terms of materials, the type of structural system and spans. When compared to conventional systems used in low rise structures, this slab system proved to be more cost-effective in the construction of the large bay sizes of 14.3 m by 14.3 m clear spans. Economics aside, the major concern of this system was punching shear around columns and the issue of buoyancy when the concrete is being placed. To overcome the issue of buoyancy the designer recommended that the voids be anchored in place until the concrete sets. This was made possible by use of metal ties over the voided tubes and then anchorage of the ties to the plywood decking. On the other hand, to minimize punching shear and allow for adequate shear transfer from the floor slabs to columns, the conventional solid slab was required. This was achieved by eliminating the voided tubes around the column sections and in sections with high punching shears.

A new system consistent with HCS concept is the Voided Biaxial Slab (VBS) that allows for the economical construction of flat floor slabs with clears of over 15m. The VBS operates under the same principle as HCS by eliminating the non-working concrete in the middle of the slab and replacing it with a lighter material. In this state-of-the-art system, the voids are made with spheres made from recycled plastic and are locked into position by the top and bottom reinforcement meshes. The elimination of ineffective concrete by the plastic voids allows for up to 40 % reduction in columns, foundation and wall elements due to the reduced dead loads on the structure. Similar to HCS, the sequence of placing concrete is equally important in ensuring that the buoyancy effects do not lift the reinforcing bars and plastic spheres out of position. As a standard, adequate concrete is first placed to cover the bottom reinforcement mesh and some portions of the void modules See Figure 2.9. The concrete is then allowed

to attain the initial set before concrete is again poured in the second placement to finish the slab. The diagonal girders between the lower and upper steel lattice and the concrete between the voids provide the composite action between the two placements as highlighted before [75].

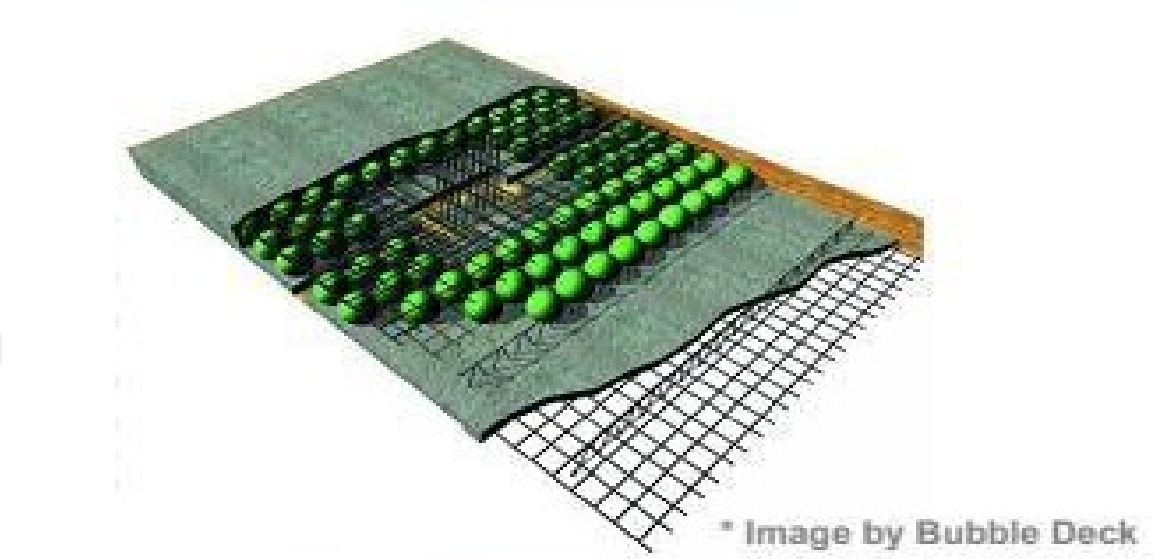

Figure 2.9 Biaxial voided slab

The innovative HCS system can be combined with the post-tensioning slab modules to produce precast members which can then be delivered to the construction site for use. This system has found widespread applications especially in office complexes, hospitals, universities, entertainment centers, museums, and high rise residential buildings.

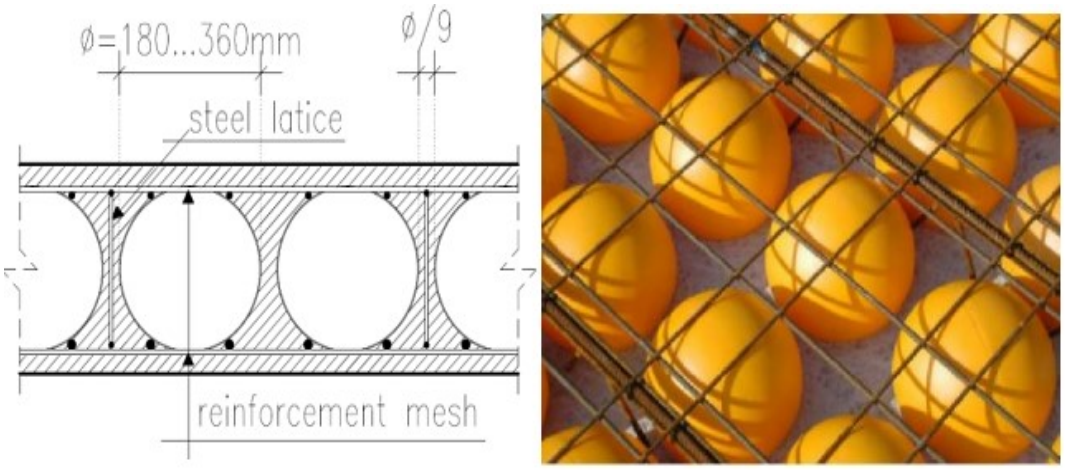

Figure 2.10 Details for the spherical hollow cores flat slab system

2.6.2 Structural Hollow Core Slabs

In 1985, Becker and Buettner [76] studied the applicability of using the existing ACI Codes and standards for shear calculations in extruded HCS. The experimental outcomes revealed that the obtained shear capacity was close to the projected shear obtained through the use of the ACI equation. Even with no shear reinforcement bars in the slab, acceptable ultimate structural behavior and service load were observed. It is therefore conclusive to say that the minimum ACI Code and Specifications for shear reinforcement is also valid for pre-stressed HCS. During the studies, the worst case scenario was encountered when the strands had 0.76 m plus the effective length beyond bearing capacity. However, the experimental results do not indicate the bond failures even with the use of theoretical ultimate flexural capacity models.

In 1992, Aswad and Jacques [77], analyzed the experimental results of tests conducted on 203 mm thick hollow slabs. In their experiment, point loads were applied at the near ends of the slabs to yield regional shear failures. Based on their findings, it was found out that the permissible edge service loads ranged between 15.6 kN to 16.9 kN for the given pre-stress forces, concrete strength and floor system. From the actual measurements, it was found that increments in area and flange properties above the minimal values were common especially in the production stage. It was investigated that the increase in the web thickness and the local flange near the end of the slabs significantly contribute to the increase in the shear capacity much that punching shear failure is triggered. The shear failures are characterized by the diagonal crack that appeared at the vertical edge of the slab and was continuous in a spiral shape along the bottom and top of the slab. Strand slippages were also observed at end of some slabs but were very minor.

In 1998, Pajari [78] suggested a more straight forward estimation technique that investigates the shear capacity of the pre-stress HCS elements. The comparison principles were based on the axial, shear and transverse shear stresses. The shear and axial stresses were calculated for the slabs braced on nonflexible bearings. On the other hand, the transverse shear stress was calculated based on the beam theory on the composite element that comprised of the beam, a slab section, joint concrete, and the elective topping. The slab width was an experimental constraint that considered the level of interaction between the beam and the slab. The width of the slab was supposed to be commensurate to the beam span. Equally, the investigators demonstrated the

modifications required for a continuous beam, HCS with ends filled with concrete and floor wrapped with concrete topping.

In 2009 Elgabbas et al. [79] presented an experimental investigation on the structural behavior of precast hollow core reinforced concrete slabs strengthened by CFRP laminates in flexure. Near-surface mounted and externally bonded laminates were used in the investigations. The transverse anchorage and the CFRP area were also examined in their experiments. From the results, it was concluded that the NSM method resulted in peak strengthening efficiency. The increased bond strength was also attributed to the full initiation of the NSM laminates at failure. However, it was noted that the NSM flexural reinforcing level should be cautiously designed so that unfavorable shear tension failure modes can be eliminated. Note that moderate efficiency levels in the externally bonded method were linked to the premature de-bonding. However, the strengthening efficiency can be optimized by the use of transverse CFRP laminates as anchors which resulted in re-direction of the de-bonding further from the laminates end which in turn delayed failure. For this, a rational investigative study was carried out. The comparison between the analytical and the experimental results yielded satisfactory agreements.

In 2013, Cuenca et al. [80] established that the HCS are mostly pre-casted by extrusion and it is thus difficult to place stirrups. In this sense, it is difficult to assure the shear resistance in some cases. Thus, a cautiously designed system that uses Fiber Reinforced Concrete (FRC) to produce HCSs by extrusion was investigated to analyze the gain in shear reinforcement. For this, an experimental program was developed that entailed 26 HCSs. The elements were formed and tested in shear according to the variables below:

- The shear span-depth ratio of between 2.3-4.4 and 8.6, and
- Amount of SFs (0.50 kg/m^3 and 70 kg/m^3)

Different failure modes occurred and conclusively determined that the introduction of the SFs greatly improved the material quality against shear. The fiber reinforced HCS achieved greater loads capacity than normal HCS and achieved improved ductility.

In 2016, Abed [81], conducted an experimental and numerical investigation that evaluated the performance of RC slabs having longitudinal hollow cores at different volumes and loading conditions. The study comprised of eight moderately thick reinforced concrete slabs that were 2.05 m in length, 0.6 m in width and 0.25 m in thickness. The experimental results deduced that the ultimate load capacity reduced by

approximately 21 % and 33 % for solid slabs with the increasing area to depth proportion from 2 to 3 respectively. It was noticed that the ultimate load capacity of circular hollow cores also reduced by about 5.49 %, 15.7 % and 20.6 % with circular diameters 75, 100 and 150 respectively. Similarly, when the area depth ratios were increased from 2 to 3.5 and 3 respectively, the ultimate load strength of the HCSs reduced by 31 % and 45 % respectively. Statistically, the FE method using ANSYS computer software was utilized to evaluate the behavior of these RC slabs.

In 2016, Ibrahim et al [82] carried out an experimental study to investigate the shear flexure capacity of composite slabs using concrete toppings and HCU. Full-scale 3-point load tests were conducted on 14 composite slab samples using different surface roughness and condition of the HCU before placement of the concrete topping. The surface roughness was measured as smooth or rough whereas the moisture condition considered either as the pond, dry or optimum wet. The overall effect of the longitudinal joint between the HCU sections was also considered. The obtained experimental results were then compared with the predicted values using the approximate models available in Euro Code 2 in addition to other equations published by earlier researchers. The experimental results evidently demonstrate that HCU longitudinal joint and surface condition significantly affect the shear flexure strength and stiffness of the slabs. It was noted that the optimum HCU surface condition that produces the highest shear strength and stiffness is wet and rough conditions. Also noted was that the longitudinal joint between the HCU panels decreases the shear strength of the slab. Interestingly, the interfacial horizontal shear was found not to be the factor that governs the behavior or strength of the slab. The empirical equations derived from Euro code 2 provides the non-conservative estimate of the shear strength of the slab. Contrary to this, the equations published by the earlier researcher offers a more conservative prediction of the shear strength of the slab.

In 2017, Prakashan et al [83] conducted an experimental investigation on four different HCS together with the solid slab as the control specimen. The load-deflection curves were analyzed in addition to the load and failure deflection at the first crack. The effectiveness of the traditional flexural capacity equation in calculating the capacity of HCS was also evaluated. Experimental results from the study were used to analyze the comparative study among the samples studied. The study comprehensively concluded that the traditional flexural strength equations can be utilized in HCSs. Conclusively,

it was found out that the HCS has improved performance than solid slabs both in terms of serviceability and load-deflection behavior.

In 2017, Wariyatno et al [84] tested samples comprising of a solid slab ad the control specimen, HCS Type 1 with cavities made from PVC pipes and HCS Type 2 with cavities made from Styroform. The thickness of the slab in this experiment was considered to be 12 cm. The experimental results demonstrated that HCS Type 1 and Type 2 can decrease the weight of the slab by 24 % and 25 % respectively as rightly compared to the solid slab system. Additionally, it was investigated that the flexural strength of HCS Type 2 is relatively higher than that of HCS Type 1 but expectedly lower than that of the solid slab. In simple terms, the flexural stiffness of the solid slab was significantly greater than both the HCS Type 1 and Type 2. The cracks that appeared in the solid slab are regarded as flexural cracks with the cracks occurring in HCS Type 1 and Type 2 distinguished as shear cracks.

A study conducted by Helén and Karin (2002) [85] presented an analytical study of the FEM analysis using the DIANA program. The study proved the ability of such concrete slabs to provide better resistance to shear and torsion. Also, an experiment was conducted to measure the failure modes, ultimate load, cracking load and the deflection of two types of concrete slabs under a load [86]. The types of concrete slabs used were HCSs and solid slabs (used for reference). It was even found out that flexural equations could be used to predict the ultimate load of HCSs. In addition, another experiment was conducted by Cuenca and Serna [80], on HCSs with and without reinforcement. The study was aimed at determining the shear capacity of a sample of high strength concrete slabs with and without SF reinforcement. It was discovered that slabs containing SF reinforcement performed better under shear load than those without reinforcement.

CHAPTER 3

EXPERIMENTAL PROGRAM AND METHODOLOGY

3.1 Introduction

The properties of SCGCs using FA and GGBFS were investigated through an experimental model, which was made up of two components. First of all, SCGC was manufactured with the replacement of FA with various levels of GGSFS. The first stage was alternating the FA with a new percentage of GGSFS, while the second stage was manufacturing a hollow unit slab using SCGCs. The slump flow, T_{500} flow time, V-funnel flow time and L-box height ratio tests were carried out to recognize the describable properties and features of the fresh SCGCs. The hardened concrete was tested for compressive strength, splitting tensile and fracture toughness at 28 days for the assessment of its mechanical properties. HCS was pour with the best mixture composition obtained for SCGCs, and a testing program recognized, four-point bending test outcomes, strength, failure mode and crack width, were assessed.

3.2 Materials

3.2.1 Cement

Ordinary Portland Cement (OPC CEM, I 42.5R) was used adhering to the TS EN 197-1 [87], which is composed mainly of the European EN 197-1. It had a specific gravity, and a Blaine fineness of 3.15 and 326 m^2/ kg respectively. Below are its various chemical and physical properties are given in Table 3.1 The chemical and physical properties of the binder components.

3.2.2 Fly Ash (FA)

The FA used in the production of SCGCs was classified according to ASTM C 618 [88] to class F group, which was obtained from Ceyhan Sugözü thermal 46 Power Plant as shown in Figure 3.1. It possessed a Blaine fineness, and specific gravity of 2.29 and 387 m^2/kg respectively. The FA physical and chemical properties are shown in Table 3.1.

3.2.3 Slag (GGBFS)

Ground Granulated Blast Furnace Slag (GGBFS) was manufactured by quenching molten iron slag obtained from a blast-furnace, by immersing in water or steam which results in a glassy, granular, end-product that is subjected to a drying process and then broken down to a fine powder using a grinding process as shown in Figure 3.1. It was obtained from ADANA cement manufactured by (T.A.S) ISKENDERUN, TURKEY. Two types of slag were mainly used for this, and Table 3.1 describes the chemical and the physical properties of these types of slag.

Table 3.1 The chemical and physical properties of the binder components

Analysis report (%)	Portland cement	FA	Slag (1)	Slag (2)
CaO	63.60	1.60	34.19	38.26
SiO_2	20.25	62.40	40.42	38.02
Al_2O_3	5.31	21.14	10.60	11.33
Fe_2O_3	4.04	7.85	1.28	0.75
MgO	2.82	1.76	7.63	7.22
SO3	2.73	0.10	0.63	0.58
K_2O	0.92	0.73	2.83	----
Na_2O	0.22	2.45	0.17	----
Loss on ignition	3.02	2.07	2.74	2.29
Specific gravity	3.15	2.29	2.80	2.88
Blaine fineness (m^2/kg)	326	387	575	504

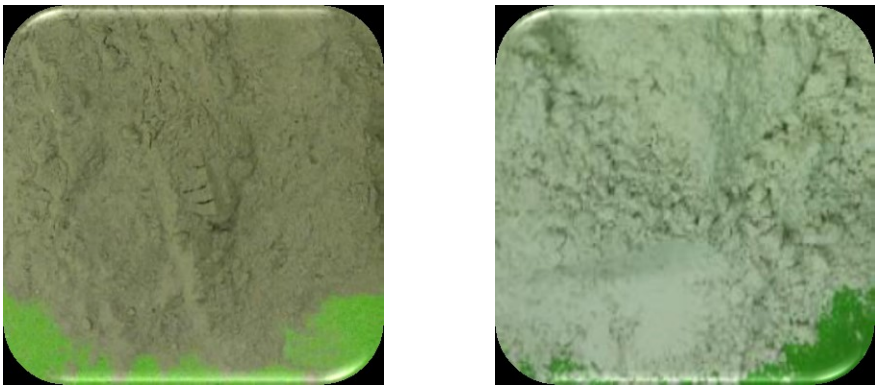

a) FA b) Slag

Figure 3.1 Binder component of SCGCs

3.2.4 Alkaline Liquid

Typically, sodium silicate (Na_2SiO_3) and sodium hydroxide (NaOH) solutions were used as the alkaline solution. The sodium silicate solution (Na_2O= 13.7 %, SiO_2=29.4 % and water=55.9 % by mass) was purchased locally. Sodium hydroxide (NaOH), in the form of chips or pellets with a 97 to 98 % purity value, was procured from a local vendor. The concentration of the NaOH solution was prepared in a range from 8 M to 12 M, as seen in Table 3.2. The mass of NaOH solids found in the solution, varied depending on the concentration of the solution. The preparation of the alkaline solution was done 24 hours before its usage.

Table 3.2 Concentration of alkaline solutions

NaOH	% of solids	Solids (grams)	% of water
8M	26.23	262	73.77
10M	31.37	314	68.63
12M	36.09	361	63.91
14M	40.43	404	59.57

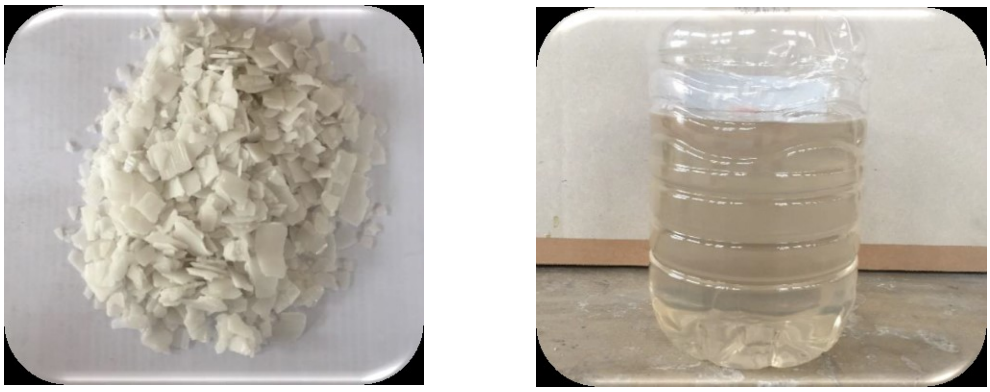

a) Sodium hydroxide b) Sodium silicate

Figure 3.2 Alkaline component solutions

3.2.5 Steel Fiber (SF)

SF are a form of concrete reinforcing material, which used in combination with concrete, give additional benefits when compared to conventional forms of reinforcement. Two types of SF were used for this purpose, macro and micro SFs. Macro possessed hooked ends (SF1) and Micro was straight (SF2) as shown in Figure 3.3. SF1 had a tensile strength and a specific gravity of 1100 MPa and 7.85, while the SF2 had 2000 MPa and 7.17. SF1 had a length and aspect ratio of 30 mm and 55, while these were 6 mm and 37.5 in SF2. SF2 was produced using high strength steel, with a brass coating which gave the fibers a uniformly smooth surface. In the case of the mixtures, (0.5, 1 and 1.5 %) by volume were adopted for each of the SF types, with the concrete mixture.

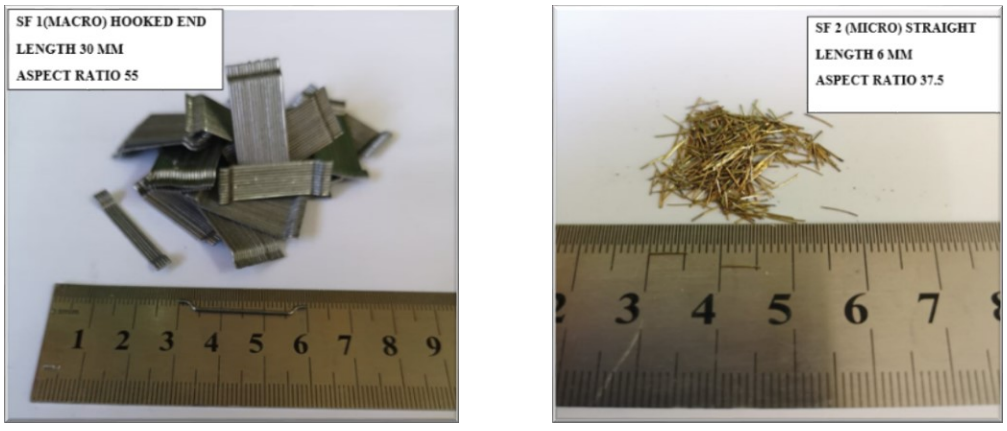

a) Macro steel b) Micro steel

Figure 3.3 Types of SF

3.2.6 Super-Plasticizer

Polycarboxylic-ether type super-plasticizer (SP) was used. The main function of the SP was to improve the plasticity of the concrete, to make it workable enough so that it could compact itself without external compaction or vibration. The SP was purchased locally. It possessed a pH of 5.7 and a specific gravity of 1.07. The physical properties and description of the super-plasticizer are shown in Table 3.3.

Table 3.3 The properties of super-plasticizer.

Properties	superplasticizer
Name	Glenium51
Specific gravity	1.07
Stat	Liquid
Color tone	Dark brown
Description	Modified polycarboxylic type of polymer

3.2.7 Aggregate

The coarse aggregate used for this project was obtained after crushing gravel to reach an average maximum size in the range of 12 mm. For the fine aggregate, limestone was crushed to obtain aggregates with a maximum size of 4 mm. The specific gravity of the coarse aggregate was 2.72, and the water absorption was 0.45 %. The limestone had a specific gravity of 2.45 and water absorption of 0.92 %. The gradients of the particle sizes obtained, following a thorough sieve analysis, as well as the physical properties of the fine and coarse aggregates [89], are given in Table 3.4, while the fine and coarse aggregates linked to the control mixture are seen in Figure 3.4

Table 3.4 Sieve analysis and physical properties of the fine and coarse aggregates

Sieve Size (mm)	16	8	4	2	1	0.5	0.25	Fineness Modules	Specific Gravity	Abs. %
Fine Aggregate	100	100	95.4	63.3	39.1	28.4	16.4	2.57	2.45	0.92
Coarse Aggregate	100	31.5	1	0.5	0.5	0.5	0.4	5.66	2.72	0.45

a) Coarse aggregate b) Fine aggregate

Figure 3.4 Types of aggregate

3.3 Concrete Mixture Details

In the first stage of this study, five SCGCs mixtures were formulated to encompass a wide range of various mixture combinations with a constant liquid/binder ratio (0.5) and a total binder content of 500kg/m^3. GGBFS was used to replace the FA at percentage levels of 25 %, 50 %, 75 % and 100 % by mass, as shown in Table **3.5**. During the second stage, the casting of 21 panels of HCS was done considering the results that were derived from the initial stage with 50 % percentage replacement of GGBFS, by making use of the best SCGCs mixed with SF as shown in Table 3.6

.

Table 3.5 Concrete mixture proportions in (kg/m^3)

Mix ID.	Binder	FA	GGBFS	Fine agg.	Coarse agg.	Mol.	SP	Water
	kg/m³	%	%	kg/m³	kg/m³		%	%
F100S0	500	100	0	830.65	723.55	12	5	9
F75S25		75	25	846.39	737.26			
F50S50		50	50	862.13	750.97			
F25S75		25	75	877.87	764.68			
F0S100		0	100	893.61	778.40			

Table 3.6 HCS mixture proportion in (kg/m^3)

Mix ID.	Macro steel (Ma)	Micro Steel (Mi)
	%	%
SO-Ma-0	0	0
RH-Ma-0		
CH-Ma-0		
SO-Ma-05	0.5	0
RH-Ma-05		
CH-Ma-05		
SO-Ma-10	1	0
RH-Ma-10		
CH-Ma-10		
SO-Ma-15	1.5	0
RH-Ma-15		
CH-Ma-15		
SO-Mi-05	0	0.5
RH-Mi-05		
CH-Mi-05		
SO-Mi-10	0	1
RH-Mi-10		
CH-Mi-10		
SO-Mi-15	0	1.5
RH-Mi-15		
CH-Mi-15		

3.4 Concrete Casting, Testing, and Curing.

In the manufacturing of SCGCs, the order of mixing and the time taken play an important role. This is important as it determines the homogeneity and uniformity found in every mixture. The mixing was done in two stages. In the beginning, sand, coarse aggregate with a wet surface, dry condition, and binder, were combined in the concrete mixer for a time period of 2.5 minutes as shown in Figure 3.5. Once this was done, a well-stocked, premixed alkaline solution that had been stored in plastic or glass containers for 24 hours at room temperature, SP and extra water were added into the concrete mixer, and the process of wet mixing took place for an additional 3 minutes, as shown in Figure 3.6. In order to ensure a uniform mixture, the fresh concrete was subjected to the mixing process for an additional duration of 2 to 3 minutes. To evaluate the nature of the SCGC, once the mixing procedure completed, the tests (slump flow time and diameter, V-funnel flow time, L-Box height ratio) were carried out to assess the fresh properties of the SCGCs according to EFNARC [90].

Figure 3.5 Dry material (binder, fine and coarse aggregate)

Figure 3.6 Wet mix (dry material, alkaline solution, sp, and water)

First step the pre-oiled molds were filled with fresh concrete in three layers and covered with plastic sheets to minimize the carbonation effect and prevent water evaporation. After 24 hours of casting, the samples were then cured for 48 hours in the oven, at a temperature of 70-80^{o}C as seen in Figure 3.7 & Figure 3.8, after which the samples were removed from the molds and kept outside at room temperature until the aging for the testing was achieved. Each of the specimens was poured without subjecting them to any form of compaction or vibration. Specimens poured in a standard mold as following formats:

- Three 100 mm cubes for the compressive strength test.
- Three 100x200 mm cylinders for the splitting tensile test.
- Two 100x100x500 mm prisms for the fracture toughness test.

Figure 3.7 Filling the molds with fresh concrete

Figure 3.8 Curing samples by heating

Second step Twenty-one 1000x350x125 mm HCS were divided into seven groups with three panels as shown in Table 3.6 (solid and hollow core) in each group were also used:

- Rectangular hollow cores were formed using electric tri-cables, each with a wall thickness of 2 mm. Only one size of tri-cables, with dimensions of 60x80mm, was used in the formation of the hollow core, SF reinforced, SCGCs of equal area as shown in the Figure 3.9.

- Circular hollow cores were formed utilizing Polyviny1 Chloride (PVC) pipes with an equal wall thickness of 2 mm. Only one size of PVC pipes, with a diameter of 75mm, was used in the formation of the hollow core, SF reinforced, SCGCs of equal area as shown in the Figure 3.9.

The same procedure was used for the casting and curing (as in step 1).

a) Pre-Oiled Frame Panel

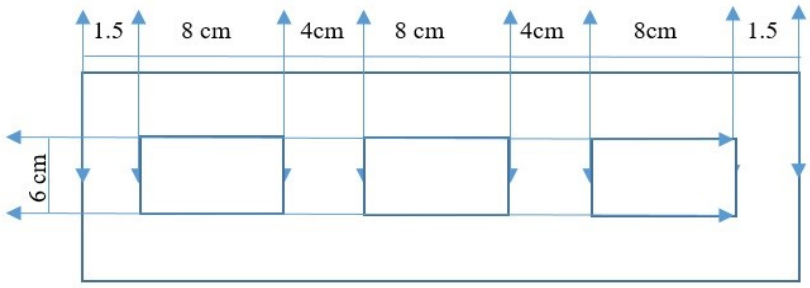

b) RH Schematic details

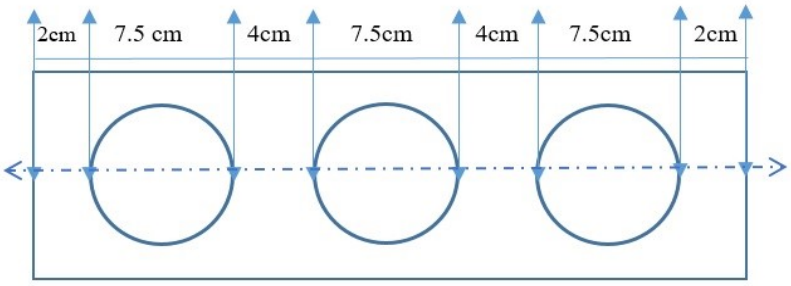

C) CH Schematic details

Figure 3.9 Slab panel details: a) Pre-oiled frame panel b) RH schematic details c) CH schematic details

3.5 Tests for Fresh Properties

The slump flow, T_{500mm} flow time, V-funnel flow time and L-box height ratio tests were carried out to assess the necessary properties, and the features of the new SCGCs mixtures based on the recommendations according to EFNARC [90].

3.5.1 Slump Flow Test

To evaluate the slump flow, an ordinary slump flow cone was filled with SCGC without using any form of compaction. Then the cone was elevated, and the average diameter of the concrete spread was noted down, as seen in Figure 3.10. There was a decreased slump flow in every mixture. The time (T_{500mm}) was noted, which effects the time required for the concrete to fill the 500 mm spread circle. A lesser time reflects an increased rate of flow. EFNARC suggests a T_{500mm} of 2 to 5 sec for SCCs.

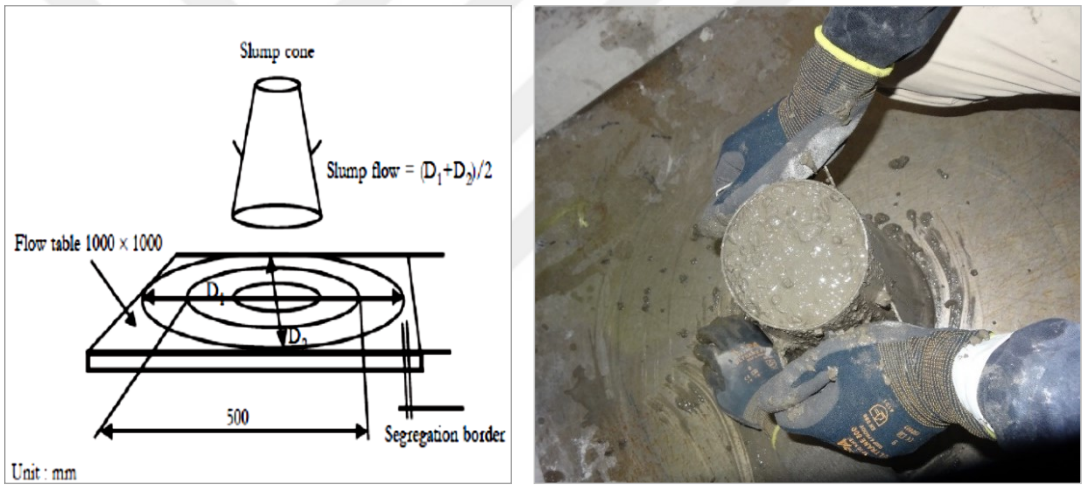

a) Schematic details b) Test application

Figure 3.10 Slump flow test

3.5.2 V-Funnel Flow Test

To assess the filling capacity and the viscosity of the SCGCs, the V-Funnel test was shown as presented in Figure 3.11. The fill time was observed using a process where the funnel was filled with fresh concrete, after which the time was taken for the flow from the orifice opening to the complete emptying of the funnel. The best fill-able and stable concrete took a short time to flow out. According to EFNARC, t (V-f) ranging from 6 to 12 sec is considered adequate for SCCs.

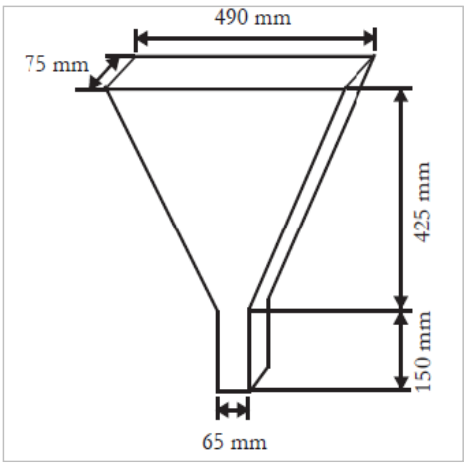

`a) Schematic details b) Test application

Figure 3.11 The V-funnel flow test.

3.5.3 L-Box Test

The L-box unit was made of a rectangular-section box in the form of an 'L' shape, with a vertical and horizontal section, which were then segregated using a mobile gate. In the anterior aspect, the vertical portions of reinforcement used three or four bars as shown in Figure 3.12. The vertical section was loaded with concrete, and the gate was raised to allow the concrete flow into the other section. Following the stoppage of the flow, the concrete level seen at the end of the horizontal section was noted to be a ratio of that remaining within the vertical section. This highlights the passing ability of SCGCs and any concerns about the inadequacy of stability (segregation) can be appreciated visually. Segregation was also noted by assessing, sawing and analyzing the horizontal sections of the concrete. The acceptable value according to the EFNARC ranges from 0.8 to 1.0. If the passage of concrete is similar to the flow of water, when at rest, it will remain at a horizontal, so H_2/H_1 reaches (1).

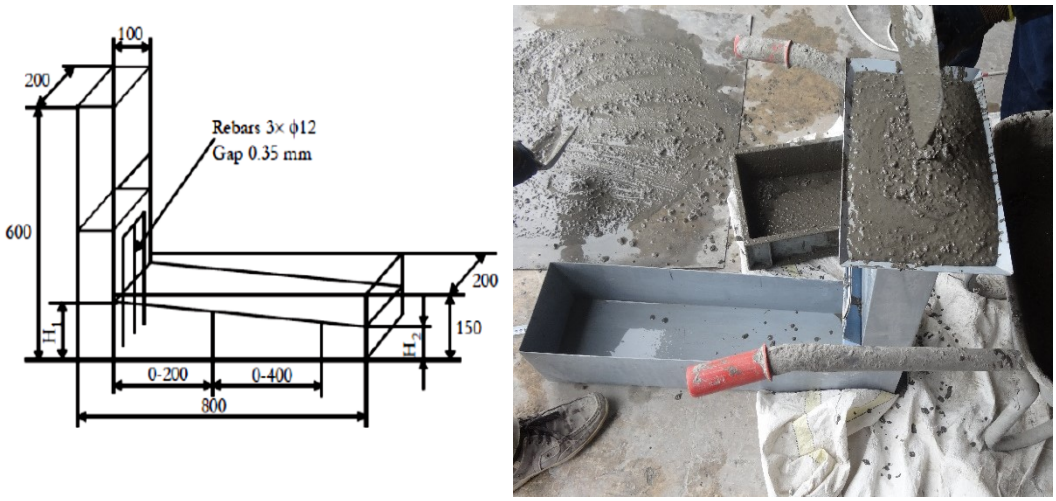

a) Schematic details

b) Test application

Figure 3.12 L-box test

3.6 Tests for Mechanical Properties

3.6.1 Compressive Strength

According to ASTM C39 [91], the compressive strength of the concrete was assessed by using cube samples of 100x100x100 mm for 28 days' age as seen in Figure 3.13. The compressive strength was calculated by taking the average of the results derived from the three tested cubes samples. A 2500 kN capacity testing machine was used for this purpose.

Figure 3.13 Photograph of the compressive test

3.6.2 Splitting Tensile Strength

The splitting tensile test was performed on cylinder specimens of 100x200 mm according to ASTM C496 [92], as seen in Figure 3.14. The test was done on three samples for each mix for 28 days. The cylindrical concrete specimens' splitting tensile strength (f_{st}) was assessed using the Equation (3.1).

$$f_{st} = {}^{2P}/_{\pi h \varphi} \quad \textbf{(3.1)}$$

For the above equation P, h, and φ are the maximum load, length and cylinder specimen diameter respectively.

Figure 3.14 Photograph of the tensile test

3.6.3 Fracture Energy

A closed-loop 250 kN testing machine was used as mentioned in the guidelines of RILEM 50-FMC/198 Committee [93] to evaluate the fracture toughness (G_f) of the beam specimens. A linear variable displacement transducer (LVDT) was applied to assess the mid-span displacement of the beam specimens. The description of the machine used, specimens and the placement of the LVDT are described in Figure 3.15. The ratio of the notch to height (a/w) for prismatic specimens was 0.4. In order to reduce the effective cross-section to 60×100 mm^2, a notch was opened in the prismatic

test specimens by cutting. Also, the distance between the supports was 400 mm. All prismatic beams were tested using displacement control with a rate of loading of 0.02 mm/minute. The fracture energy of the prismatic specimens was achieved under three-point loading according to RILEM [93] as shown below:

$$G_f = \frac{(w_0 + mg\delta_s)}{A_{lig}} \quad \textbf{(3.2)}$$

Where w_0 is the area under the load-displacement curve (N-m), m is the mass of the beam (Kg); g is the gravity acceleration (9.81 m/s^2), δ_s is the specific displacement (m), and A_{lig} is the area of the ligament (m^2). The details of the specimens and test set up are indicated in Figure 3.16. The net flexural strength was obtained according to the following equation [94]

$$f_{flex} = \frac{3P_{\max} S}{2B(W-a)^2} \quad \textbf{(3.3)}$$

Where, P, B, W, and a are the peak load (N), span length (mm), the width of the beam (mm), depth of beam (mm), and depth of the notch (mm) respectively.

The critical stress intensity factor (f_{flex}) was used to specify the magnitude of stress concentration in cracks. The (K_{IC})values were obtained according to the equation (3.4) [95].

$$K_{IC} = \frac{3P_{\max} l}{2bd^2}\sqrt{a_0}\left(1.93 - 3.07A + 14.53A^2 - 25.11A^3 + 25A^4\right) \quad \textbf{(3.4)}$$

Where $P_{\max}$, l, b, d, and a_0 are the peak load, the span of the prism, the width of the prism, the depth of prism, and the depth of the notch respectively, since (A = a$_\circ$/d).

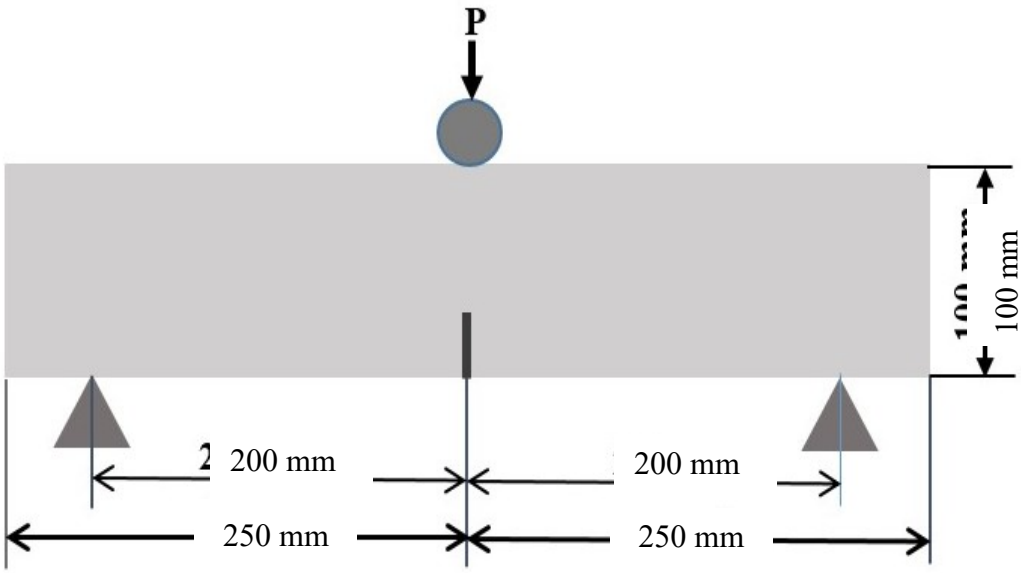

a) Schematic details

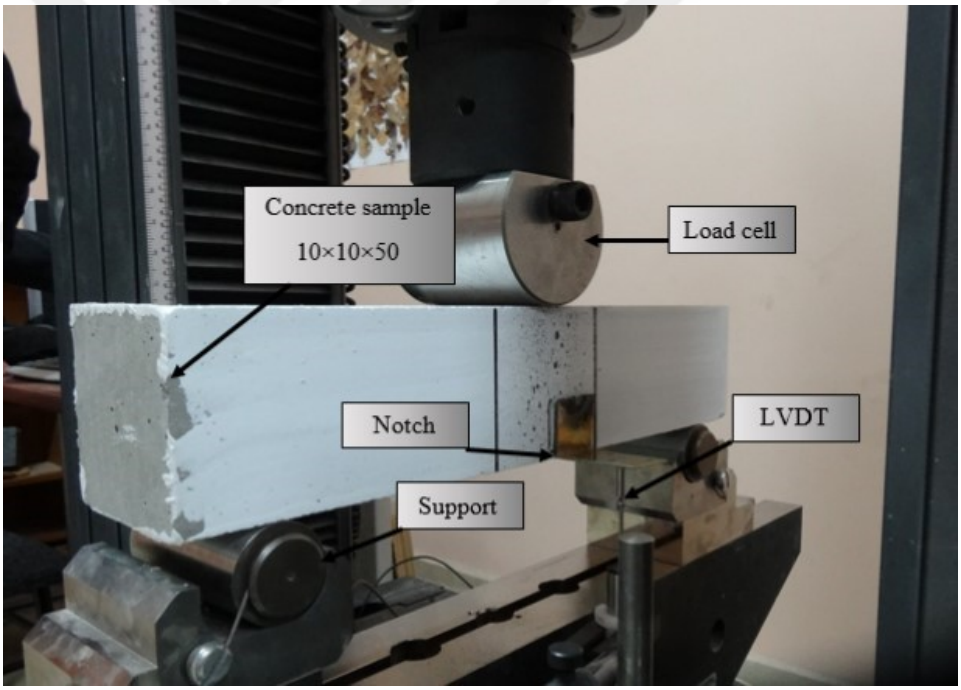

b) Three-point test application

Figure 3.15 Specimen geometry and test setup for three-point bending load

3.6.4 Flexural Panel Test

Panel specimens were tested under a static four-point load to study the flexural behavior and show the difference between the hollow and control solid panels. A universal testing machine (INSTRON) with a capacity of 250 kN was used. The experiments were executed in displacement control as shown in figure 3.16. The rate

of the load was increased slowly at about 0.05 kN/min to record the growth of cracks, strains and the deflections of the panel. The crack was remarked and drawn on the front face of the slabs during, and after, the test. The deflections were obtained by using a high precision LVDT that was placed on the bottom near the mid-span of the panel. All specimens were placed on the testing machine by aligning the marked support and the loading positions. The first crack and the development of cracks during the increase of load were recorded. After the initial cracking, the loading continued and was stopped when the panel was just at the stage of collapsing.

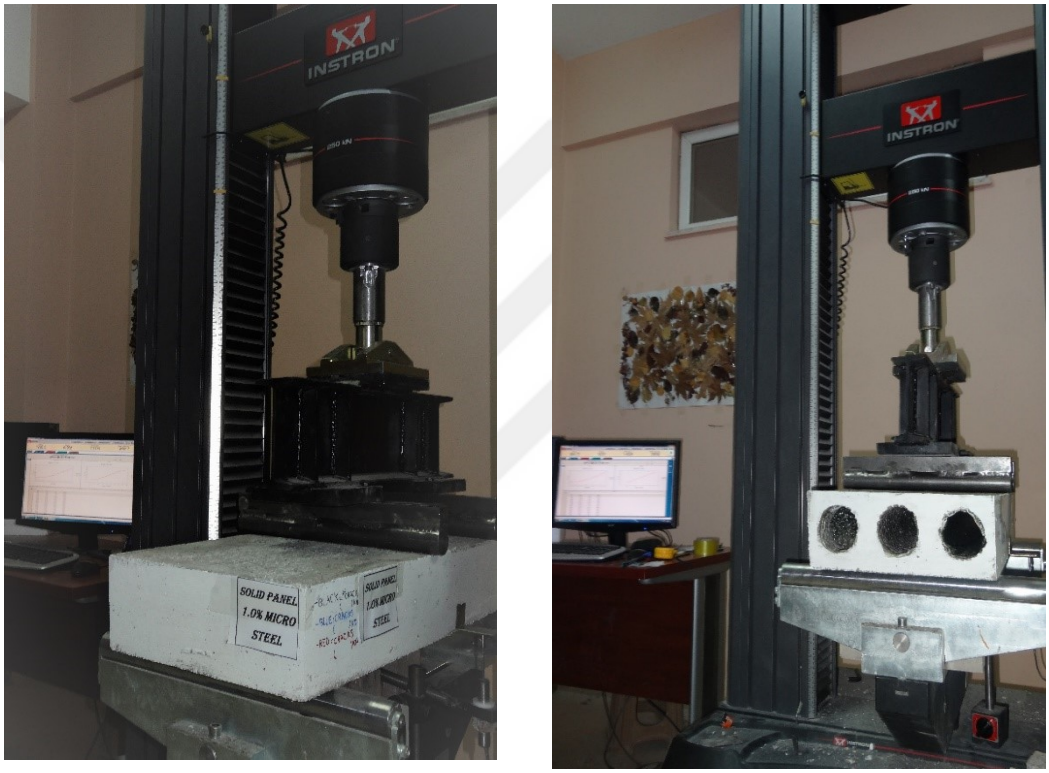

Figure 3.16 Specimen test setup for four-point bending load

CHAPTER 4

TEST RESULTS AND DISCUSSIONS

4.1 General

All results of the tests for the mixtures design that were estimated in Chapter 3, are explained in this chapter. This tests includes the fresh properties (slump flow, T_{500mm}, V-funnel and L-Box height ratio) and the hardened properties (compressive strength, tensile strength), and structural performance (fracture energy, flexural behavior). The hardened test results and structural performance of concrete were determined at 28 days.

4.2 Fresh Properties of SCGC

The fresh properties of SCGC can be specified by the following four critical characteristics: passing ability, viscosity, flowability, and segregation resistance, each of them can be addressed by one or more test methods described by EFNARC [90]. For example, viscosity may be measured by the T_{500mm} slump flow time and V-funnel flow time tests, while the fallibility can be determined via a slump flow test. One or more of above mentioned four critical properties should be satisfied for the requirements of self-compacting concrete in a fresh state that are appropriate for a given application. Then the self-compacting concrete must specify the class or target value defined in Table 4.1 in order to specify the flowability, viscosity and passing ability of the manufactured SCGCs, slump flow diameter, T_{500mm} slump flow time, V-funnel flow time and L-box height ratio.

Table 4.1 EFNARC classes of slump flow, viscosity and passing ability of SCC mixes

Slump flow classes		
Classes		Slump flow dia (mm)
Slump flow 1		550-650
Slump flow 2		660-750
Slump flow 3		760-850
Viscosity classes		
Class	T_{500mm} (sec)	V-funnel time (Sec)
Viscosity 1	≤2	≤8
Viscosity 2	>2	9 to 25
Passing ability classes		
Passing ability 1		≥0.8 with two rebar
Passing ability 2		≥0.8 with three rebar

4.2.1 Slump Flow Diameter

From this study, the design limits for all of the concrete mixtures were to give a slump flow diameter of 785 to 672 mm, which was achieved by using a superplasticizer as seen in Table 4.2 conforming to EFNARC recommendations, which states that the lower and upper approval limits of slump flow diameter should be between 550 and 850 mm respectively. Figure 4.1 shows the highest slump flow diameter was measured for the control mixture (F100S0) and it's about 785 mm, while the mixture with 100 % GGBFS replacement (F0S100) had the lowest slump flow 670 mm.

The slump flows for the SCGCs of all mixtures were in the range of Slump flow 2 class, except the control mix which was in the range of Slump flow 3 class. According to EFNARC [90], the SCGCs in Slump flow 2 can be used for structures with complex shapes, vertical applications in very congested structures, or for filling under formwork. However, SCGCs in the range of Slump flow 3 exhibit a better surface finish compared to Slump flow 2 when used in normal vertical applications. However, it is more challenging to control segregation resistance.

Table 4.2 The result of fresh properties

Mix code	Slump flow dimeter (mm)	T_{500mm} (sec)	V funnel (sec)	L box height ratio		
				H_1	H_2	H_2/H_1
F100S0	785	2.25	8.02	8.2	8.2	1.0
F75S25	765	2.47	11.5	8.3	8.0	0.97
F50S50	730	2.96	13.57	8.5	7.8	0.92
F25S75	690	3.56	16.18	8.6	7.4	0.86
F0S100	672	4.03	18.05	8.8	7.1	0.81

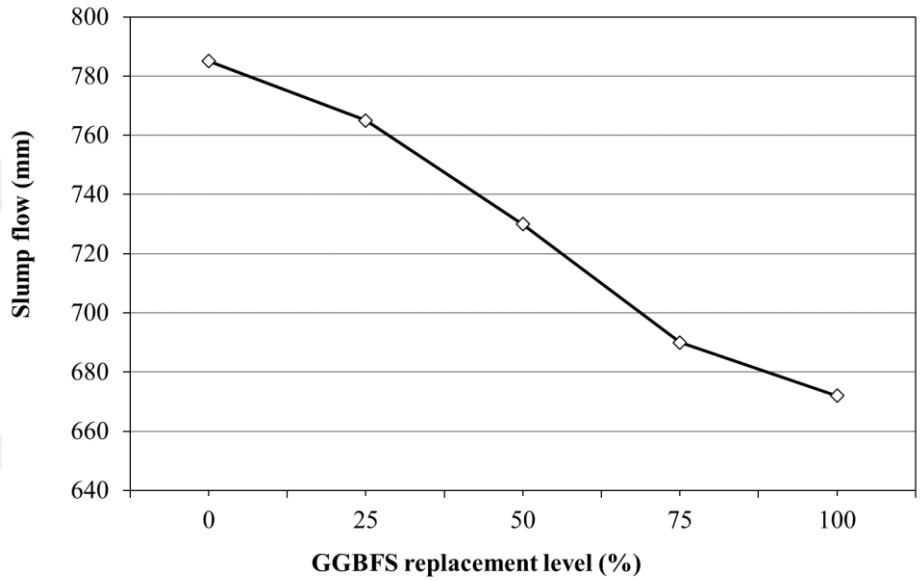

Figure 4.1 Effect of GGBFS level on slump diameter values

4.2.2 Times of Slump Flow and V-Funnel Flow

T_{500mm} slump flow and V-funnel flow times of the produced SCGCs were also presented in Table 4.2 and Figure 4.2 and Figure 4.3, respectively. It was observed that increasing the replacement level of GGBFs increased both the T_{500mm} slump flow and the V-funnel times of SCGCs. For example, T_{500mm} slump flow and V funnel flow times were 2.25 and 8.02 sec respectively, for the control mixture. However, as the GGBFs were replaced with 100 % FA as in the case of mixture S100F0, the corresponding measurements increased to 4.03 sec for the slump flow time and 18.05 sec for the V-funnel.

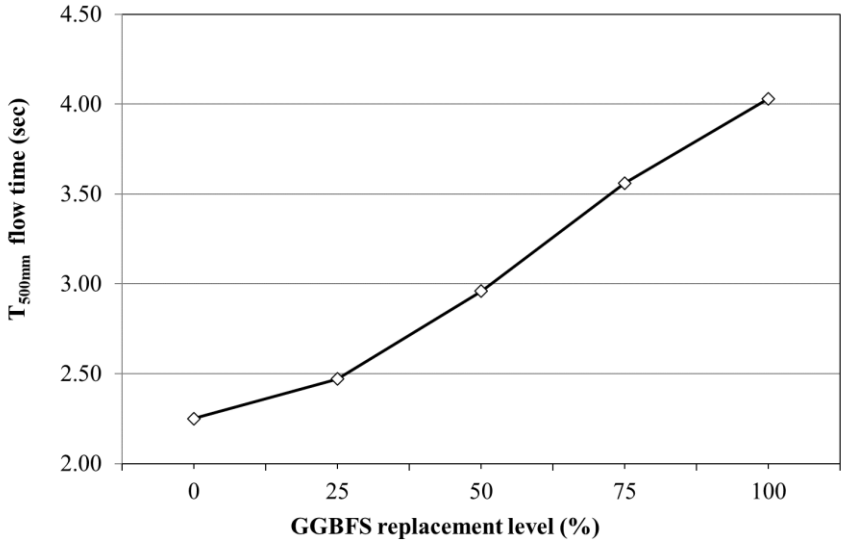

Figure 4.2 Effect of GGBFS level on T_{500mm} flow time values

That means that when there was a 100 % replacement level of GGBFs, it resulted in about 80 % and 125 % increases in T_{500mm} and V-funnel flow times for the SCGCs respectively. When taking the interaction of V-funnel flow and slump flow times, as indicated in Figure 4.4, into account, it was observed that all of the SCGCs mixtures were within the boundaries of the viscosity class (VS2/VF2) where (VS2 or VF2) mean the viscosity class as defined in Table 4.1 by the EFNARC. In addition, it was emphasized that such concrete might be helpful in improving segregation resistance or limiting the formwork pressure [90].

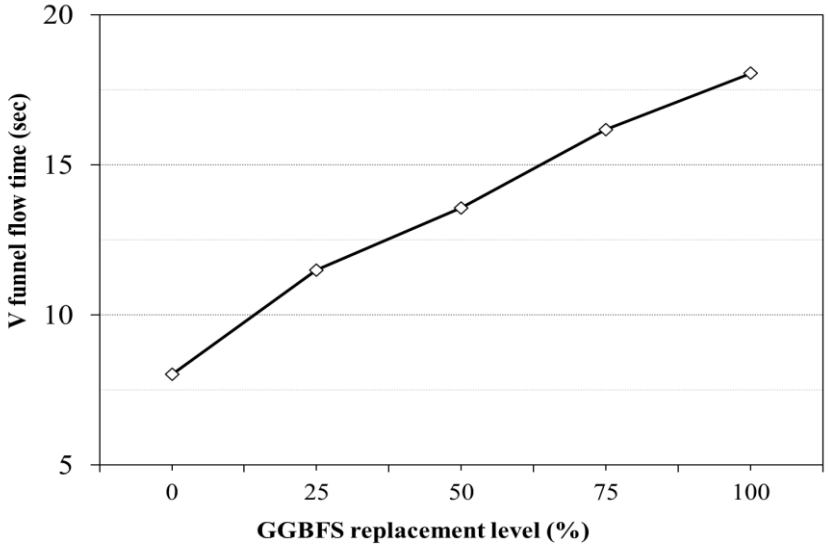

Figure 4.3 Effect of GGBFS level on V-funnel time values

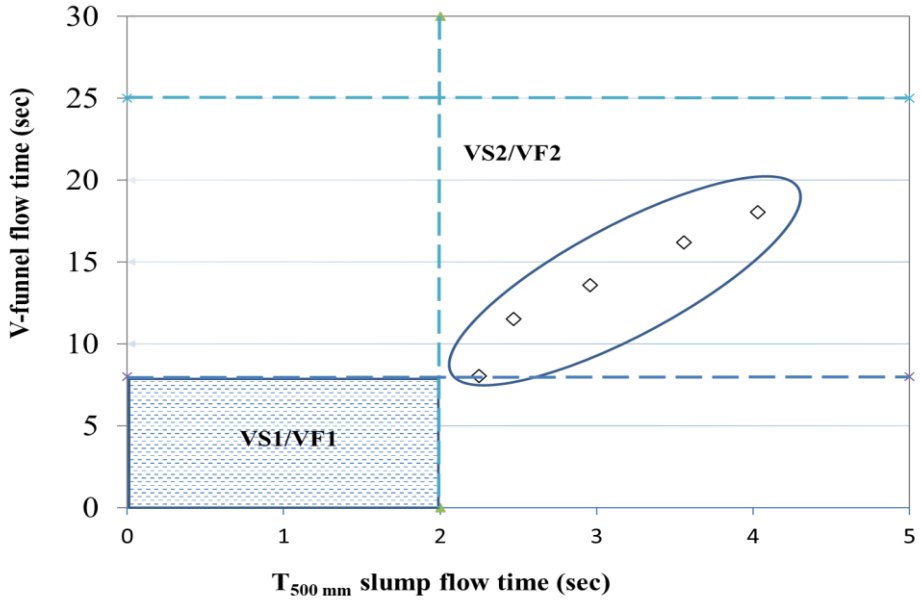

Figure 4.4 Variation of viscosity classes with T_{500mm} slump flow and V-funnel flow time

4.2.3 L-Box Height Ratio

In order to identify the passing ability of the produced SCGCs, the L-box height ratio was determined. The test provided H_2/H_1 ratio as a measure of the passing ability among the reinforcing bars. The variations in the three bar L-box height ratio is presented in Figure 4.5. To declare that a self-compacting concrete has the passing ability, L-box height ratio must be equal to, or greater than, 0.8. It should be noted that this ratio is 1.0 for perfect fluid behavior of concretes. It was obviously monitored in Table 4.2 The result of fresh properties and Figure 4.5 that all of the mixtures satisfied the EFNARC limitation given to the L-box height ratio.

The findings of this test showed that the absorption of the GGBFs replacement provided a systematic decrease in the L-box height ratio of up to 20 % as listed in Table 4.2 The result of fresh properties. Since the minimum height ratio had been reached at that replacement level, increasing the GGBFs replacement to 100 % also yielded the same height ratio as expected.

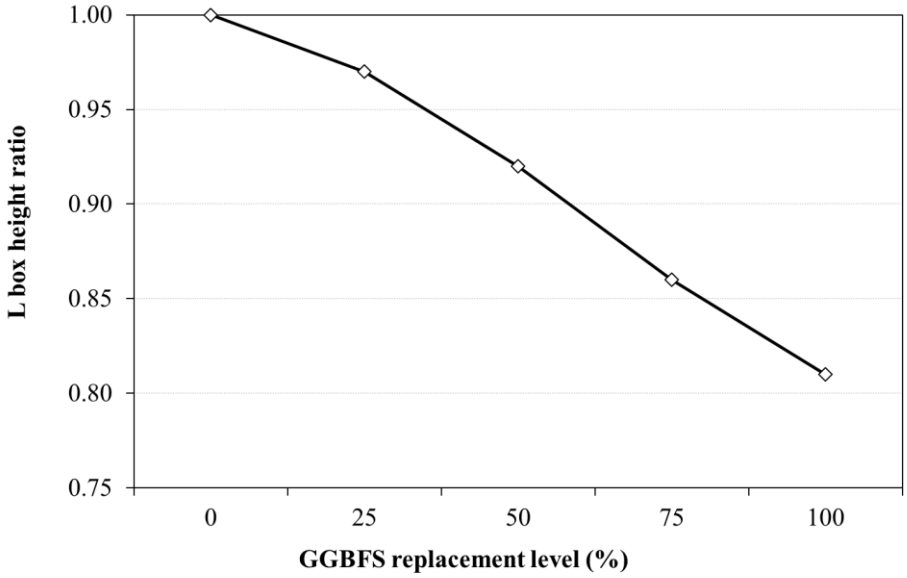

Figure 4.5 Effect of GGBFS level on L-Box height ratio

4.3 Hardened Properties

The hardened specimens of various SCGCs were tested to determine compressive strength, splitting tensile strength and fracture energy test.

4.3.1 Compressive Strength ($f_{c'}$)

Concrete is widely recognized for its compressive strength, and it is one of the most vital mechanical properties of concrete. The structure's service life completely relies on the hardened properties of concrete. The compressive strength was conducted on cubes as shown in Figure 4.6 at 28 days. The variation trends of compressive strength for different SCGC mixes, tabulated in Table 4.3 The result of material hardened properties and graphically presented in Figure 4.7. It can be seen that the compressive strength of SCGC free of GGBFs was 24.25 MPa for the control mix, and 76.19 MPa with 100 % GGBF at 28 days, also it was noted that the specimens with 0 % GGBFS (100 % FA) had to be removed from the molds two or three days after they were cast, since they failed to meet the target hardening level after one day due to the low amount of CaO in FA, which is the main factor affecting the initial setting time of concrete. The addition of GGBFS in the FA-based GPC accelerated the setting time. The average of the three identical samples was applied to measure the value of the compressive strength of each mix of concrete.

The compressive strength of SCGC was increased by the addition of GGBFS. Furthermore, it was indicated that the compressive strength of mixtures was between 24.25 to 76.19 MPa, since the compressive strength of SCGC improved by up to more than 200 % for (F0S100) specimens. These results showed the substantial effect that GGBFS has on the compressive strength values of SCGCs mixtures. The lowest compressive strength in the FA-based GPC specimens were attributed to the low calcium content [96]–[98] and low activity of FA [99], [100].

The influence of GGBFS, FA, and GGBFS/FA combinations on the compressive strength of OPC and GPCs were also examined and it was concluded that the compressive strength of the GPCs were increased in the order of 100 % with FA-based GPC< OPC<FA/GGBFS combination GPC<100 % GGBFS-based GPC. A lesser content of reactive calcium was observed after the XRD results on the 100 % FA specimens, resulting in the low amount of Calcium Silicate Hydrate (C-S-H) (the main form that is responsible for strength). As a result, a lower mechanical performance was obtained for the FA-based geopolymer specimens, since the lesser amount of CaO in the FA did not contribute to the C-S-H creation [99].

Figure 4.6 Compression test sample

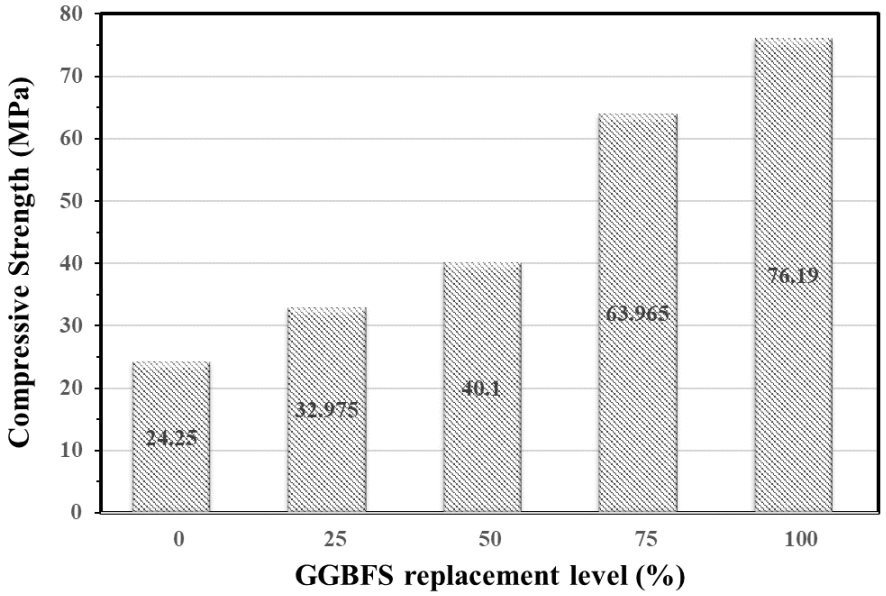

Figure 4.7 Effect of GGBFS replacement on compressive strength

4.3.2 Splitting Tensile Strength (f_{st})

The relationship between the tensile and compressive strength in FA-based SCGC with GGBFS were observed to be very similar to that of OPC concrete. The increase in the amounts of compressive strength normally causes a parallel relative increase of the tensile strength values. Splitting tensile strength values, evaluated from cylindrical specimens shown in Figure 4.8 with the Equation (3.1), are presented in Table 4.3 The result of material hardened properties. The variation in splitting tensile strength of 28 days, for all SCGCs with respect to content of GGBFS is given in Figure 4.9. Splitting tensile strength values ranging from 1.58 MPa to 6.45 MPa were achieved in this study. The lowest splitting tensile strength result was obtained from the control mixture, and a systematic increasing of splitting tensile strength was observed as the GGBFS increased. The increase in the amounts of splitting tensile strength that resulted due to the incorporation of GGBFS compared to the control mix F100S0, were 40.5 %, 121.5 %, 226 %, and 308 % for the mixes F75S25, F50S50, F25S75, and F0S100 respectively.

All concrete typically has a low tensile strength (~10 % of compressive strength) and a low strain capacity [101]. However, tensile strength is important in highway design, airfield slabs, and when shear strength and crack resistance are a priority. The addition of GGBFS to SCGC decreases these shortcomings, as shown in Figure 4.9 where there

is a general tendency towards increasing tensile strength, which may be attributed to the same reasons affecting the compressive strength. The relationship between compressive and splitting tensile strength is controlled by numerous factors including aggregate type, particle size distribution, and curing age [102].

Figure 4.8 Tensile strength specimen

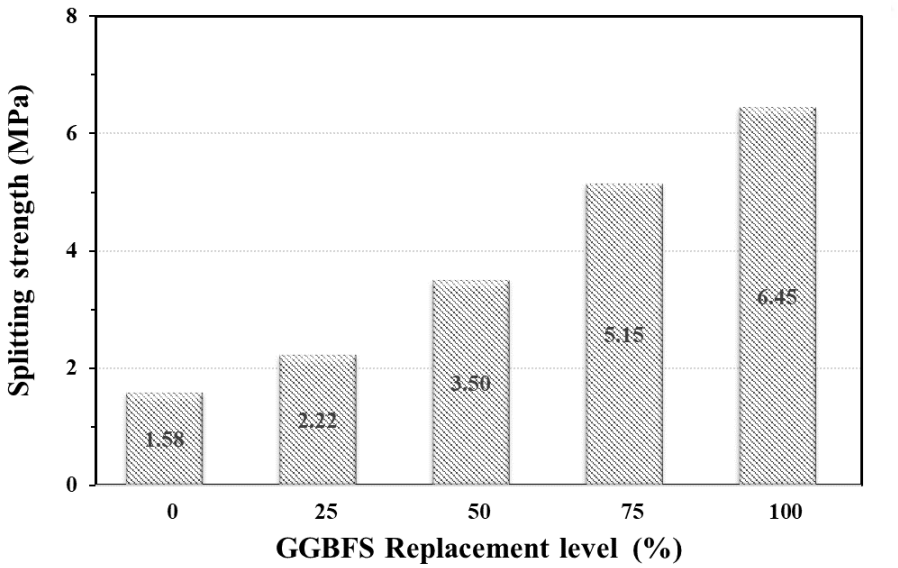

Figure 4.9 Effect of GGBFS replacement on splitting strength

Table 4.3 The result of material hardened properties

Mix code	$f_{c'}$	f_{st}	P_{max}	f_{flex}	Δ_{max}	Area (under the curve)	G_f	K_{IC}
	(MPa)	(MPa)	(N)	(MPa)	(mm)	(N.mm)	(N/m)	(MPa.mm$^{0.5)}$
F100S0	24.25	1.58	1398.00	2.33	1.03	641.82	133.86	11.04
F75S25	32.98	2.22	1661.00	2.77	1.02	664.40	145.54	13.11
F50S50	40.10	3.50	2206.76	4.18	1.07	736.83	173.53	17.42
F25S75	63.97	5.15	2607.82	4.35	1.10	882.63	195.68	20.59
F0S100	76.19	6.45	2723.00	4.54	1.01	885.84	213.54	21.50

4.3.3 Fracture Toughness

The fracture process region is recognized as being created in front of an existing crack in concrete. The fracture energy in concrete is usually achieved by a three-point bending on a notched prismatic specimen as illustrated in the previous chapter.

4.3.3.1 Load-Displacement

The load-displacement patterns of SCGC at 28 days are presented in Figure 4.10, and the results are summarized in Table 4.3 The result of material hardened properties. In general, all SCGC curves exhibited a linear upward slope until load at the first cracking on specimens. During the test process, after the load reaches the peak load, cracks appeared, which resulted in a descending curve after the peak load. However, the slope of the descending part of the curve after the peak load represented the property of the crack propagation inside the specimen until failure. (The failure after peak load is a relative issue depending on the displacement at peak load). Figure 4.10 indicated that the peak load values of SCGC specimens increased with an increase in the replacement percentages of GGBFS that was attributed to the high strength of the specimens when compared with the control specimens (100 % FA), accompanied by decreasing values of displacement with an increase in GGBFS variance. The maximum increase/reduction (load/displacement) was achieved in specimens containing 100 % GGBFS that exhibited maximum compressive strength value.

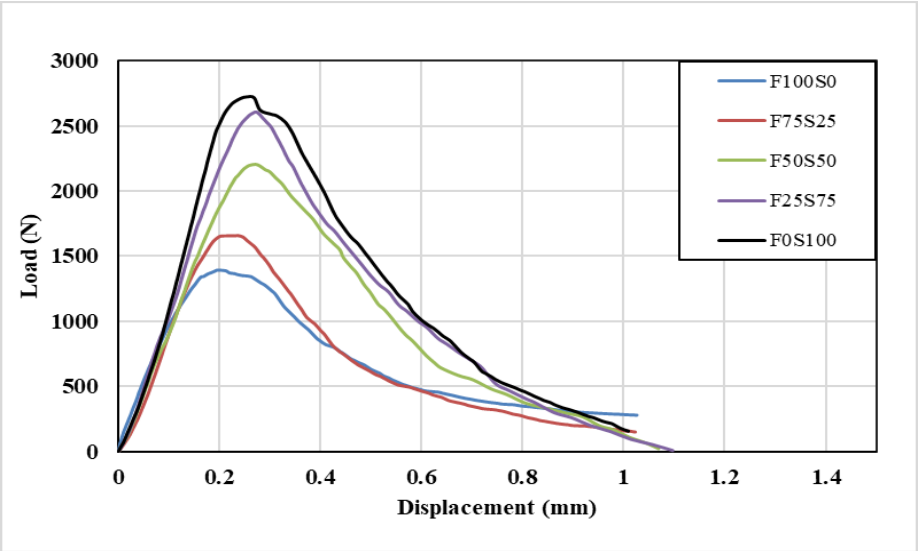

Figure 4.10 Effect of variance replacement percentage of GGBFS on load displacement

4.3.3.2 Fracture Energy

The energy required to breakdown the material, the product of force and distance, is signified by the area under the curve of the stress-strain diagram. The word toughness is a measure of this energy. The area under the load-displacement curve for each prismatic specimen was estimated and utilized in Equation (3.2) to achieve the fracture energy (G_f) for notched beams subjected to the three-point bending test Table 4.3 The result of material hardened properties. It was presented as the values of (G_f), and the final displacement at mid-span was recorded when the specimen failed.

The fracture energy for all mixes is represented in Figure 4.11. It was detected that the fracture energy of SCGC specimens had increased as compared with control specimens. Generally, the fracture energy of SCGC inclined to increase with an increase in compressive strength, as shown in Figure 4.11. [23], [44] investigated that fracture energy improved with the increase in compressive strength for heat-cured FA-based GPC.

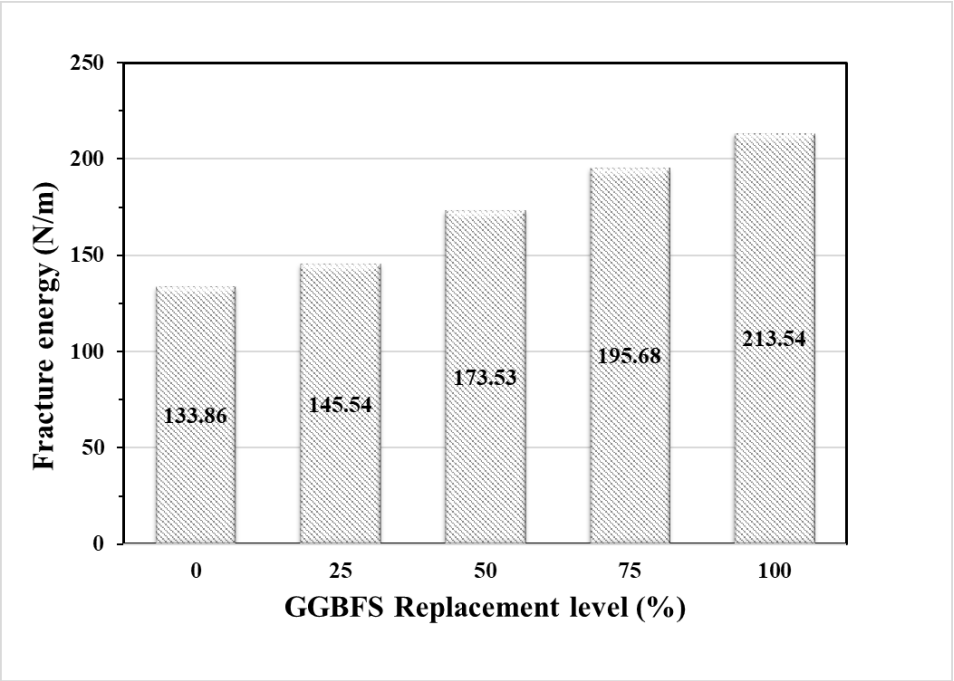

Figure 4.11 Effect of GGBFS replacement on fracture energy (G_f)

4.3.3.3 The Net Flexural Strength

The net flexural strength and critical stress intensity factor (K_{IC}) of SCGC at 28 days were estimated by Equations (3.3) and (3.4) respectively and represented in Figure 4.12 and Figure 4.13 respectively and summarized in Table 4.3 The result of material hardened properties. The stress intensity factor refers to the amount of stress concentration near the crack tip when the crack starts to propagate. Similar to the aforementioned mechanical performance of SCGC, incorporating GGBFS had a superior effect on flexural strength and stress intensity factor values.

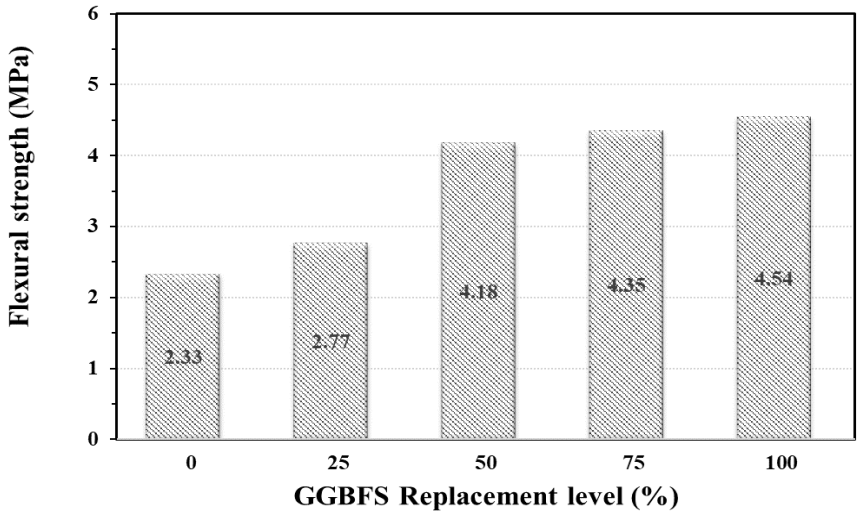

Figure 4.12 Effect of GGBFS replacement on flexural strength

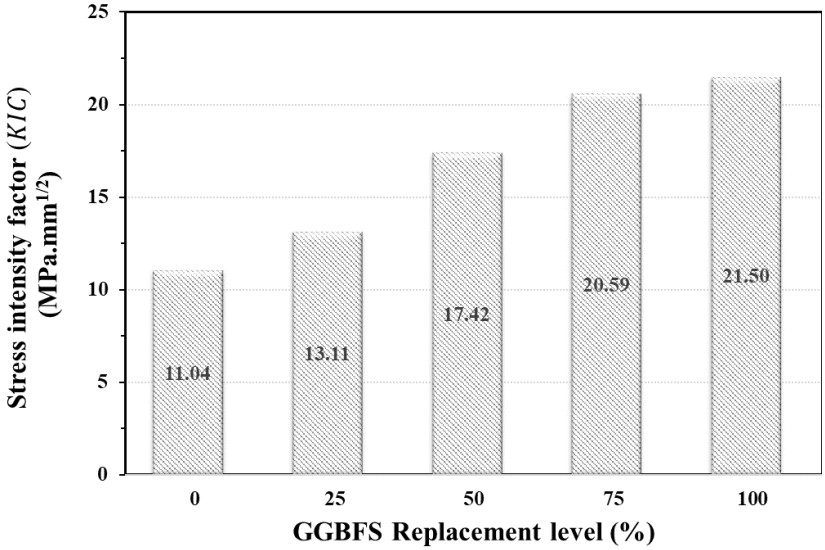

Figure 4.13 Effect of GGBFS replacement on stress intensity factor (K_{IC})

4.4 Correlation Between the Fresh and Hardened Properties of SCGC:

The correlation of the experimental data can be considered one of the most widespread applies among the researchers to evaluate the results were obtained. Theoretically, the relative volume fractions of the cementitious binder and aggregate are the major fundamentals that regulate the fresh and hardened properties of concrete. As shown previously, the higher compressive strength reflects the enhanced mechanical behavior.[32], [103] showed that the behavior of GPC is very similar to OPC. In order to estimate the relationship among the properties of SCGC, the following correlation was found:

4.4.1 Correlation Between the Fresh Properties of SCGC

Good relationships were found between the fresh properties of the SCGC mixtures. The R^2 for the relationship between slump flow and T-500 flow, and L-Box was (R^2: 0.987) and (R^2:0.9892) and are shown in Figure 4.14. The high value of (R^2), the coefficient of determination, specified that the slump flow and the other two properties were well correlated, despite the use of GGBFSs. This finding indicated the strong relationship between the fresh properties of SCGC in the study.

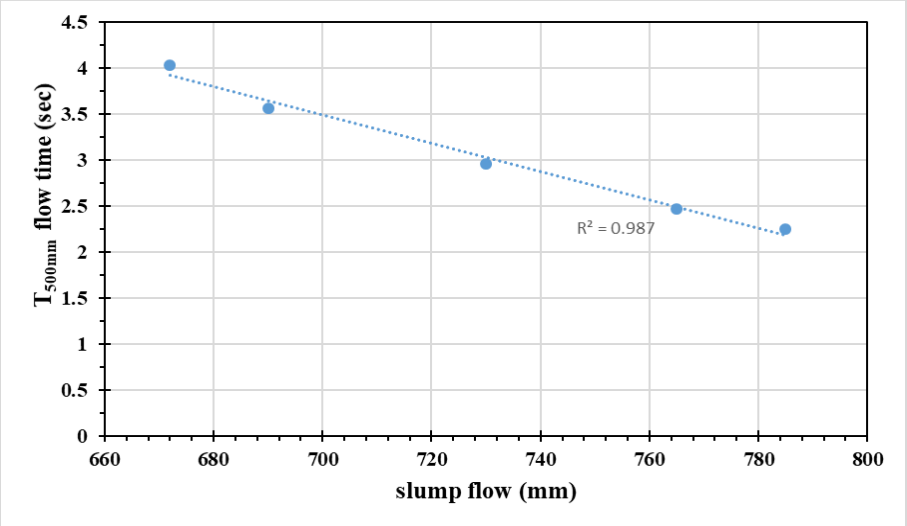

a) Correlation between T_{500mm} and slump flow dimeter

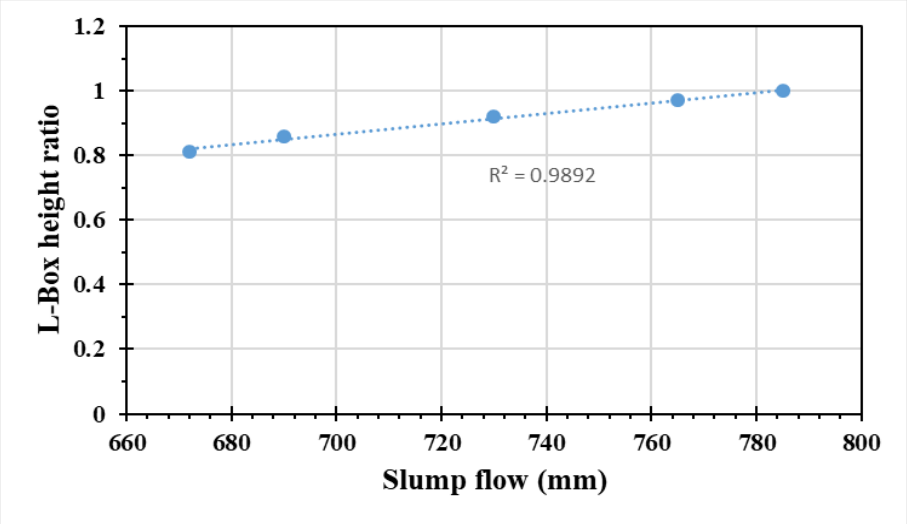

b) Correlation between L-Box height ratio and slump flow dimeter

Figure 4.14 Relationship between the fresh properties of SCGC

4.4.2 Correlation Between the Hardened Properties of SCGC

The compressive strength values of FA-based SCGC with variance replacement of GGBFS was found to exhibit similar performance to that of OPC concrete. In general, as the compressive strength increased, this resulted in a similar relative increase in terms of the value of mechanical properties. It was observed from the results of compressive strength and other mechanical properties of SCGC that the incorporation of GGBFS significantly increased the mechanical properties of the SCGC. Additionally, the improved performance for all mechanical properties was observed to have a similar trend.

An excellent relationship was found between the compressive strength and the other mechanical performance, as shown in Figure 4.15. The value of (R^2) obtained from the relation between experimental compressive strength and splitting tensile strength with the theoretical values of the stress intensity factor (K_{IC}) and the net flexural obtained from the different equations was the same. Therefore, it can be concluded that both equations are close to each other, in addition to the experimental results.

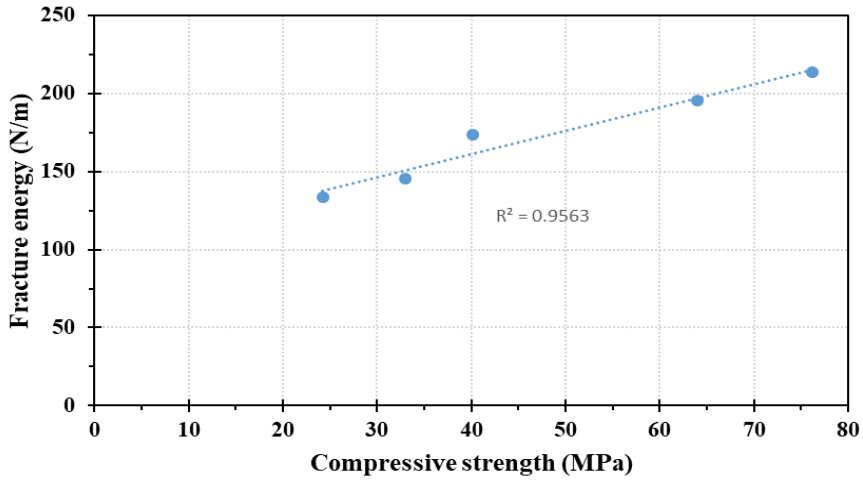

a) Correlation between Fracture energy and Compressive strength

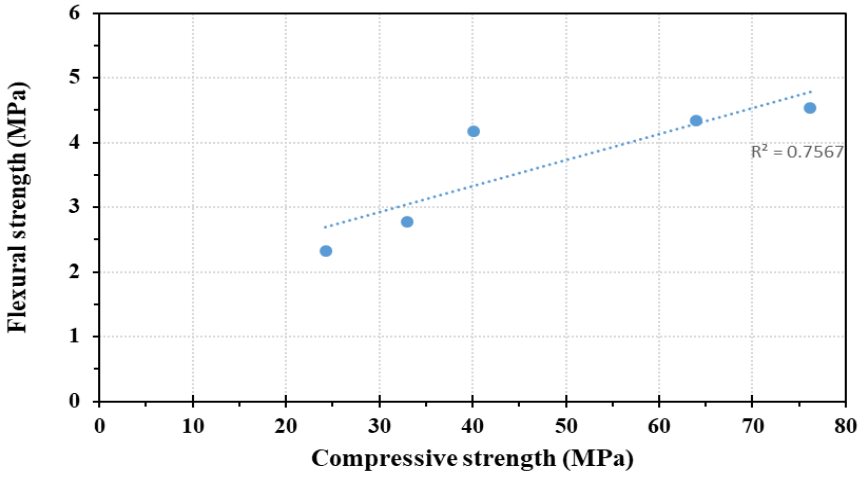

b) Correlation between Flexural strength and compressive strength

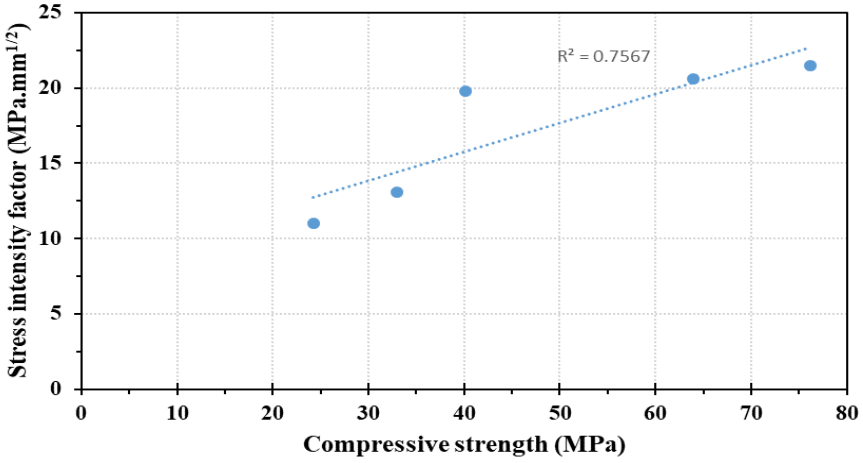

c) Correlation between compressive strength and splitting tensile strength

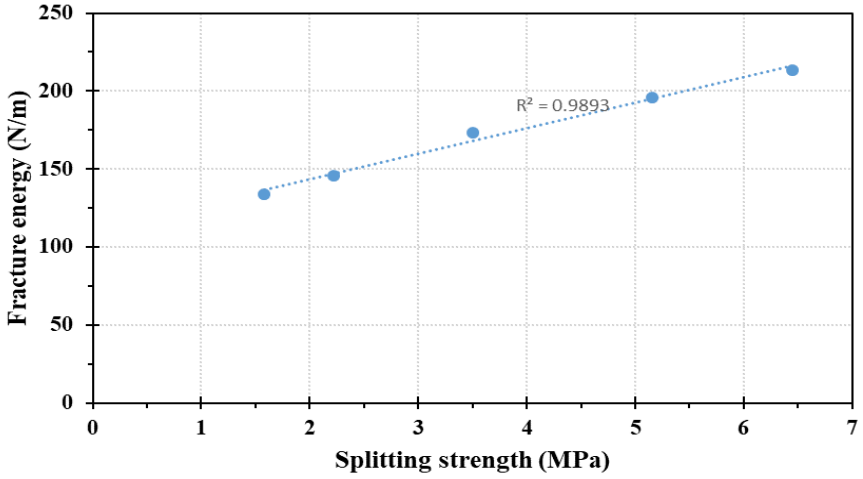

d) Correlation between Fracture energy and Splitting strength

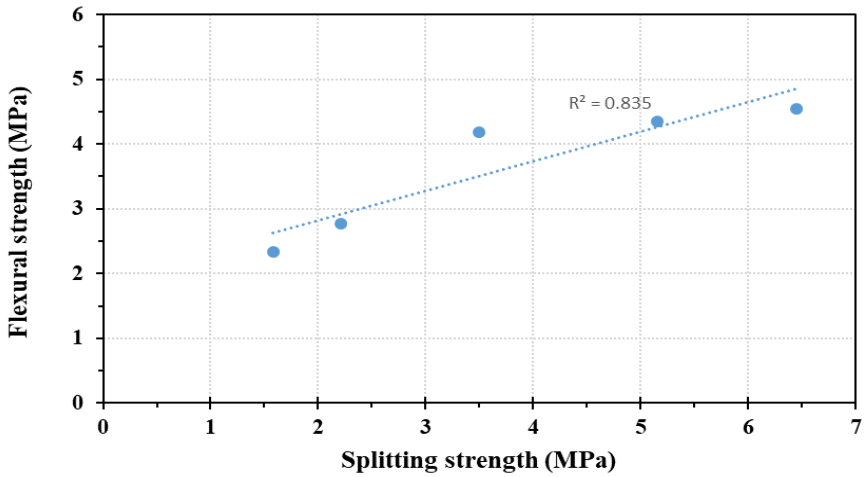

e) Correlation between Flexural strength and splitting tensile strength

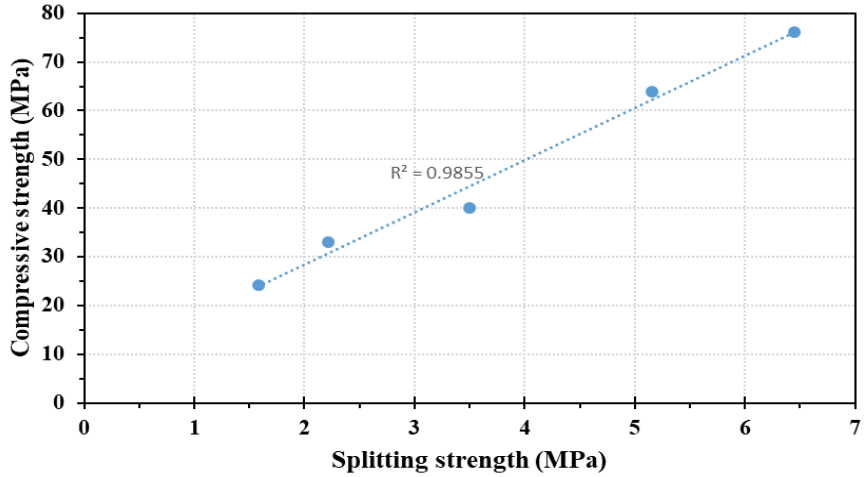

f) Correlation between stress intensity factor and compressive strength

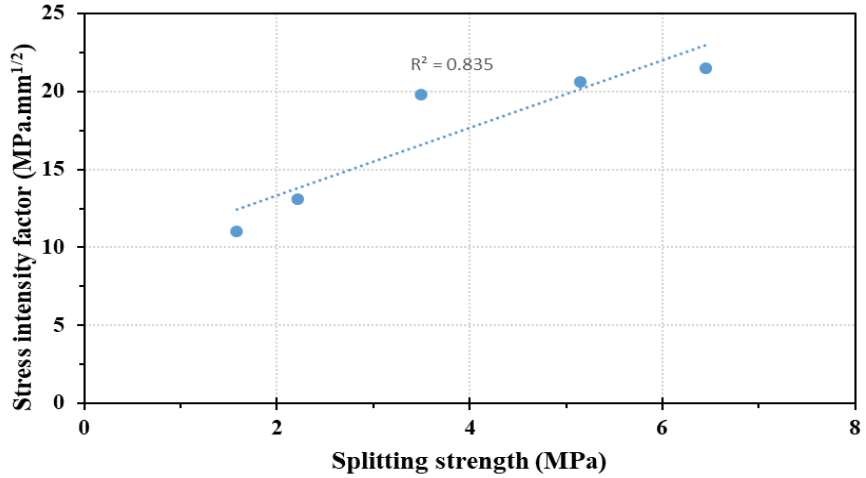

g) Correlation between stress intensity factor and splitting tensile strength

Figure 4.15 The relationship between the hardened properties of the SCGC

4.5 Statistical Evaluation of the Test Result

A general linear model analysis of variance (GLM-ANOVA) was performed at a significant level of 0.05 in order to estimate the variation in the tested performance of the SCGC with the different level of GGBFS in a quantitative form. For this, slump flow diameter, slump flow time (T_{500mm}), V-funnel flow time, L-Box height ratio, compressive strength, splitting strength, flexural strength, and the critical stress intensity factor of the concretes were assigned as the dependent variables, while the replacement level of GGBFS was the factor. A statistical analysis was conducted to indicate the statistically significant factors (p-level <0.05). Table 4.4 A statistical analysis presents the contributions of the factors to the evaluated test results. The column below the percent contribution shows the effect of the independent factors on the evaluated response, for example, the higher the contribution, the higher efficiency of the factors on that specific response. Also, a low influence of the factors on that specific response will be observed if the percent contribution is low. It was indicated by the results in Table 4.4 that all of the independent variables had a significant influence on the fresh and mechanical properties of the SCGC. When detecting the contribution amounts of the factors, it was observed that the most effective parameter in the variation of the fresh and hardened properties of the SCGC is the GGBFS replacement level. In addition, the combination of the GGBFS was observed to be most impactful factor on all of the mechanical properties of SCGC.

Table 4.4 A statistical analysis

Dependent Variable	Independent variable	Computed F	P Value	significant
Slump flow diameter	GGBFS replacement level	106.41	0.000	Yes
T_{500mm}	GGBFS replacement level	985.29	0.000	Yes
V- funnel flow time	GGBFS replacement level	441.68	0.000	Yes
L-Box height ratio	GGBFS replacement level	205.15	0.000	Yes
Compressive strength	GGBFS replacement level	4307.66	0.000	Yes
Splitting strength	GGBFS replacement level	94.72	0.000	Yes
Flexural energy	GGBFS replacement level	1.04	0.484	No
Critical stress intensity factor	GGBFS replacement level	40.60	0.002	Yes

CHAPTER 5

STRUCTURAL PERFORMANCE OF HOLLOW CORE SLAB PANEL

5.1 General

Although the results obtained in building materials from the previous chapter are a good step in the right direction, they must also be applied to the structural members to show this advantage. Therefore, the structural properties of HCS, with and without SF, are investigated. As stated previously, twenty-one HCS were created with two types of SF (macro and micro SF) with three volume fractions of each type (0.5, 1.0, and 1.5 %), and compared with the control HCS and the results presented herein.

This chapter encloses the results of the experimental test carried out, as outlined in chapter 3 for the HCS. These tests include the first crack loads, the load capacity of the panels, load-deflection behavior, crack patterns and failure modes. The test results, as conducted in this research, were determined at 28 days.

Table 5.1 The mechanical properties of slabs mix

MIX ID	SF %		Mechanical properties of concrete		
	Ma	Mi	Compressive strength (MPa)	Tensile strength (MPa)	Density(Kg/m^3)
normal	0	0	67.6	3.97	2332.06
Control	0	0	72.5	4.86	2176.33
Ma-05	0.5	0	74.7	5.97	2225.00
Ma-10	1.0	0	82.1	8.33	2266.83
Ma-15	1.5	0	76.6	10.82	2302.83
Mi-05	0	0.5	73.96	5.00	2224.33
Mi-10	0	1.0	77.51	5.16	2265.17
Mi-15	0	1.5	78.19	5.78	2283.67

5.2 Mechanical Properties

5.2.1 Compressive Strength

As previously highlighted, the compressive strength is one of the most important tests for concrete in the engineering world. For this, the compression test was conducted on cube specimens (100x100x100 mm) by a 250 kN capacity testing machine with respect to ASTM C39 [91]. The test was conducted on three samples for each mix of slab panels at 28 days and the results are shown in Table 5.1 and Figure 5.1.

The result observed that the addition of any type of SF (macro or micro) greatly improved the compression resistance values. These increases in the amounts of compressive strength resulted due to the addition of macro (Ma) SF. The addition of 0.5 %, 1.0 % and 1.5 % of Ma resulted to an increase in compressive strength of approximately 2.95 %, 13.3 %, and 5.6 % respectively as compared to the control mixes. The results showed that the addition of 1.0 % of Ma resulted in the best possible compressive strength of the specimens.

Also, the addition of micro (Mi) SF enhanced the compressive strength and gave a good result close to that of Ma as shown below whereby 2 %, 6.9 %, and 7.8 %, increases in compressive strength were obtained from the addition of 0.5 % 1.0 % and 1.5 % of Mi respectively.

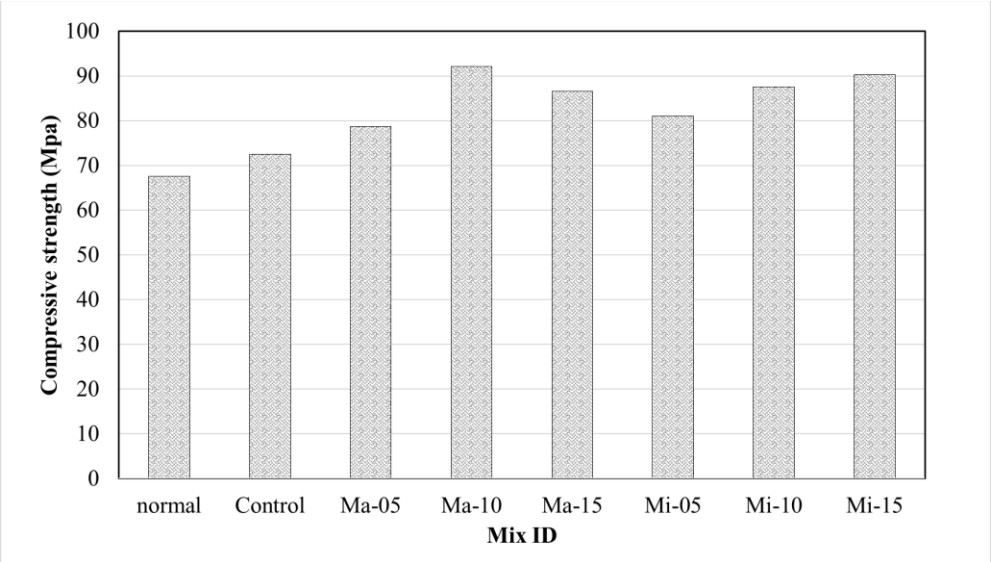

Figure 5.1 Compressive strength

5.2.2 Tensile Strength

The average of three cylinders was taken as the value for tensile strength for each mix, as per the standard method of tensile testing as highlighted in the previous sections. Table 5.1 and Figure 5.2 show the effect of adding Ma and Mi.

The results showed that the increase was significant in cylinders containing fiber size of 0.5 %, 1.0 %, and 1.5 % with the tensile strength increasing by 22.8, 71.4, and 122.6 % respectively as compared with the control mix. On the other hand, when Mi was added in the same percentage the increment in tensile strength was 2.9 %, 6.2 %, and 19 %. It is evidently seen that there is a big difference between the result for Ma and Mi because of the variations in length and the tensile strength of each type.

The increase in tensile strength, when the SF was added, lies in the capability of this fiber to attack the creation of cracking as well as its development. It also helps the fiber to carry and redistribute the stresses placed on the cylinder. Ganesan and Santhakumar reported that the main objective of the addition of SFs was to increase the tensile strain capacity of the concrete [19]. Also, it was reported in the literature that tensile strength could significantly increase when fibers were added to the concrete due to the crack arresting effect of the fibers.

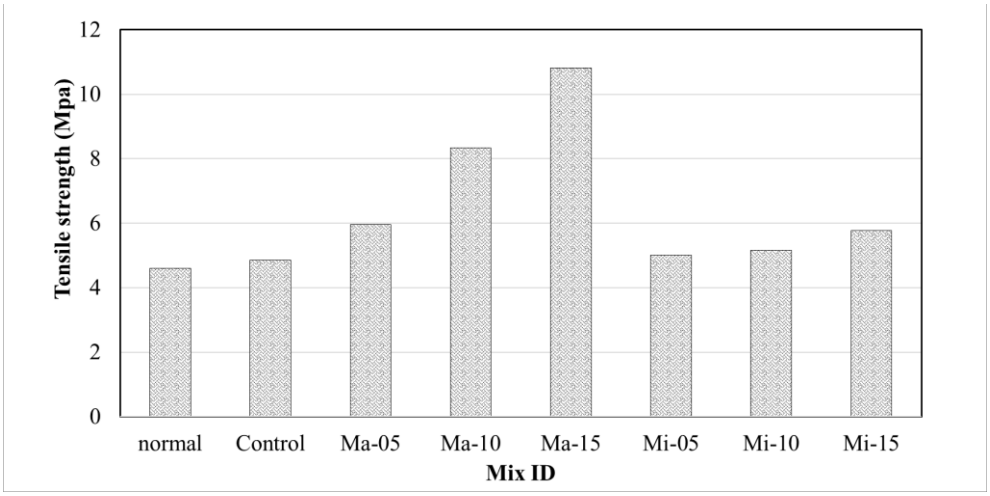

Figure 5.2 Variation in tensile strength

5.3 Structural Characteristics

5.3.1 Test Setup and Procedure

In the beginning, the front faces of all the concrete panels in the specimens were painted white to help identify the starting areas of cracks and to observe the length of those cracks. The white color was also applied to help accurately install the LVDT (Linear variable differential transformer) at the center of the sample.

Panel specimens were tested under a standard static four-point load in the study of the flexural behavior of concrete, showing the difference between hollow core and solid panels. A universal testing machine (INSTRON) having a capacity of 250kN was used. The rate of load application was about 0.05 kN/min, enough to record the growth of cracks, strains and deflections. The cracks were remarked and drawn on the face of slabs during, and also after, the test. Deflections were obtained using high precision LVDT placed at the bottom (near the mid-span of the concrete slab panel). Specimens were placed on the machine by aligning the marked support and positions of loading. The initial (first) crack and successive cracks, as the load was increased, were recorded. After the first cracking, loading was continued and was finally stopped when the concrete slab panel was just at the stage of collapsing.

5.3.2 Failure Modes and First Crack Strength

The shape of the openings affects the type of failure mode of HCSs. Also, the span to effective depth ratio (a/d) was noted. This ratio also affects the failure mode of a HCS specimen. This ratio was calculated as follows

a/d= 35/12.5 = 2.8

For the same a/d ratio of 2.8, the HCSs will experience similar failure modes i.e. there should be no difference when the a/d ratio is considered (because it is the same for all slabs); what should make the failure modes different is the shape of the openings and the SF type and percentage used.

There are three major types of failure modes that are exhibited in reinforced concrete slabs, as shown in Table 5.2.

Table 5.2 Failure modes in reinforced concrete slabs

Failure mode	Description
Shear	Cracks appear near the edge of the slab
Flexural	Cracks appear within the mid-span area of the slab
Shear-flexural	Cracks appear at both near the edge and mid-span of the slab

Table 5.3 Test results of unit slab panels (failure mode, loads and deflections)

Mix ID.	Failure mode	SF %		load (KN)		Deflection	
		Ma	Mi	P_{cr}	P_{max}	Δ_{cr}	Δ_{max}
SO-normal	Shear-flexural	0	0	26	80	1.02	25.83
RH-normal	Shear			20	45	1.35	3.42
CH-normal	Shear			23	58	1.04	3.44
SO-control	Shear-flexural	0	0	31	81	1.05	21.75
RH-control	Shear			23	54	1.12	4.22
CH-control	Shear			26	63	1.09	3.58
SO-Ma-05	Flexural	0.5	0	41	88	1.85	32.61
RH-Ma-05	Shear			25	60	1.84	4.01
CH-Ma-05	Shear-flexural			28	71	1.41	4.30
SO-Ma-10	Flexural	1.0	0	43	93	7.39	34.45
RH-Ma-10	Shear			40	75	1.12	4.21
CH-Ma-10	Flexural			44	84	1.64	7.29
SO-Ma-15	Flexural	1.5	0	48	95	7.06	37.30
RH-Ma-15	Shear-flexural			54	72	1.52	3.50
CH-Ma-15	Flexural			56	85	1.72	5.25
SO-Mi-05	Flexural	0	0.5	32	87	1.06	18.67
RH-Mi-05	Shear			24	57	1.08	4.29
CH-Mi-05	Shear			25	67	1.33	3.76
SO-Mi-10	Flexural	0	1.0	64	101	1.16	3.53
RH-Mi-10	Shear			35	62	1.15	3.69
CH-Mi-10	Shear-flexural			37	76	5.54	5.33

Mix ID.	Failure mode	SF %		load (KN)		Deflection	
		Ma	Mi	P_{cr}	P_{max}	Δ_{cr}	Δ_{max}
SO-Mi-15	Flexural	0	1.5	84	106	1.26	3.52
RH-Mi-15	Shear			36	77	1.21	4.52
CH-Mi-15	Flexural			40	86	1.40	14.86

When the results of the control HCS panels were compared with those of the SF reinforced HCS panels, it was noted that SFs had an impact in the flexural strength of the concrete slabs. SFs were used to improve the bending, stiffness, tensile strength, shear and fracture energy of the SCGC. Cracking begins in the tension zone because concrete (without reinforcement) is itself weak in tension. The fiber controls cracking, by capturing the cracks and preventing them from progressing further into the compression zone. Fiber bridges the cracks and transfers the stresses across it, and has the ability to work in many directions, leading to an increase of the ultimate load (P_{max}). For solid slab panels, with and without steel, the type of failure mode exhibited was flexural Table 5.3 and Figure 5.3. Solid slabs have higher flexural strength because of the arrangement of concrete fibers in the concrete. The arrangement is in such a way that stresses act uniformly throughout the concrete. Solid slabs are intact structural units with fibers arranged in the same direction; there are no breaks in the concrete created by the change in shape or hollowness of a section.

a) Control panel

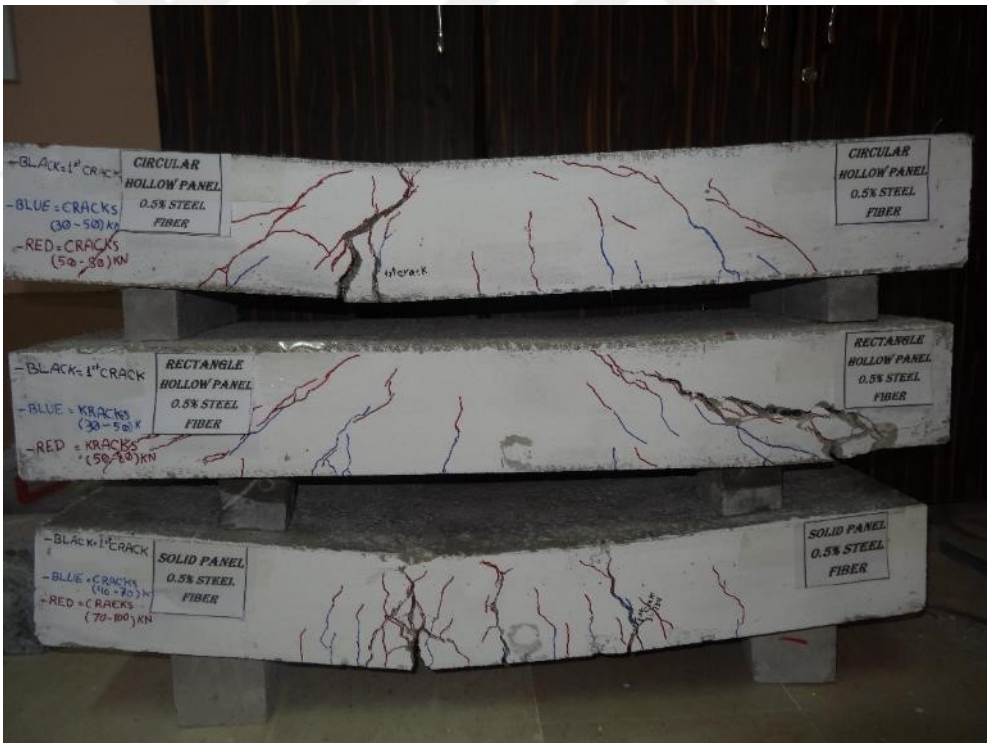

b) Panel with Ma-05

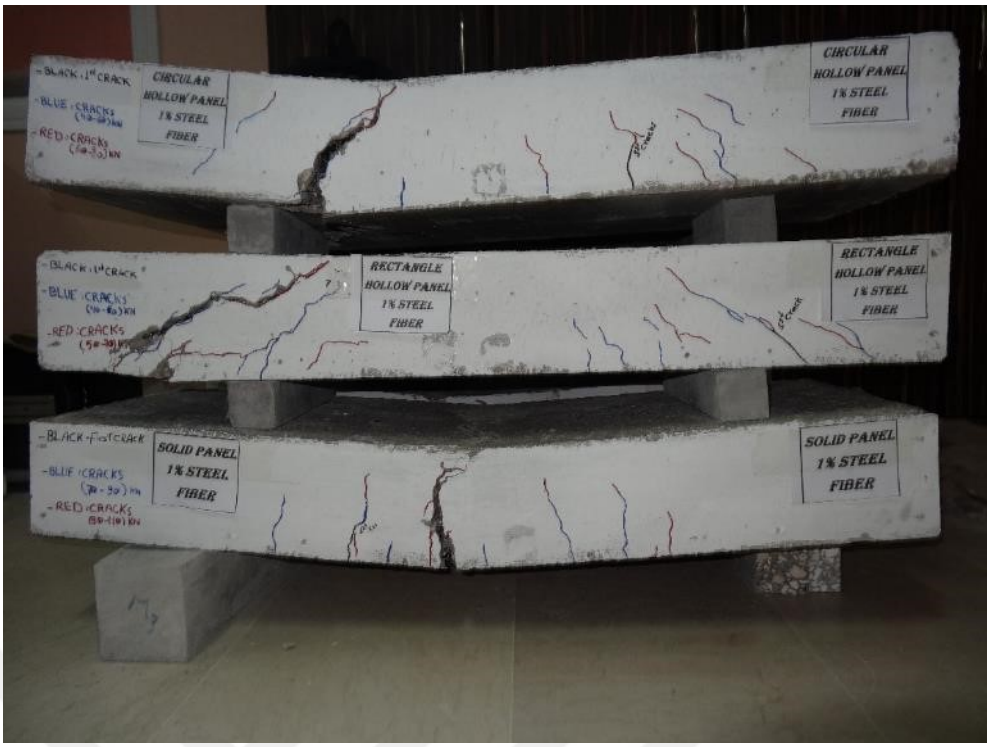

c) Panel with Ma-10

d) Panel with Ma-15

e) Panel with Mi-05

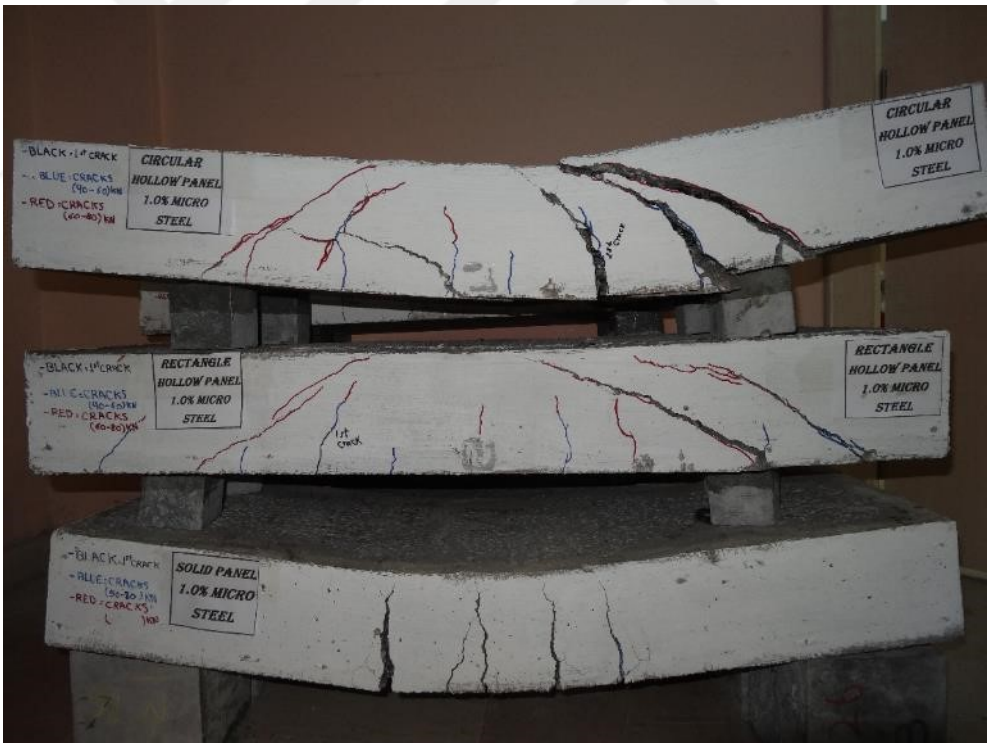

f) Panel with Mi-10

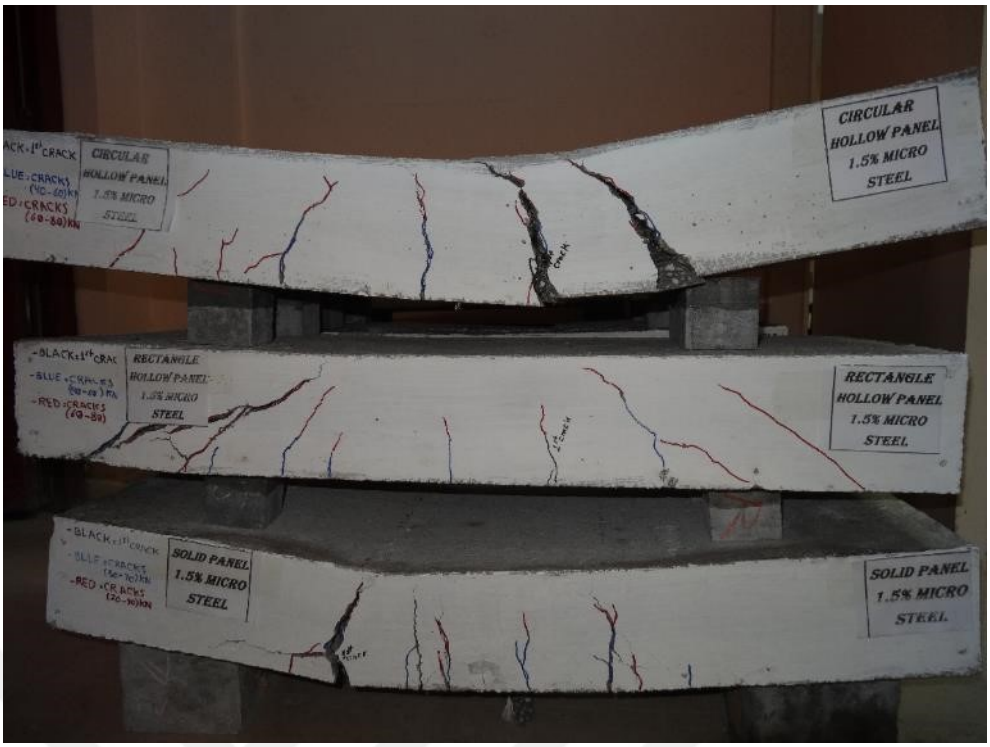

g) Panel with Mi-15

Figure 5.3 Effect of hollow shape on failure mode

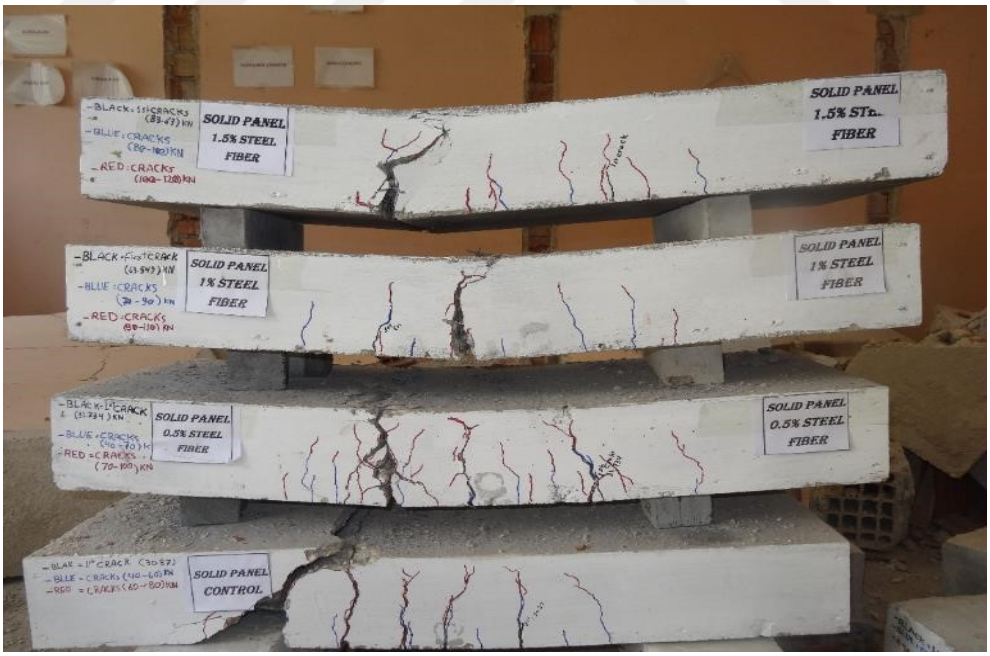

a) Solid panel with Ma

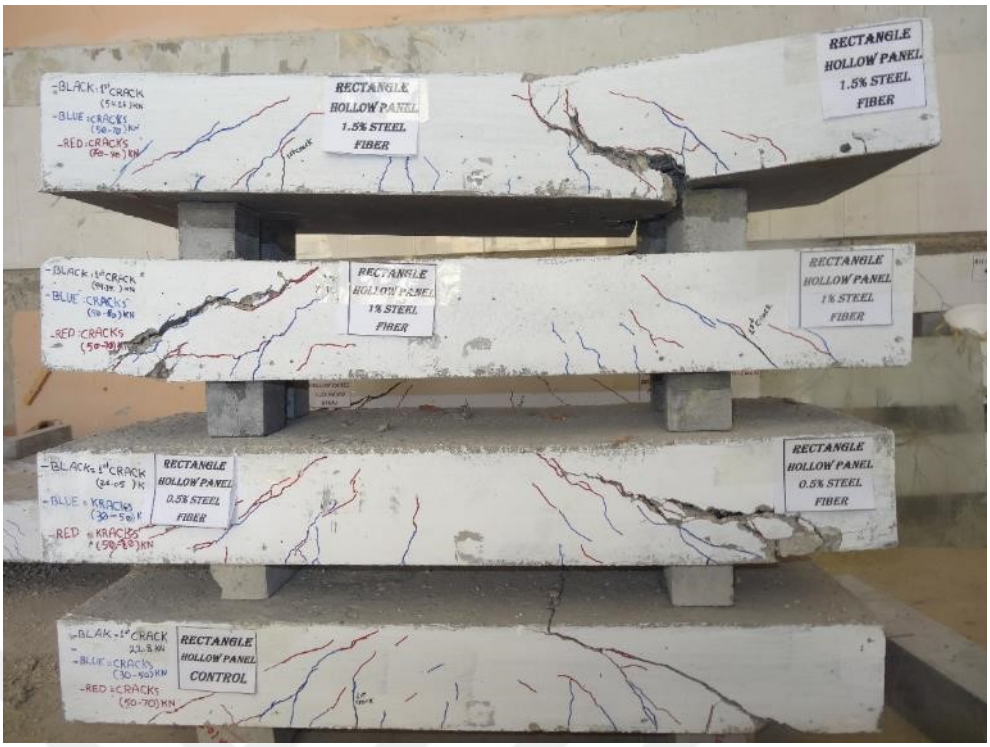

b) RH with Ma

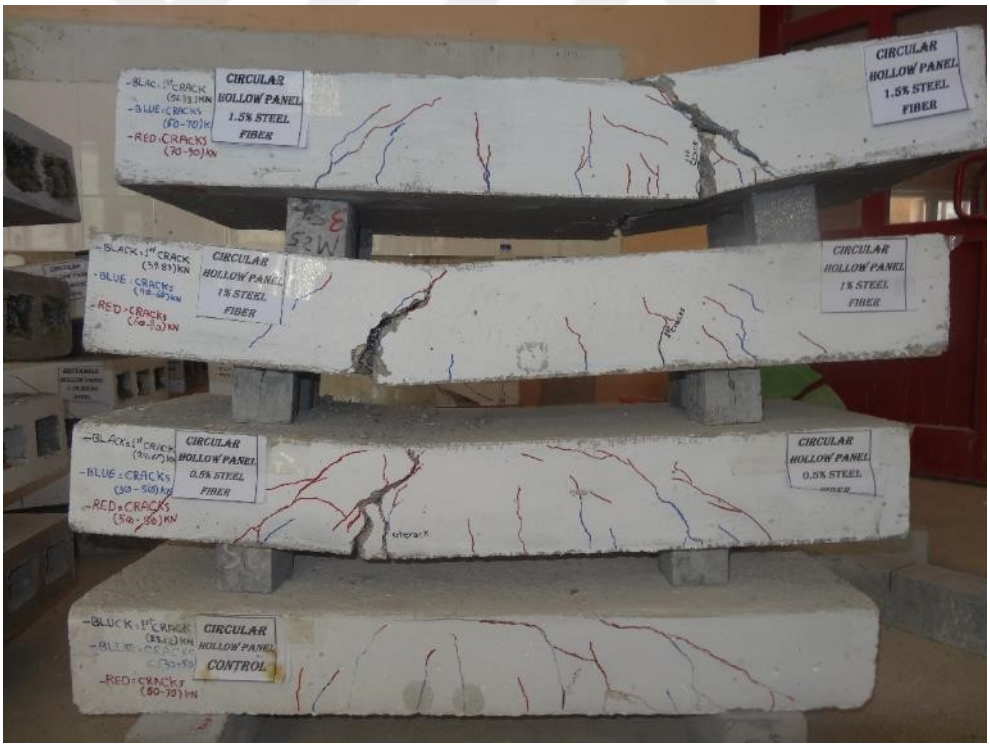

c) CH with Ma

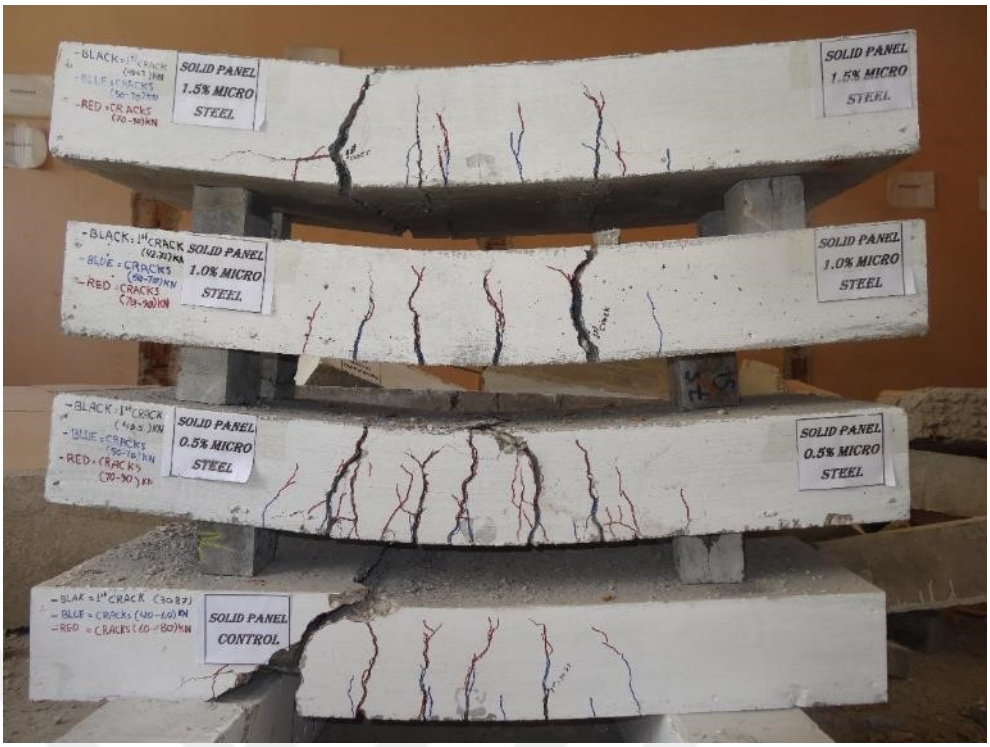

d) Solid with Mi

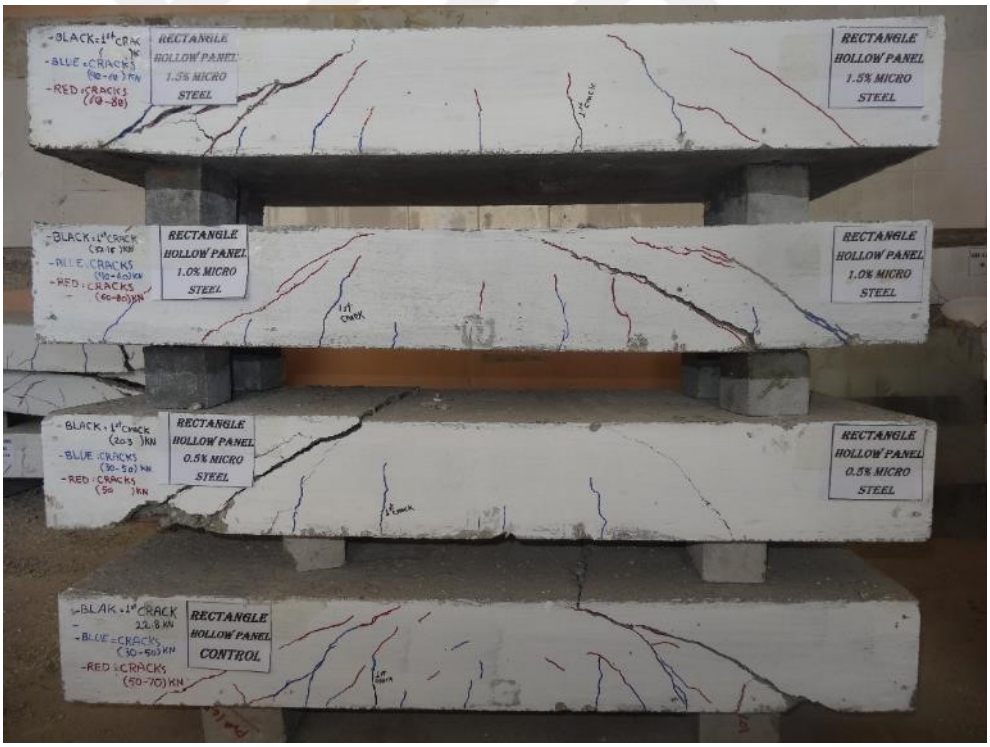

e) RH with Mi

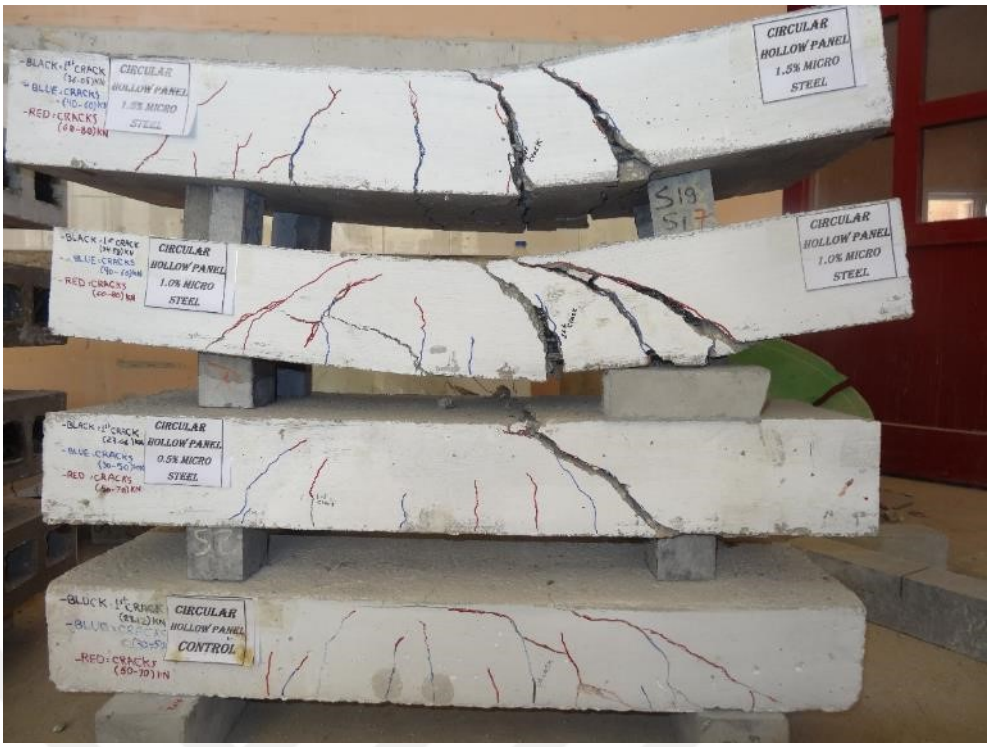

f) CH with Mi

Figure 5.4 Effect of steel percentage and type, on failure mode

Also, Rectangular Hollow (RH) core slab panels exhibited poor flexural strength. They had the lowest first cracking loads (P_{cr}) and ultimate loads (P_{max}) when compared with the Circular Hollow (CH) core slab panels. Also, they exhibited shear failure quickly. This is because a rectangular shaped opening has four corners, which are stress concentration areas within the concrete. These stress concentration areas contribute to the poor flexural strength of RH core slab panels. Therefore, they will also likely experience first cracking earlier (under a relatively low load), than the other slab panels, as observed in Table 5.3 and Figure 5.4. In addition, Ma proved to provide better flexural strength than Mi. Values of P_{cr} and P_{max} for Ma were higher than those for Mi, for corresponding types of HCS panels. Difference in the flexural strength can also be noted from the observation of RH-Mi-15 slab panel and RH-Ma-15 slab panel in Table 5.3 and Figure 5.5. The RH core slab panel experiences shear failure when only 0.5 % of Ma is used while the same shear failure will occur when 1 % of Mi is used. This is because Ma is longer, has a higher aspect ratio and has hooked ends that provide better bonding between the fibers and the cement paste. The first cracking strength and ultimate strength is higher in slab panels reinforced with Ma than those reinforced with Mi as shown in Figure 5.6. Similarly, when the percentage of steel is

increased, the flexural strength improves across all types of HCS panels with both macro and micro steel as shown in Figure 5.6.

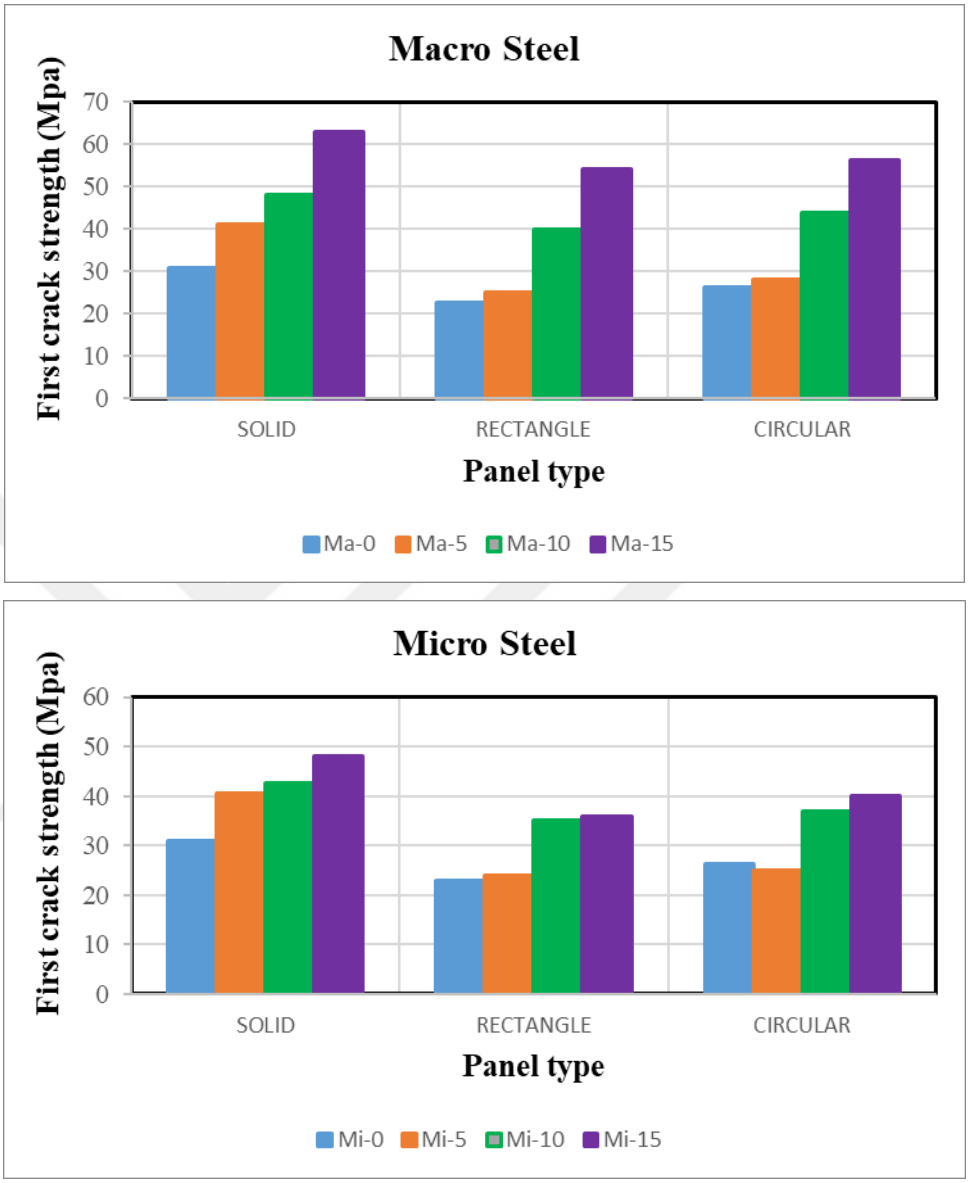

Figure 5.5 Effect of panel type on the first crack load

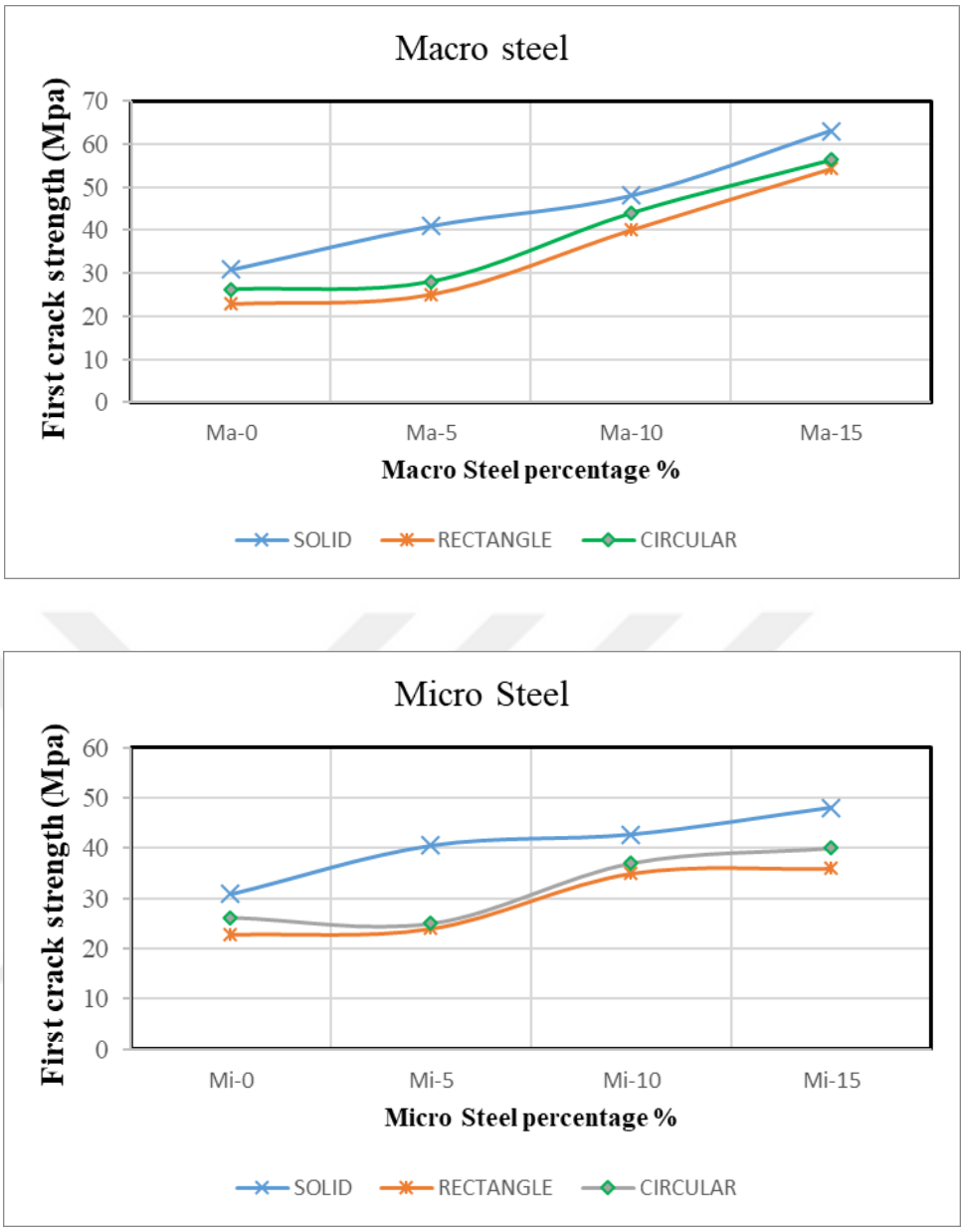

Figure 5.6 Effect of SF type and percentage on the first crack load

5.3.3 Ultimate Strength

As can be observed on Figure 5.7 and Figure 3.8, the ultimate strength of solid slab panels is higher than that of other slab panels. Likewise, the ultimate strength of HCS panels is noted to be less than that of solid slab panels; in particular, the ultimate strength of RH core slab panels is much less than that of other slab panels. Solid slabs have higher ultimate strength because the complete mass of concrete is intact and acts as one unit when load-imposed stresses are acting on the slab. The strength of any material greatly depends on the built-in properties of the material. In the case of solid slabs, grains are well arranged with fibers aligned in the same direction. Therefore,

there is no undesirable localization of stresses due to the irregularity of a concrete section. This is different for HCSs because the whole mass of concrete is not intact; breaks are created (at the hollowed out sections), which is an indication that fibers are misaligned. This results in localization of stresses in some areas. In particular, RH core slab panels experience the lowest ultimate load because the opening has corners that act as stress concentration (localization) areas. The ultimate strength is predicted by the elastic behavior of concrete. As it shall be described later, when looking at the effect of SF type and percentage on the ultimate strength of SF reinforced SCGC, a high ultimate strength results from improved elastic behavior of reinforced concrete. Both the shape of opening and SF affect the elastic behavior of reinforced concrete.

SF has the effect of increasing the ultimate strength of SCGC. As can be seen in Figure 5.8, control slab panels (without SF reinforcement) have a relatively low ultimate strength. SF improve the elastic behavior of reinforced concrete by increasing the modulus of elasticity such that the concrete slab panel is able to accommodate a higher load prior to permanent deformation and failure; the modulus of elasticity (E) is the gradient of the proportional line of the load-deflection graph in the elastic region. SF affects the concrete section properties by increasing the effective tension zone; the neutral axis is raised from the tension zone to the compression zone, as cracks are effectively controlled within the SCGC. However, Ma increases the ultimate strength more than Mi, as illustrated in Figure 5.9; Ma increases the modulus of elasticity of concrete. This is because Ma is longer, has a higher aspect ratio and has hooked ends that provide better bonding between the fibers and the cement paste. In spite of the difference in type of SF reinforcement, an increase in the volumetric ratio of steel will surely increase its ultimate strength, as shown in Figure 5.8.

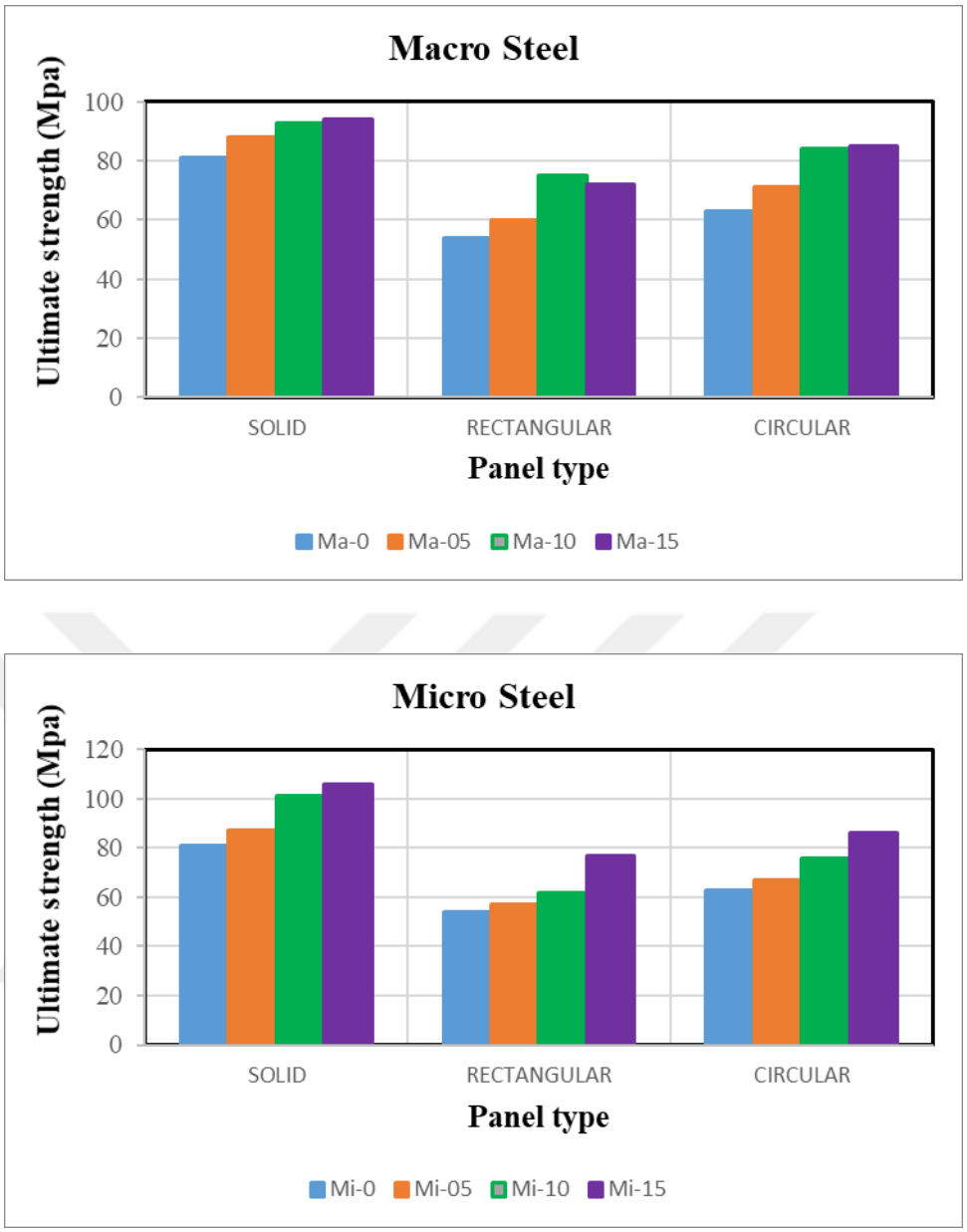

Figure 5.7 Effect of panel type on the Ultimate strength

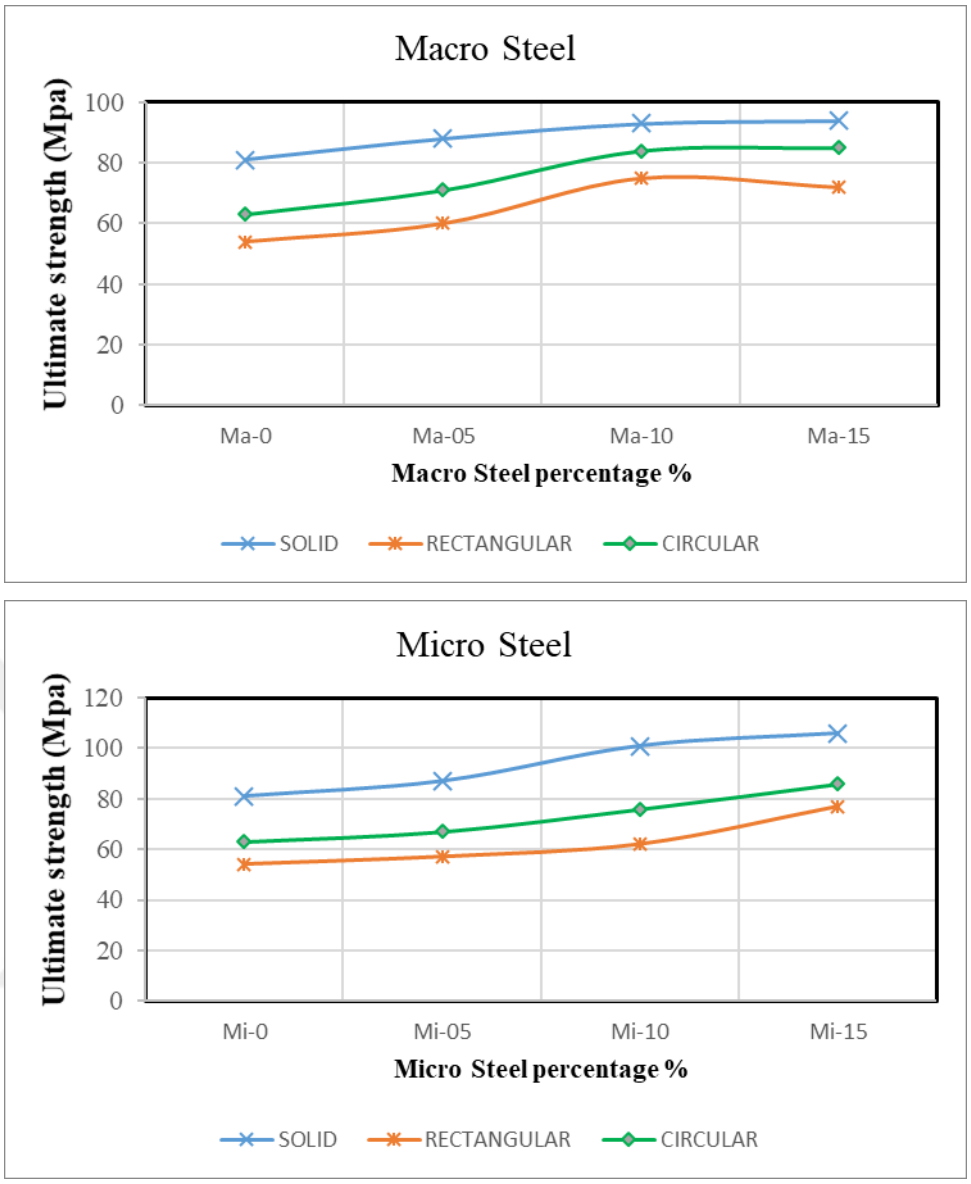

Figure 5.8 Effect of steel type and percentage on the Ultimate strength

5.3.4 Load-Deflection Behavior

As seen in Table 5.4, the deflection at failure is higher than both the deflection at first crack and deflection at ultimate load as shown in Table 5.3. This is because, the concrete zones have been overstressed. However, the failure load is less than the ultimate load because of the inelastic behavior of concrete; the load-deflection assumes a straight line (elastic range) followed by a downward curve with a peak at the top (inelastic range). The ultimate load is higher than the failure load, as shown in Figure

5.10; the ultimate load occurs at the peak of the load-deflection line graphs while the failure load occurs at the downward end of the curve.

Solids slabs have higher failure loads and deflections than HCS panels. This is because, solid slabs have a higher flexural strength that results from the fact that non-occurrence of breaks, or irregularities, contributes to the effective transmission of stresses uniformly within the concrete. Also, RH core slab panels exhibited the least failure loads and deflections. This is because a rectangular shape opening has corners that act as stress localization points. These stress concentration areas contribute to the poor flexural strength of these slab panels.

In addition, Ma has smaller deflections than Mi. This is because of the physical behavior of concrete as shown in Figure 5.9 (the peak of the curve represents the ultimate load). Concrete with Ma behaves as illustrated by curve M1, whereas concrete with Mi behaves as illustrated by curve M2. Ma increases the modulus of elasticity (E). However, when the modulus of elasticity (E) is increased, the inelastic region becomes smaller thus subsequent deflections tend to be small. On the other hand, Mi results in a smaller modulus of elasticity (E). A smaller modulus of elasticity (E) due to Mi creates a corresponding increase in the inelastic region of concrete thus subsequent deflections tend to be larger.

Table 5.4 Test results of unit slab panels (loads and deflections at failure) and ductility index

Mix ID.	Failure load P_F	Deflection at failure Δ_F	Ductility index
SO-normal	40	36.81	1.02
RH-normal	15	3.92	1.35
CH-normal	13	4.65	1.04
SO-Ma-0	53	32.17	1.05
RH-Ma-0	14	6.88	1.12
CH-Ma-0	50	11.43	1.09
SO-Ma-05	44	35.43	1.06
RH-Ma-05	19	8.93	1.18
CH-Ma-05	57	26.88	1.64
SO-Ma-10	45	41.28	1.16
RH-Ma-10	35	10.94	1.75

Mix ID.	Failure load P_F	Deflection at failure Δ_F	Ductility index
CH-Ma-10	71	20.86	1.41
SO-Ma-15	75	47.02	1.26
RH-Ma-15	51	28.95	1.54
CH-Ma-15	69	27.85	1.72
SO-Mi-05	39	34.82	1.85
RH-Mi-05	10	8.2	1.08
CH-Mi-05	30	11.54	1.33
SO-Mi-10	47	27.87	7.39
RH-Mi-10	16	7.19	1.15
CH-Mi-10	53	42.33	5.54
SO-Mi-15	46	26.14	7.06
RH-Mi-15	31	8.08	1.21
CH-Mi-15	55	38.27	1.40

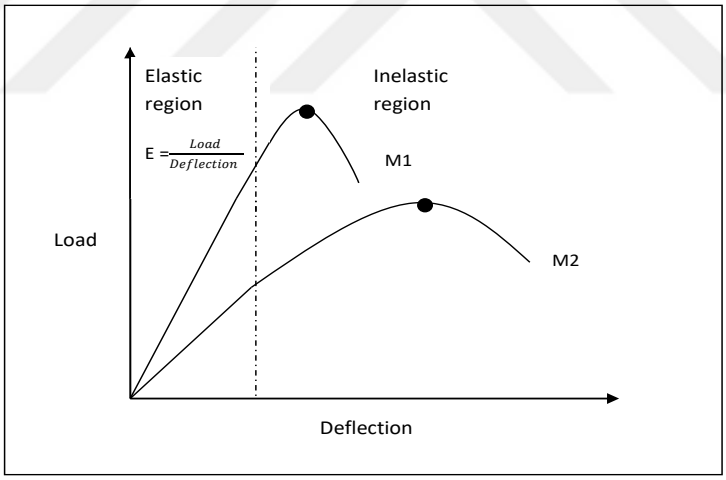

Figure 5.9 Graph of load against deflection for concrete with macro steel (curve M1) and concrete with micro steel (curve M2).

Similarly, when the percentage of steel is increased, the flexural strength improves across all types of HCS panels with both Ma and Mi as shown in Figure 5.10

.

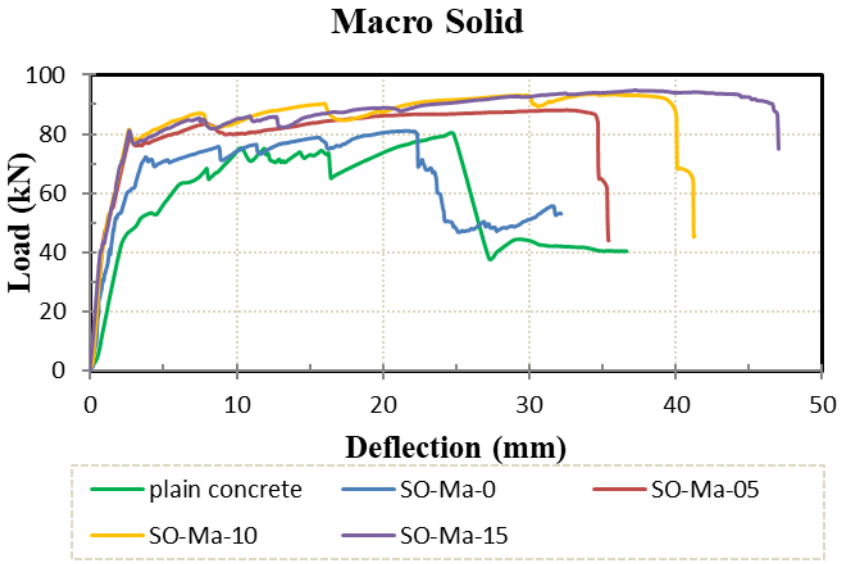
Macro Solid
Load (kN)
Deflection (mm)
plain concrete
SO-Ma-0
SO-Ma-05
SO-Ma-10
SO-Ma-15

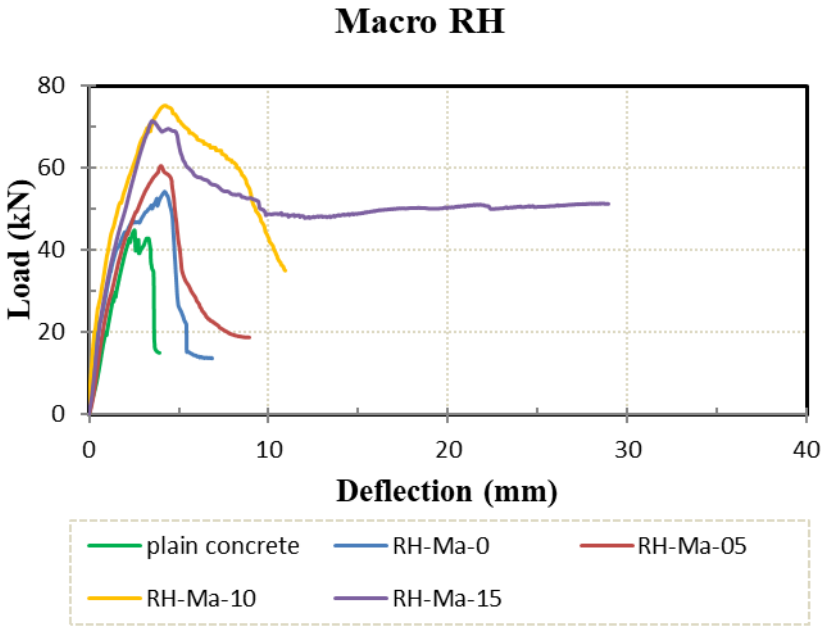
Macro RH
Load (kN)
Deflection (mm)
plain concrete
RH-Ma-0
RH-Ma-05
RH-Ma-10
RH-Ma-15

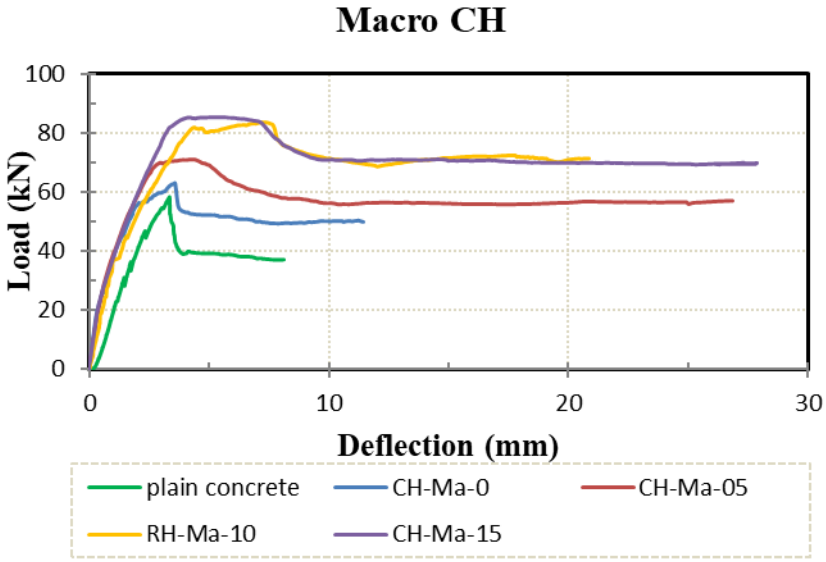
Macro CH
Load (kN)
Deflection (mm)
plain concrete
CH-Ma-0
CH-Ma-05
RH-Ma-10
CH-Ma-15

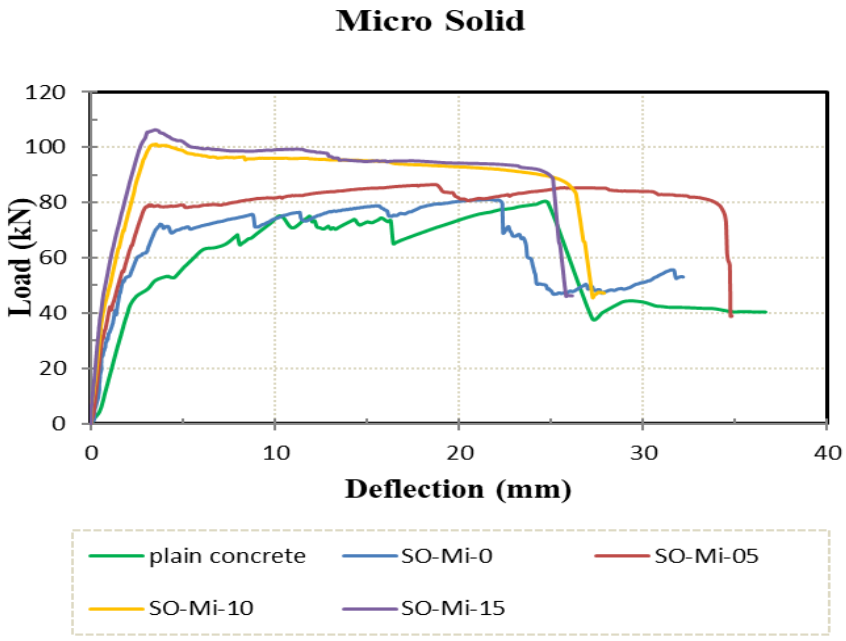
Micro Solid
Load (kN)
Deflection (mm)
plain concrete
SO-Mi-0
SO-Mi-05
SO-Mi-10
SO-Mi-15

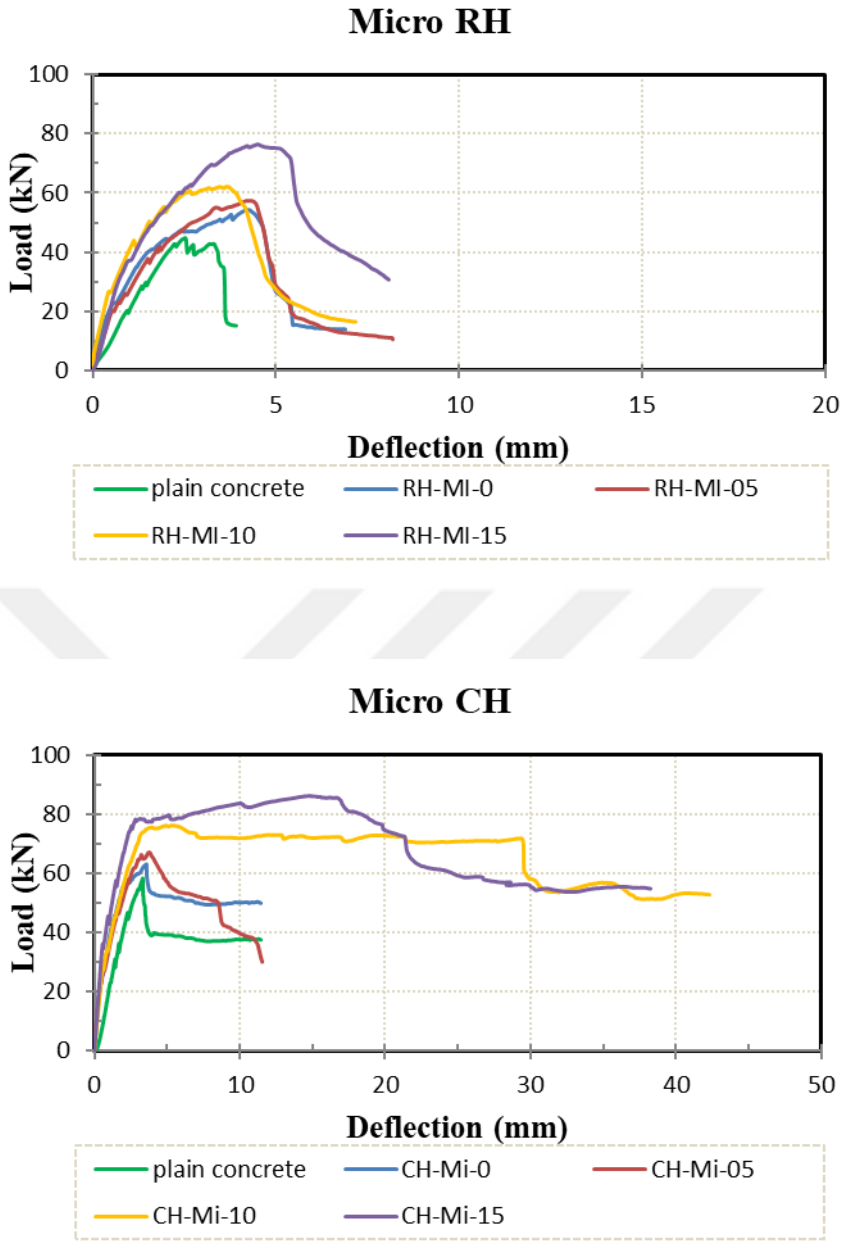

Figure 5.10 Load – Deflection curve

RH core slab panels exhibited lower ductility indices. This is because a rectangular shape opening has four corners which are the maximum stress concentration areas within the concrete. “Stress concentration is defined as the localization of high stress due to the irregularities present in the component and abrupt changes of the cross-section” [104]. These stress concentration areas result in some concrete fibers being stressed up to their strength limit earlier than other fibers. Ductility is the property of a material to continue to deform when subjected to additional loads from the time concrete stops deforming elastically up to the time of failure. This property is

important because it looks at the ability of an element to deform further, without collapsing, even after reaching the elastic limit. In consideration of this behavior, the first cracking load and deflection are related to the time at which the concrete reaches the elastic limit, while the failure load and deflection are obviously the time at which the concrete collapses, and is now no longer serviceable. High ductility is the ability of the SCGC to deform further, when subjected to more changing loads (a greater range of loads), from the time it undergoes first cracking; ductility is defined as the ratio of the extent of the additional deflection (further deflections from first cracking up to failure) to the deflection at first cracking load, (Δcr). RH core slab panels cannot deflect so much, when subjected to a wide range of changing loads, after the elastic limit, depicted by the low values of ductility indices observed in Table 5.4. This arises from the fact that RH core slab panel sections have built up high stress concentration areas at the corners, which reduce the flexural (deflection) capacity of the concrete.

The ductility index of Ma fiber reinforced SCGC is higher than that of Mi fiber reinforced SCGC as seen in Table 5.4. This is because Ma is longer, has a higher aspect ratio and has hooked ends that provide better bonding between the fibers and cement paste. Due to this superior property of Ma, the SF reinforced SCGC is able to accommodate a relatively wider range of loads, from the time concrete stops deforming elastically, up to the time of failure, than SCGC reinforced with Mi. Similarly, when the percentage of steel is increased, the ductility index increases across all the types of HCS panels with both Ma and Mi.

CHAPTER 6

CONCLUSION

6.1 General

In order to decrease the environmental effects from the manufacture of cement, the struggle for alternative materials must continue. These innovative materials should not only be environmental friendly but should also prove to be effective construction products. In the recent past, huge attempts have been made to reduce the negative effects on the environment as a result of cement manufacture. One such development is the use of alternative material such as Geopolymer Concrete (GPC) instead of the conventional OPC. [9,10]

6.2 Conclusion

Based on the experimental results of this thesis, the following conclusions have been made on how GGBFS replacement can affect the fresh and hardened properties of FA based SCGCs, and the effects of hollow type and SF percentages on the structural performance of hollow core slab.

- It can be deduced from the interaction of the V-funnel flow and slump flow times that all of the SCGCs mixtures belonged to the boundaries of the viscosity class (VS2/VF2) as defined by the EFNARC. In addition, it was emphasized that such concrete might be helpful in improving segregation resistance or limiting the formwork pressure.
- It was indicated that the FA based SCGC had to be removed from the molds two or three days after they were cast since they failed to reach the target hardening after one day, due to the low amount of CaO in FA, which is the main factor affecting the initial

setting time of concrete. However, this problem can be avoided by the incorporating of GGBFS in FA based GPC.

- The FA based SCGC exhibited low compressive strength due to the low calcium content and low activity of FA. In addition, the use of GGBFS in the mixes of SCGC significantly improved the compressive strength, since the amount of enhancement increased to more than 200 % for the S100SF0 specimens. This result showed the significant effect of GGBFS on the compressive strength values of SCGCs mixtures.
- It was indicated that splitting tensile strength, flexural strength, fracture toughness, and stress intensity factor values were increased with an increase in compressive strength, and improved with an increase in GGBFS contents, compared to the control mix (100% FA).
- FA and GGBFS were the special elements used to create SCGC- this kind of concrete has a lower carbon footprint, lowers the heat of hydration, has a fairly higher compressive strength of up to 80 MPa and provides, both, better fire resistance and acid/corrosion resistance. Although this type of concrete is considered superior, it still exhibits poor tensile strength, shear and low fracture energy of conventional concrete. Therefore, steel fibers were used to improve the bending, stiffness, shear and tensile strength for SCGC.
- The GGBFS replacement level significantly affects the fresh properties of SCGC. Increasing the amount level of GGBFS in the mixes had a negative effect on the fresh properties. However, the addition of SF had a significant effect on the fresh properties of SCGC, but still within the accepted range according to EFNARC.
- The incorporation of SF had very little influence on the fresh properties and compressive strength. However, the addition of either Ma or Mi SFs is the most dominant factor in splitting tensile strength and flexural strength.
- The results showed that the increase in SF ratios leads to an increase in the first crack load, ultimate load and deflection values compared with control mix.
- The incorporating of SF gives the structural part a degree of ductility that prevents it from sudden collapse and thus gives time for the emigration measures of the structure without collapse of the facility and in some cases, the damaged part can be repaired according to the type of damage.

- From the load-deflection curve appears to be an obvious effect for the type and percentage of SFs, the result showed that Ma is better than Mi because of the aspect ratio and the length of Ma.
- To produce lightweight slabs as a result of reduced cross-sectional areas of slabs. Hollow Core Slab (HCS) panels, also known as void slabs, are super materials in engineering due to low seismic zones, relatively small weight and cheap price. Considerably noticeable is the opening that is created through the panel, which reduces its total weight.
- The reduction in weight of HCS was more than 32 % in both of RH and CH, while the decrease in the ultimate load of control panels was 22 % and 33 % for CH and RH respectively.
- For same HCS, CH core shows an increase in cracking and ultimate loads by 11.5 % and 14.3 % respectively compared to RH core. The shear mode of failure is obtained for RH while shear flexure mode of failure is obtained for RH when the loosest percentage of SF was added.
- RH core concrete slab panels have inferior structural properties compared to solid and CH core concrete slab panels.

REFERENCE

[1] V. S. Ramachandran, (1981) "Waste and by-products as concrete aggregates," *Can. Build. Dig.*, **215**.

[2] G. Baykal and A. G. Döven, (2000) "Utilization of fly ash by pelletization process; theory, application areas and research results," *Resour. Conserv. Recycl.*, **30(1)**, pp. 59–77.

[3] C. R. Cheeseman, A. Makinde, and S. Bethanis, (2005) "Properties of lightweight aggregate produced by rapid sintering of incinerator bottom ash," *Resour. Conserv. Recycl.*, **43(2)**, pp. 147–162.

[4] G. Joseph and K. Ramamurthy, (2009) "Influence of fly ash on strength and sorption characteristics of cold-bonded fly ash aggregate concrete," *Constr. Build. Mater.*, **23(5)**, pp. 1862–1870.

[5] K. Sakai and T. Noguchi, (2012) *The sustainable use of concrete*. CRC press.

[6] O. Kayali, 2008 "Fly ash lightweight aggregates in high performance concrete," *Constr. Build. Mater.*, **22(12)**, pp. 2393–2399.

[7] H. Wilts, N. von Gries, and B. Bahn-Walkowiak, (2016) "From waste management to resource efficiency the need for policy mixes," *Sustainability*, **8(7)**, p. 622.

[8] B. V. Rangan, (2008) "Fly ash-based geopolymer concrete,".

[9] D. L. Y. Kong and J. G. Sanjayan, (2008) "Damage behavior of geopolymer composites exposed to elevated temperatures," *Cem. Concr. Compos.*, **30(10)**, pp. 986–991.

[10] J. Temuujin, R. P. Williams, and A. Van Riessen, (2009) "Effect of mechanical activation of fly ash on the properties of geopolymer cured at ambient temperature," *J. Mater. Process. Technol.*, **209(12–13)**, pp. 5276–5280.

[11] J. Davidovits, (1999) "Chemistry of Geopolymeric Systems, Terminology In: Proceedings of **99** International Conference," *eds. Joseph Davidovits, R. Davidovits C. James,Fr.*.

[12] A. R. Sakulich, (2011) “Reinforced geopolymer composites for enhanced material greenness and durability,” *Sustain. Cities Soc.*, **1(4)**, pp. 195–210.

[13] M. Alzeer and K. MacKenzie, (2013) “Synthesis and mechanical properties of novel composites of inorganic polymers (geopolymers) with unidirectional natural flax fibres (phormium tenax),” *Appl. Clay Sci.*, **75,** pp. 148–152.

[14] S. Wallah and B. V. Rangan, 2006“Low-calcium fly ash-based geopolymer concrete: long-term properties,”.

[15] H. Xu and J. S. J. Van Deventer, (2000) “The geopolymerisation of alumino-silicate minerals,” *Int. J. Miner. Process.*, **59(3)**, pp. 247–266.

[16] C. K. Yip, G. C. Lukey, J. L. Provis, and J. S. J. van Deventer, (2008) “Effect of calcium silicate sources on geopolymerisation,” *Cem. Concr. Res.*, **38(4)**, pp. 554–564.

[17] H. K. Tchakouté and C. H. Rüscher, (2017) “Mechanical and microstructural properties of metakaolin-based geopolymer cements from sodium waterglass and phosphoric acid solution as hardeners: a comparative study,” *Appl. Clay Sci.*, **140**, pp. 81–87.

[18] H.-L. Yip, S. K. Hau, N. S. Baek, H. Ma, and A. K.-Y. Jen, (2008) “Polymer Solar Cells That Use Self-Assembled-Monolayer-Modified ZnO/Metals as Cathodes,” *Adv. Mater.*, **20(12)**, pp. 2376–2382.

[19] N. Ganesan and P. V Indira, (2013) “Engineering properties of steel fibre reinforced geopolymer concrete,” *Adv. Concr. Constr.*, **1(4)**, pp. 305–318.

[20] P. Jeyaraj, D. Sugumar, K. Thandavamoorthy, and S. J. Xavier, (2014) “Students Perceived Value towards Quality of Distance Education in Tamil Nadu.,” *Turkish Online J. Distance Educ.*, **15(2)**, pp. 201–208.

[21] O. Gencel, C. Ozel, W. Brostow, and G. Martinez-Barrera, (2011) “Mechanical properties of self-compacting concrete reinforced with polypropylene fibres,” *Mater. Res. Innov.*, **15(3)**, pp. 216–225.

[22] A. Khaloo, E. M. Raisi, P. Hosseini, and H. Tahsiri, (2014) “Mechanical performance of self-compacting concrete reinforced with steel fibers,” *Constr. Build. Mater.*, **51**, pp. 179–186.

[23] V. Midhun Mohan and A. M. Sajeeb, (2018) “Improving the efficiency of DASC by adding CeO2/CuO hybrid nanoparticles in water,” *Int. J. Nanosci.*,**17(1-2)**, p. 1760011.

[24] C. Frazão, A. Camões, J. Barros, and D. Gonçalves, (2015) “Durability of steel

fiber reinforced self-compacting concrete," *Constr. Build. Mater.*,**80,** pp. 155–166.

[25] M. Zhang, M. Zhao, G. Zhang, D. Mann, K. Lumsden, and M. Tao, (2016) "Durability of red mud-fly ash based geopolymer and leaching behavior of heavy metals in sulfuric acid solutions and deionized water," *Constr. Build. Mater.*, **124**, pp. 373–382.

[26] L. V Prakashan, J. George, J. B. Edayadiyil, and J. M. George, (2016) "Experimental Study on the Flexural Behavior of Hollow Core Concrete Slabs," *Appl. Mech. Mater. Submitt.*, **857**, pp. 107–112.

[27] M. Baker, (1984) "Evaluation on the utilization options, combustion by products utilization manual," *EPRI Rep. no. CS-3122*.

[28] M. Ahmaruzzaman, (2010) "A review on the utilization of fly ash," *Prog. energy Combust. Sci.*, **36(3)**, pp. 327–363.

[29] G. Qian, S. Bai, S. Ju, and T. Huang, (2012) "Laboratory evaluation on recycling waste phosphorus slag as the mineral filler in hot-mix asphalt," *J. Mater. Civ. Eng.*,**25(7)**, pp. 846–850.

[30] P.-C. A. (2011) "itcin and S. Mindess, *Sustainability of concrete*. CRC Press.

[31] D. Suresh and K. Nagaraju, 2015 "Ground Granulated Blast Slag (GGBS) In Concrete--A Review," *IOSR J. Mech. Civ. Eng.*,**12(4)**, pp. 76–822.

[32] M. M. A. Abdullah, K. Hussin, M. Bnhussain, K. N. Ismail, and W. M. W. Ibrahim, (2011) "Mechanism and chemical reaction of fly ash geopolymer cement-a review," *Int. J. Pure Appl. Sci. Technol*,**6(1)**, pp. 35–44.

[33] J. L. Provis and J. S. J. Van Deventer, (2009) *Geopolymers: structures, processing, properties and industrial applications*. Elsevier.

[34] A. Fernández-Jiménez, A. Palomo, I. Sobrados, and J. Sanz, (2006) "The role played by the reactive alumina content in the alkaline activation of fly ashes," *Microporous Mesoporous Mater.*, **91(1–3)**, pp. 111–119.

[35] P. Duxson, G. C. Lukey, and J. S. J. van Deventer, (2007) "Physical evolution of Na-geopolymer derived from metakaolin up to 1000 C," *J. Mater. Sci.*, **42(9),** pp. 3044–3054.

[36] J. Davidovits, (1994) "High-alkali cements for 21st century concretes," *Spec. Publ.*,**144**, pp. 383–398.

[37] Z. Xie and Y. Xi, (2001) "Hardening mechanisms of an alkaline-activated class F fly ash," *Cem. Concr. Res.*,**31(9)**, pp. 1245–1249.

[38] H. Du, S. Du, and X. Liu, (2014) “Durability performances of concrete with nano-silica,” *Constr. Build. Mater.*,**73**, pp. 705–712.

[39] J. G. S. Van Jaarsveld, J. S. J. Van Deventer, and L. Lorenzen, (1997) “The potential use of geopolymeric materials to immobilise toxic metals,” *Miner. Eng*,**10**, pp. 659–669.

[40] J. C. Swanepoel and C. A. Strydom, (2002) “Utilisation of fly ash in a geopolymeric material,” *Appl. geochemistry*,**17(8)**, pp. 1143–1148.

[41] A. Motorwala, V. Shah, R. Kammula, P. Nannapaneni, and D. B. Raijiwala, (2013) “ALKALI activated FLY-ASH based geopolymer concrete,” *Int. J. Emerg. Technol. Adv. Eng.*,**3(1)**, pp. 159–166.

[42] A. Palomo, M. W. Grutzeck, and M. T. Blanco, (1999) “Alkali-activated fly ashes: a cement for the future,” *Cem. Concr. Res.*,**29(8)**, pp. 1323–1329.

[43] P. Duxson and J. L. Provis, (2008) “Designing precursors for geopolymer cements,” *J. Am. Ceram. Soc.*,**91(12)**, pp. 3864–3869.

[44] P. Nath and P. K. Sarker, (2014) “Effect of GGBFS on setting, workability and early strength properties of fly ash geopolymer concrete cured in ambient condition,” *Constr. Build. Mater.*,**66**, pp. 163–171.

[45] J. Lindgård, Ö. Andiç-Çak\ir, I. Fernandes, T. F. Rønning, and M. D. A. Thomas, (2012) “Alkali--silica reactions (ASR): literature review on parameters influencing laboratory performance testing,” *Cem. Concr. Res.*,**42(2)**, pp. 223–243.

[46] J. Davidovits, (1991) “Geopolymers - Inorganic polymeric new materials,” *J. Therm. Anal.*,**37(8)**, pp. 1633–1656.

[47] P. Q. Europe, (2004) “Sodium and Potassium Silicates: Versitile Componants for Your Applications.”.

[48] D. Hardjito, S. E. Wallah, D. M. J. Sumajouw, and B. V. Rangan, (2004) “On the development of fly ash-based geopolymer concrete,” *Mater. J.*,**101(6)**, pp. 467–472.

[49] L. N. Assi, E. Deaver, M. K. Elbatanouny, and P. Ziehl, (2016) “Investigation of early compressive strength of fly ash-based geopolymer concrete,” *Constr. Build. Mater.*,**112**, pp. 807–815.

[50] E. Arioz, O. Arioz, and O. M. Kockar, (2012) “An experimental study on the mechanical and microstructural properties of geopolymers,” *Procedia Eng.*,**42**, pp. 100–105.

[51] J. G. S. Van Jaarsveld, J. S. J. Van Deventer, and G. C. Lukey, (2003) "The characterisation of source materials in fly ash-based geopolymers," *Mater. Lett.*, **57(7)**, pp. 1272–1280.

[52] D. Hardjito and B. V. Rangan, (2005) "Development and properties of low-calcium fly ash-based geopolymer concrete,".

[53] P. V Krivenko and G. Y. Kovalchuk, (2002) "Heat-resistant fly ash based geocements," *Geopolymers*.

[54] D. Hardjito, S. E. Wallah, D. M. J. Sumajouw, and B. V Rangan, (2004) "Factors influencing the compressive strength of fly ash-based geopolymer concrete," *Civ. Eng. Dimens.*,**6(2)**, pp. 88–93.

[55] A. Palomo, S. Alonso, A. Fernandez-Jiménez, I. Sobrados, and J. Sanz, (2004) "Alkaline activation of fly ashes: NMR study of the reaction products," *J. Am. Ceram. Soc.*, **87(6)**, pp. 1141–1145.

[56] P. Chindaprasirt, T. Chareerat, and V. Sirivivatnanon, (2007) "Workability and strength of coarse high calcium fly ash geopolymer," *Cem. Concr. Compos.*,**29(3)**, pp. 224–229.

[57] M. Olivia and H. Nikraz, (2012) "Properties of fly ash geopolymer concrete designed by Taguchi method," *Mater. Des.*,**36**, pp. 191–198.

[58] K. Vijai, R. Kumutha, and B. G. Vishnuram, (2010) "Effect of types of curing on strength of geopolymer concrete," *Int. J. Phys. Sci.*,**5(9)**, pp. 1419–1423.

[59] H. Okamura and M. Ouchi, (2003) "Self-compacting concrete," *J. Adv. Concr. Technol.*, **1(1)**, pp. 5–15.

[60] K. Maekawa and K. Ozawa, (1999) "Development of SCCs prototype," *Writ. Japanese), Self-Compacting High-Performance Concr. Soc. Syst. Inst.*, pp. 20–32.

[61] P.-C. A. (2011) "itcin, *High performance concrete*. CRC press.

[62] E. Güneyisi, M. Gesoğlu, S. Al-Rawi, and K. Mermerdaş, (2014) "Effect of volcanic pumice powder on the fresh properties of self-compacting concretes with and without silica fume," *Mater. Struct. Constr.*,**47(11)**, pp. 1857–1865.

[63] Y. Hasegawa, (1989) "Synthesis of continuous silicon carbide fibre," *J. Mater. Sci.*, **24(4)**, pp. 1177–1190.

[64] J. A. O. Barros and others, (2016) "Report on indirect method to obtain stress-strain response of fiber-reinforced concrete (FRC)," *Report on indirect method to obtain stress-strain response of fiber-reinforced concrete (FRC)*. American

Concrete Institute, pp. 1–22.

[65] B. N. Skourup and E. Erdogmus, (2010) “Mechanical characteristics of PVA fiber-reinforced PCL mortars for masonry applications,” *ACI Mater. J*, **107**, pp. 1–9.

[66] R. F. Zollo, (1997) “Fiber-reinforced concrete: an overview after 30 years of development,” *Cem. Concr. Compos.*,**19(2)**, pp. 107–122.

[67] A. E. Naaman, (1985) “Fiber reinforcement for concrete,” *Concr. Int.*,**7(3)**, pp. 21–25.

[68] F. F. Wafa and S. A. Ashour, (1992) “Mechanical properties of high-strength fiber reinforced concrete,” *Mater. J.*, **89(5)**, pp. 449–455.

[69] S. Al-Rawi and N. Taysi, (2018) “Performance of self-compacting geopolymer concrete with and without GGBFS and steel fiber,” *Adv. Concr. Constr.*,**6(4)**, pp. 323–344.

[70] S. Finazzi, I. Paegle, G. Fischer, and F. Minelli, (2014) “Influence of bending test configuration on cracking behavior of FRC,” in *Proceedings of Third All-Russia (International) Conference on Concrete and Reinforced Concrete*, **3**, pp. 196–205.

[71] S. Bernal, R. De Gutierrez, S. Delvasto, and E. Rodriguez, (2010) “Performance of an alkali-activated slag concrete reinforced with steel fibers,” *Constr. Build. Mater.*, **24(2)**, pp. 208–214.

[72] K. H. Mo, K. H. Yeoh, I. I. Bashar, U. J. Alengaram, and M. Z. Jumaat, (2017) “Shear behaviour and mechanical properties of steel fibre-reinforced cement-based and geopolymer oil palm shell lightweight aggregate concrete,” *Constr. Build. Mater.*, **148**, pp. 369–375.

[73] A. A. Yee, (2001) “Structural and economic benefits of precast/prestressed concrete construction,” *PCI J.*, **46(4)**.

[74] S. D. Nakaki, (1999) “An overview of the PRESSS five-story precast test building,” *PCI J.*,**44(2)**, pp. 26–29.

[75] PCI, (1998) “PCI Manual for the Design of Hollow Core Slabs,” *PCI Hollow Core Slab Prod. Comm.*, p. 141.

[76] R. J. Becker and D. R. Buettner, (1985) “Shear tests of extruded hollow-core slabs,” *PCI J.*,**30(2)**, pp. 40–54.

[77] A. Aswad and F. J. Jacques, (1992) “Behavior of Hollow-Core Slabs Subject to Edge Loads,” *PCI J.*,**37(2)**.

[78] M. Pajari, (1998) “Shear resistance of PHC slabs supported on beams. II: Analysis,” *J. Struct. Eng.*,**124(9)**, pp. 1062–1073.

[79] F. M. M. Elgabbas, (2009) “Cfrp Strengthening Of Prestressed Hollow Core Slabs In Positive Moment Region,” Ain Shams University Cairo.

[80] E. Cuenca and P. Serna, (2013) “Failure modes and shear design of prestressed hollow core slabs made of fiber-reinforced concrete,” *Compos. Part B Eng.*,**45(1)**, pp. 952–964.

[81] A. A. Al-Azzawi and S. A. Abed, (2017) “Investigation of the behavior of reinforced concrete hollow-core thick slabs,” *Comput. Concr.*,**19(5)**, pp. 567–577.

[82] I. S. Ibrahim, K. S. Elliott, R. Abdullah, A. B. H. Kueh, and N. N. Sarbini, (2016) “Experimental study on the shear behaviour of precast concrete hollow core slabs with concrete topping,” *Eng. Struct.*,**125**, pp. 80–90.

[83] S. K. S. Pachalla and S. S. Prakash, (2017) “Load resistance and failure modes of GFRP composite strengthened hollow core slabs with openings,” *Mater. Struct. Constr.*, **50(1)**, pp. 1–14.

[84] N. G. Wariyatno, Y. Haryanto, and G. H. Sudibyo, (2017) “Flexural behavior of precast hollow core slab using PVC pipe and Styrofoam with different reinforcement,” *Procedia Eng.*,**171**, pp. 909–916.

[85] H. Broo and K. Lundgren, (2002) “Finite element analyses of hollow core units subjected to shear and torsion,”.

[86] L. V. Prakashan, J. George, J. B. Edayadiyil, and J. M. George, (2016) “Experimental Study on the Flexural Behavior of Hollow Core Concrete Slabs,” *Appl. Mech. Mater.*, **857**, no. September, pp. 107–112.

[87] T. S. EN, “197-1 (2002) Cement-Part 1: Compositions and conformity criteria for common cements,” *Turkish Stand. Institution, TSE, Ankara (in Turkish)*.

[88] ASTM Standards C618, (2015) “Standard Specification for Coal Fly Ash and Raw or Calcined Natural Pozzolan for Use,” *Annu. B. ASTM Stand.*, pp. 3–6.

[89] ASTM C127 − 15, (2015) “Standard Test Method for Relative Density (Specific Gravity) and Absorption of Coarse Aggregate,” *ASTM Int.*, p. 5.

[90] EFNARC, (2005) “The European Guidelines for Self-Compacting Concrete: Specification, Production and Use,” *Eur. Guidel. Self Compact. Concr.*, no. May, p. 68.

[91] ASTM International, (2016) “ASTM C39 Standard Test Method for

Compressive Strength of Cylindrical Concrete Specimens," *Am. Soc. Test. Mater.*, pp. 1–7.

[92] ASTM C496/C496M-11, (2011) "ASTM C496-11 Standard Test Method for Splitting Tensile Strength of Cylindrical Concrete Specimens," *Annu. B. ASTM Stand.* ***04.02*****,** pp. 1–5.

[93] D. R. RILEM, (1985) "Determination of the fracture energy of mortar and concrete by means of three-point bend tests on notched beams," *Mater. Struct.*,**18(106)**, pp. 285–290.

[94] B. Akcay and M. A. Tasdemir, (2009) "Optimisation of using lightweight aggregates in mitigating autogenous deformation of concrete," *Constr. Build. Mater.*, **23(1)**, pp. 353–363.

[95] P. E. Peterson, (1980) "Fracture energy of concrete: Method of determination," *Cem. Concr. Res.*,**10(1)**, pp. 79–89.

[96] K. Dombrowski, A. Buchwald, and M. Weil, (2007) "The influence of calcium content on the structure and thermal performance of fly ash based geopolymers," *J. Mater. Sci.*, **42(9),** pp. 3033–3043.

[97] J. S. Belkowitz, W. B. Belkowitz, K. Nawrocki, and F. T. Fisher, (2015) "Impact of Nanosilica Size and Surface Area on Concrete Properties.," *ACI Mater. J.*,**112(3)**.

[98] B. B. Jindal, D. Singhal, S. K. Sharma, D. K. Ashish, and P. Parveen, (2017) "Improving compressive strength of low calcium fly ash geopolymer concrete with alccofine," *Adv. Concr. Constr.*,**5(1)**, pp. 17–29.

[99] M. Chi and R. Huang, (2013) "Binding mechanism and properties of alkali-activated fly ash/slag mortars," *Constr. Build. Mater.*, **40**, pp. 291–298.

[100] A. Çevik, R. Alzeebaree, G. Humur, A. Niş, and M. E. Gülşan, (2018) "Effect of nano-silica on the chemical durability and mechanical performance of fly ash based geopolymer concrete," *Ceram. Int.*,**44(11)**, pp. 12253–12264.

[101] A. Neville, (1995) "Chloride attack of reinforced concrete: an overview," *Mater. Struct.*, **28(2)**, p. 63.

[102] P. K. Mehta, P. J. M. Monteiro, and others, (2006) "Microstructure, properties and materials," *McGraw-Hill Prof. New York*.

[103] N. Arabi *et al.*, (2016) "Formation of C-S-H in calcium hydroxide – blast furnace slag – quartz – water system in autoclaving conditions To cite this version : HAL Id : hal-01366494 Formation of C-S-H in calcium hydroxide –

blast furnace slag – quartz – water system in autoclaving,".

[104] T. Hemalatha and A. Ramaswamy, (2017) "A review on fly ash characteristics – Towards promoting high volume utilization in developing sustainable concrete," *J. Clean. Prod.*,**147**, pp. 546–559

CURRICULUM VITAE

PERSONAL INFORMATION

Name and Surname: Saad Abdulrazzak MUKHLIF

Nationality: IRAQI

Birth place and date: Baghdad / IRAQ – December 17,1977

Marital status: Married

Phone number: +90 5531816420

Email: saalrawi77@gmail.com

EDUCATION

	Graduate School	Year
Master	Civil Engineering Department, College of Engineering, Gaziantep University, Gaziantep, TURKEY	2013
Bachelor	Civil Engineering Department, College of Engineering, Baghdad University, Baghdad, IRAQ	2002

WORK EXPERIENCE

	Place	Enrollment
2006 - Present	Civil Engineering Department, College of Engineering, AL-Nahrain University, Baghdad, IRAQ	Civil Engineer
2004 - 2006	Civil Engineering Department, Minstry of Higher Eduction, Baghdad, IRAQ	Civil Engineer
2002 - 2004	AL-HEETY Co. for Concrete Mix	Civil Engineer

PUBLICATIONS

S. Al-Rawi and N. Taysi, “Performance of self-compacting geopolymer concrete with and without GGBFS and steel fiber,” *Adv. Concr. Constr.*,**6,(4)**, pp. 323–344, 2018.

E. Güneyisi, M. Gesoğlu, S. Al-Rawi, and K. Mermerdaş, “Effect of volcanic pumice powder on the fresh properties of self-compacting concretes with and without silica fume,” *Mater. Struct. Constr.*,**47,(11)**, pp. 1857–1865, 2014.

FOREIGN LANGUAGE

English

HOBBIES

1. Reading.
2. Football.
3. swimming.